WESTERN POWER DISTRIBUTION

INNOVATION

NEXT GENERATION NETWORKS

DEDUCE
Low Cost Sensors – Sensor Testing

Report Title	:	Low cost sensors – Sensor Testing
Report Status	:	V1.0
Project Ref	:	DEDUCE
Date	:	10/07/18

Document Control		
	Name	Date
Prepared by:	D Strickland and B Goss	10/07/18
Reviewed by:	D Strickland	10/07/18
Approved (WPD):		<DD.MM.YYYY>

Revision History		
Date	Issue	Status
10/07/18	V1.0	Issued

Contents

Glossary

Abbreviation	Term
AI	Analogue Input
CREST	Centre for Renewable Energy Systems Technology
DI	Digital input
GND	'Ground' bus of circuit, usually at 0V potential.
GPRS	General Packet Radio Service (Mobile phone protocol).
I^2C	Inter Integrated circuit – A serial communication protocol
LV	Low Voltage (400V)
MEMS	Micro Electronic Mechanical Systems
PCB	Printed circuit board
SCL	Serial Clock (of I^2C serial bus connection)
SDA	Serial Data (of I^2C serial bus connection)
tx	transformer
WIFI	Wireless internet

1 Executive Summary

Recent growth in embedded generation such as wind and solar photovoltaic (PV) systems and the anticipated consumer uptake of electric vehicles (EVs) and heat pumps present new challenges for Western Power Distribution (WPD) to develop and operate its network which will experience greater fluctuation in electricity demand. Data from maximum demand indicators in distribution substations is inadequate to understand the spread of demand over time. Retro-fit datalogging solutions are available for substation monitoring, but cost typically >£1200, which would be difficult to justify for all WPDs 40,000 distribution substations. This NIA (Network Innovation Allowance) research project on network analogues is being conducted by CREST (Centre for Renewable Energy Systems Technology at Loughborough University in conjunction with WPD. The aim of the project is to identify and develop a novel low-cost monitoring approach with a target cost of £100 per substation.

Engineering projects usually capture the requirements first then identify the best solutions for those requirements. This project intentionally has a tightly defined cost requirement and loose technical requirements, which are as follows:

- The solution shall cost £100 or less excluding installation and operation costs.
- The solution should give an indication of substation loading.
- The solution should act as a replacement for existing MDIs (maximum demand indicator).
- The solution should provide as many channels of useful data at the highest feasible resolution within the cost requirement.
- The solution should consider how data will be transferred to a WPD datacentre or control room.

CREST have designed, built and coded 8 different sensors using three different control platforms. This document summarises the hardware requirements and laboratory testing against a set of pre-defined characteristics to determine usefulness and estimate value.

High level results

- The majority of the sensors and platforms for communication came within the target budget.
- There were 3 sensors that could give a good indication of substation loading and 1 more where results were inconclusive.
- There is capability to get at least 8 useable input/output channels on most platforms and many more on others.
- The best resolution found was data logging to a server at an average of 7ms resolution using a Raspberry Pi. Typically 10s resolution was felt to be useful.
- All the solutions can communicate via Wi-Fi or over the mobile Network (and in some cases through wired connection).

A summary of the key results is presented over.

	Sensor Type									Platform			
	Magnetometer	Hall Effect chip	I2m coil sensor	Accelerometer	Audio Microphone	Strain gauge	Thermal stickers	Thermal transducer	Low cost thermal imaging	Android Phone	Sensor with IOIO board and phone	Arduino	Raspberry Pi
Cost	£14	£2	£13	£19	£9	£31	£4	£99	£350	£13 + phone	£35 + phone	£49	£37 dongle
Application													
Monitoring load close to real time < 10s	✓	×	✓	×	×	×	×	×	×	✓	✓	✓	✓
Load profiling (30min peak)	✓	×	✓	×	×	×	×	×	×	✓	✓	✓	✓
Exception reporting (> max value)	✓	×	✓	×	×	×	×	✓	×	✓	✓	✓	✓
MDI	✓	×	✓	×	×	×	?	✓	×	✓	✓	✓	✓
Data storage													
Uploaded to a server										✓	✓	?	✓
Stored locally										✓	✓	✓	✓
Data form													
Current peak	✓	×	✓	×	×	×	×	×	×	✓			
Current RMS	✓	×	✓	×	×	?	×	×	×	✓			
1 phase	✓	×	×	×	×	×	×	×	×	✓			
3 phase (cable)	✓	×	✓	×	×	×	×	×	×	✓			
Load from transformer	×	×	×	?	?	×	?	?	×	×			
Data Quality													
Linearity	✓	×	✓	?	?	✓	?	✓	×	✓	✓	✓	✓
Correlation with load	> 0.999	×	> 0.996	0.34	0.48	-0.91	?	?	×	> 0.999			
Accuracy	> 7.5%	×	> 10%[1]	?	?	< 25%	?	?	×	> 7.5%			
Recommend for Field Trial	✓	×	✓	×	×	×	×	×	×	✓	×	×	✓

✓ Tested, satisfactory > better than

× Tested, unsuitable < worse than

? Test not conclusive

[1]There is still significant theory needed to back calculate current for distributed windings and this value could be easily improved.

It is recommended that the i2m coils, mobile phone and magnetometer be taken forward for field trials. Possible follow on applications for these low cost sensors are shown over and include benefits already identified by UKPN projects DNV;

- Quick identification of substations where new load is able to be connected.

• Improving the potential to defer costly reinforcement of the network through the use of demand profiles.
• Improving network and asset reliability by monitoring trends.
• Improving the management of substation and network utilisation.
• Providing information on network to better support operational activity.

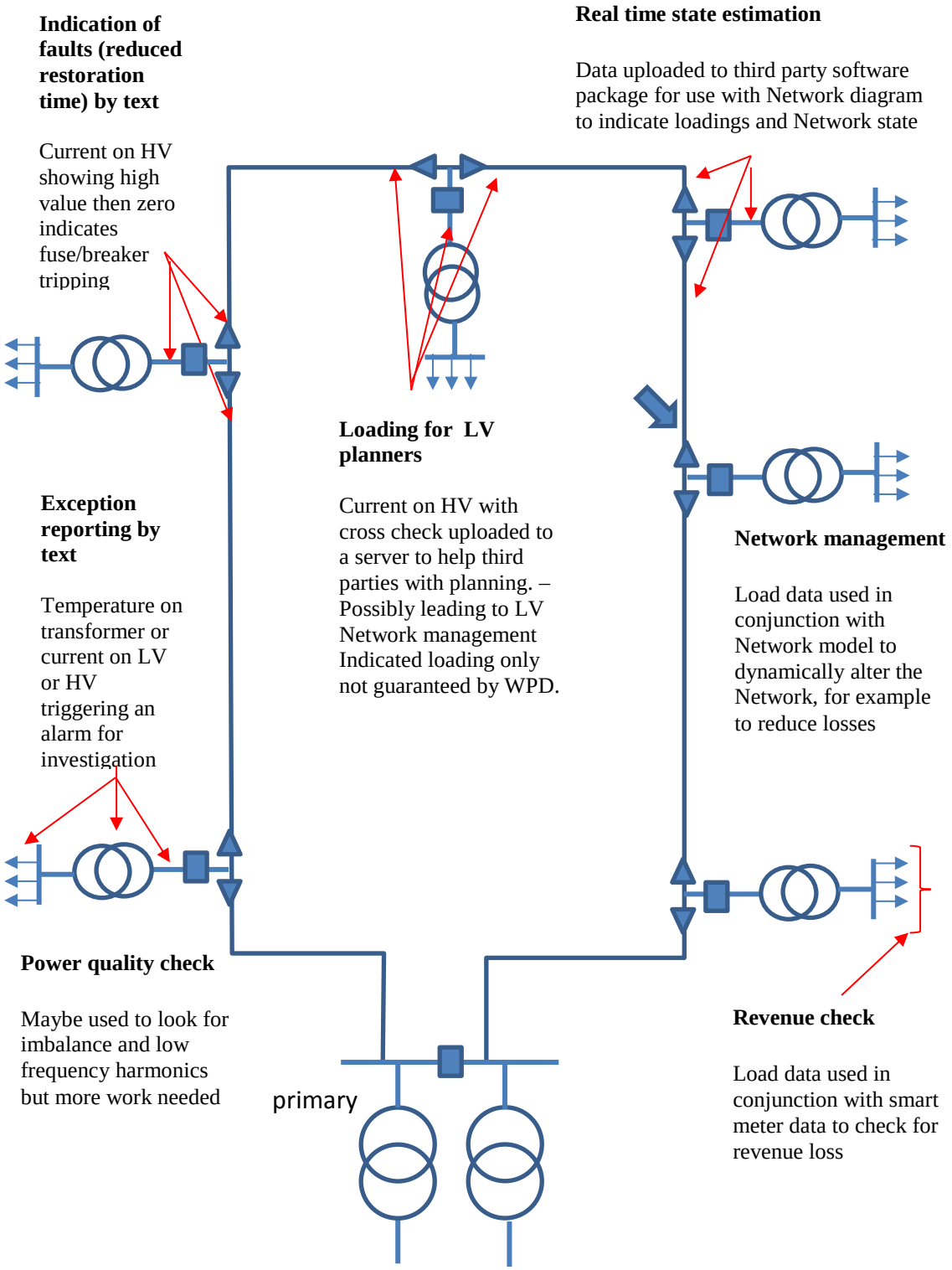

Figure 1: Sensor - platform interface options

2 Introduction

2.1 Background

DNOs currently have very limited visibility of LV networks. With Supervisory Control And Data Acquisition (SCADA) systems generally limited to 11kV feeders, visibility of LV network loading is restricted to Maximum Demand Indicators (MDI). These manual readings are generally supplemented with industry metering flows to develop an understanding of network loading. MDIs are restricted by their need to be reset periodically as well as the potential for network back-feeds to distort readings.

Several previous LCNF projects have investigated LV monitoring. This has pushed the market for LV monitoring forward significantly from the custom-built units used for the Low Voltage Network Templates project, to several commercially available units available to date. WPD currently has Standard Techniques (STs) for the installation of ground mounted and overhead monitoring as well as a fully tendered framework agreement for the supply of such units.

These units depend primarily on the measurement of voltage and current to determine loading. Voltage is generally measured directly using busbar clamps or modified fuse holders with a voltage take off point. Current is generally measured using Rogowski coils. These units can measure the detailed loading of each phase on each feeder and provide a significant level of detail and granularity. However, these devices are also costly due to the requirement for multiple sensors. This has limited their roll out to date.

This project looks to develop a low cost (sub £100) distribution substation monitor based on indirect loading measures (for example; magnetic field, temperature, noise and vibration). At a minimum this must give access to more granular and less error prone data than is currently acquired through MDIs. The substation monitor is expected to develop a methodology for the acquisition of basic whole substation loading profiles as well as the optimal method for the delivery of such data to planning teams and simplicity of installation.

To meet these aims the following approaches are proposed:

- To investigate existing low-cost sensors that can be used for indirect substation loading monitoring.
- To investigate new disruptive technologies to determine their suitability and accuracy for monitoring
- To use existing low-cost measurement devices or packages (such as a smart phone or raspberry pi) to indirectly provide measurement
- To run a university-based competition to enable non-traditional solutions to be explored

Several different sensors technologies were identified in the review document. These have now been designed, built and tested. The designs went through an iterative procedure as improvements were identified as part of testing and lessons learned were captured. This

document contains the “as built” hardware details of the sensors that have been manufactured prior to testing, the changes to hardware as testing has progressed and a summary of that testing.

2.2 Scope

The project is aimed at 11kV:400kV 50Hz distribution substations connected to public distribution networks. The project focuses on ground mounted substations on the 11kV distribution network since these account for the bulk of final LV demand. As such pole mounted transformers and substations on legacy 6.6kV networks are not specifically covered since they are a small proportion of overall demand. Likewise, primary substations are not specifically considered since the smaller number of primaries and greater power flow means more accurate and robust solutions are more like to be justified economically. Monitoring at the DNO/meter operator/consumer interface is not considered since a wide range of parameters will be available from smart meters as they are commissioned as part of a national program.

The findings of this project may have relevance for monitoring of pole mounted transformers, 6.6kV substations and primary substations which could be determined as part of a successor project.

2.3 Presentation of learning

Throughout the document, key learning outcomes are presented in a box as follows:

LP x	Brief description of learning.

Each piece of project feedback is referenced as a uniquely numbered Learning Point (LP).

All learning points are collected together in Appendix A. In addition there are a set of technical tips which contain technical pointers for anyone looking to replicate this work

TT x	Brief description of a technical tip for anyone trying to replicate this work

3 Sensors to be tested

The following sensors were identified as part of the literature review as being suitable for prototyping.

Table 3-1 : Summary of sensors and platforms to be tested

ID	Sensor type	Variable measured
A	MEMS Magnetometer	Magnetic field
B	Hall effect chip	Magnetic field
C	Novel magnetic field coil sensor	Magnetic field
D	Accelerometer	Vibration
E	Audio microphone	Noise
F	Strain gauge	Strain through a Wheatstone bridge
G1	Temperature labels	Temperature
G2	Thermistor remote alarm	Temperature
H	Thermal imaging	Temperature
ID	**Platform type**	**Variable measured**
I	Android phone	Magnetic field
J	IOIO interface unit	With a sensor above
K	Arduino	With sensors above
L	Raspberry Pi	With a sensor above

The sensors produce a range of output signals. In theory, each sensor could be connected through to each platform. However, the reality is that it is easier to connect certain sensors with associated platforms. This is for ease of setup and coding, for example where coded libraries are available. Figure 2 shows a summary of these combinations.

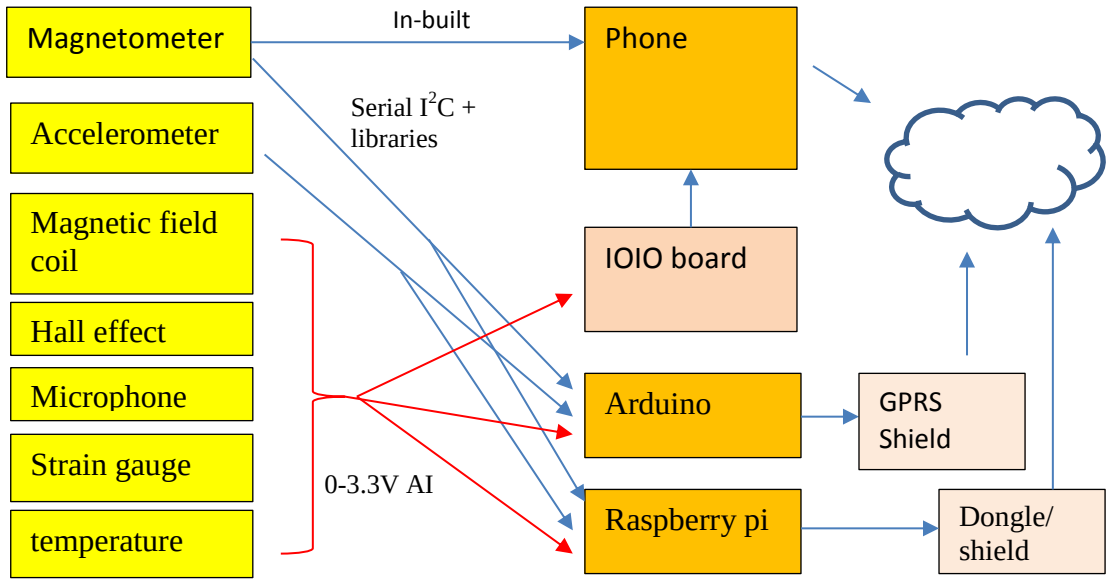

Figure 2: Sensor - platform interface options

Not all the sensors can measure loading on all types of cable. Usually, sensors only measure single core or three core cable types.

LP 1	Sensors to measure current in multicore/trefoil cables are not commercially available and there is no available published literature on measurement solutions. These are the most popular type of cable on the Distribution Network. Therefore, measuring these types of cable without separating the cores with a single sensor may be valuable.

Section 4 looks at the testing facilities while section 5 onwards considers each sensor and the platform in turn. Each section includes details about the hardware, parts list and its cost, how each sensor is set up ready for testing, followed by test results where applicable.

Where the sensor looks a promising candidate for taking forward to field trial the theory behind the back calculation of current is also included.

4 Electrical test facilities at CREST.

4.1 CREST Test Rig with Simulated Substation

For initial testing, a simulated substation has been setup which recreates many of the characteristics of an LV substation without requiring high voltages to be used.
There are two main aspects of the lab facility:

1) A 3 phase, 45kVA air cooled transformer with variable voltage supply
2) A high current, low voltage power supply which can supply up to 150A into a shorted 3 phase cable as shown in Figure 3. This means that any DNO 1,2, 3 or 4 core cables can be connected, and their electromagnetic field measured with sensors under test. It could also be used for other tests such as temperature and strain.

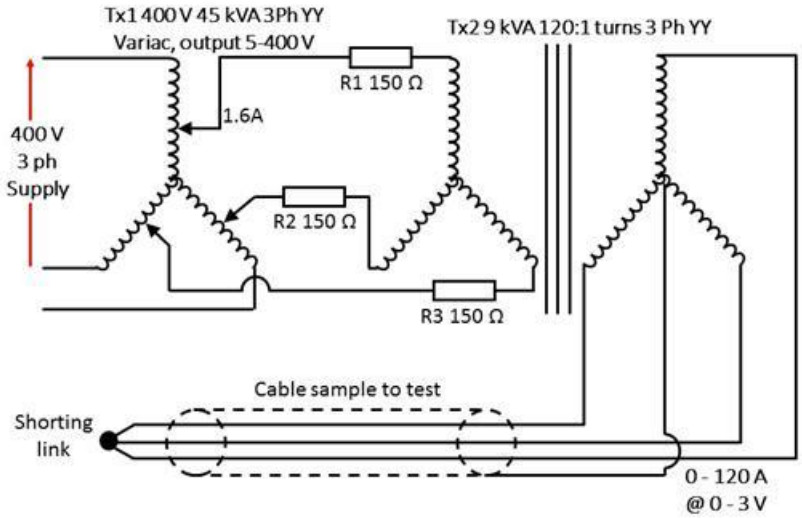

Figure 3: Simplified schematic of the test system used at Loughborough University. Note that earthing and protection is omitted in this drawing.

The following systems were used to validate current sensor measurements:

- Fluke 435 II Power Quality Analyser (PQA).
- Fluke i430 Flex-TF-II Rogowski Coil
- Teledyne Lecroy HDO6104 High Definition Oscilloscope
- CP0150 Current Probe

The Fluke 435 and i430 have been internally checked for accuracy, linearity and response to harmonics and reactive power with a calibrated Fluke 9100 multifunction calibrator.

The cables used in the test rig include a small selection of LV and HV cable types based on availability and can be used to represent some typical cable specifications found in secondary substations

The following cables (Figure 4-Figure 6 and Table 4-1) were used for testing in the Loughborough Test Rig.

Figure 4: single phase welding cable

Figure 5: 11kV 3-core Trefoil XLPE cable

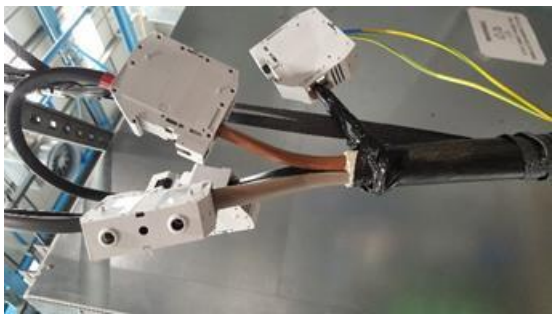

Figure 6: 11kV 3-core Waveform PVC cable

Table 4-1 : Cable types used in the testing

Type	Voltage rating [kV]	Conductor	Screen / Sheath	Cores	Cross sectional area [mm2]	Outside diameter [mm]
Waveform	11	Al	Al	3	95	33.5-35.3
Trefoil	11	Al	Al	3 (singles)	95	31-33*
Welder	0.4	Cu	Rubber	1	16	11.8

*Diameter given is of an individual core of the trefoil formation – outside diameter of the bundle is about 66.8mm

Loughborough have developed several measurement criteria to test against requirements. These were undertaken in the laboratory at Loughborough under controlled conditions which were then extended to substation facilities at Loughborough University under real world conditions.

The table below shows a summary of tests that were considered.

Table 4-2 : Key tests identified in scoping document

Test	
Range of values	Test for linearity between min and max expected values
	Test for measurement factors; saturation, impact of temperature, and other tests as determined appropriate
Accuracy	Test for accuracy, sensitivity and repeatability
Data Storage	Test for data capture and communication

Any measurement solution will also need to be scalable to deal with the whole Network. Data storage, analysis and monitoring will need to be considered in relation to this.

To get maximum demand (MD) indication, a power or current measurement is required directly or should be implied through indirect measurement. The number of measurements available will depend on the cost and methodology.

Note: the sensing circuit is not just the sensor but also includes components such as;

- Primary sensing element
- Excitation control/ power requirements
- Amplification
- Analogue filtering
- Data conversion
- Compensation
- Digital information processing
- Digital communication processing
- Communication

4.2 Testing summary table

The following steps were undertaken as part of the test process.

1) Design sensor system
2) Manufacture sensor system
3) Conduct detailed tests on the test rig
4) Modify design following 3
5) If Appropriate - Conduct tests on active 11:0.4kV substation
6) Document results & plan phase 2 of project

The results were then collated as part of a testing table shown below.

Table 4-3 : Testing table

	Sensor type										Platform type			
	Magnetometer Android Phone	Magnetometer chip	Hall Effect chip	l2m coil sensor	Accelerometer	Audio Microphone	Strain gauge	Thermal stickers	Thermal transducer	Low cost thermal imaging	Mobile phone	Arduino	Raspberry Pi	Sensor with IOIO board and phone
Cost	£18 phone	£14	£2	£13	£19	£9	£31	£4	£100	£350	£13 phone	£49	£37 dongle	£35 phone
Rough testing	✓	✓	✓	✓	✓	✓	✓	✓	✓	✓	✓	✓	✓	✓
Sensor value measured on scope/similar	✓	✓	⛔	✓	✓	✓	✓	✓	✓	✓	✓	✓	✓	✓
Sensor value related to load	✓	✓	⛔	✓	?	?	✓	✓	✓	×	✓	✓	✓	✓
Sensor value on platform	✓	✓	⛔		✓	×	×	✓	-	⛔	-	-	-	-
Rig testing	✓	✓	×	✓	×	×	✓	✓	✓	×	✓	✓	✓	✓
Linearity	✓	✓	×	✓	⛔	⛔	✓	?	?	⛔	✓	✓	✓	✓
Accuracy	✓	✓	×	✓	⛔	⛔	×	?	?	⛔	✓	✓	✓	✓
Saturation	✓	✓	⛔	✓	⛔	⛔	×	?	?	⛔	✓	✓	✓	✓
Other testing (as determined)	✓	✓	⛔	✓	⛔	⛔	×	?	?	⛔	✓	✓	✓	✓
Rig testing rerun	✓	✓	×	✓	×	×	×	×	×	×	✓	✓	✓	✓
Design improvement	✓	-	⛔	✓	⛔	⛔	⛔	⛔	⛔	⛔	✓	✓	✓	✓
Re-testing	✓	✓	⛔	✓	⛔	⛔	⛔	⛔	⛔	⛔	✓	✓	✓	✓
Data storage	-	-	-	-	-	-	-	-	-	-	✓	✓	✓	As per phone
locally	-	-	-	-	-	-	-	-	-	-	✓	✓	✓	-
server	-	-	-	-	-	-	-	-	-	-	✓	-	✓	-
1 days' worth	-	-	-	-	-	-	-	-	-	-	✓	-		-
Substation testing	✓	✓	×	✓	✓	✓	×	×	✓	×	✓	✓	✓	⛔
Correlation	✓	✓	⛔	✓	?	?	⛔	?	?	⛔	✓	✓	✓	-
Recommend for Field Trial	✓	✓	×	✓	?	?	×	?	?	×	✓	?	✓	?

✓ tested ok
× test failed
⛔ decision not to proceed with testing
? inconclusive result
- not applicable

4.3 Testing in a live substation

Tests were conducted at Holywell Building substation 8. This substation is convenient because it is close to the laboratory and the University Wi-Fi Network may be used. However, the building has recently been emptied and there is a low load on the substation. This makes it difficult to get very accurate results. In particular the current on the 11kV side of the transformer was calculated to be approximately 3A.

The cables in the substation are SWA XLPE cables as shown in Table 4-4. There was access to the 11kV cable in two places as shown in Figure 7. Access to the LV cables is straightforward – but there are a number of feeders leaving the transformer and to calculate the total loading accurately on the 11kV cable can't be accurately done using conventional measurements with the equipment available at Loughborough. This was therefore approximated by using a fluke to measure the red phase current on each LV feeder and then assuming the currents are balanced – add these together to determine the total current. Multiply this by the 433V (rating of the transformer) and √3 to get the approximate LV VA and then assuming that this VA is supplied by the primary and the transformer is lossless and dividing by √3 x 11kV to get an estimate of the primary current.

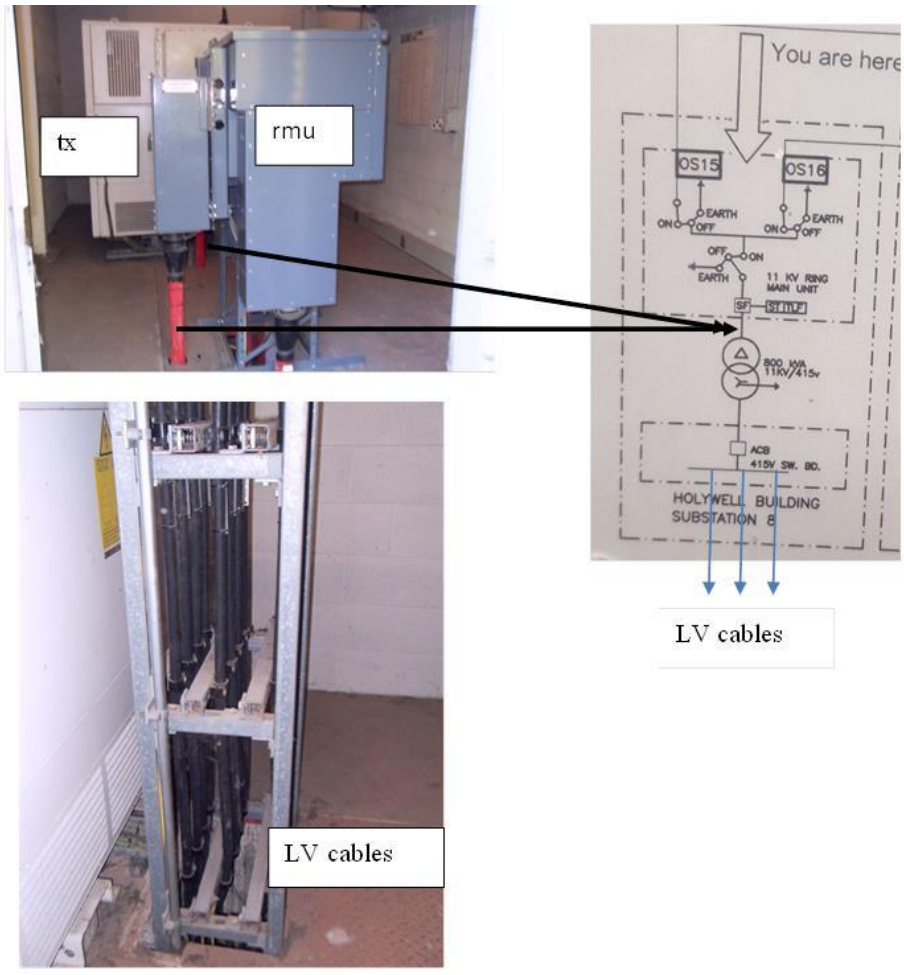

Figure 7: Substation, Holywell Building, Substation 8, schematic and photo

Table 4-4 : Cable types in the substation testing

Type	Voltage rating [kV]	Conductor	Screen / Sheath	Cores	Cross sectional area [mm2]	Outside diameter [mm]
XLPE	11	Cu	SWA	3	185	75
XLPE	0.4	Cu	SWA	1	185	27.14

Another issue with the substation is that the transformer was not directly available as this had been enclosed in a stainless steel covering. This impacted efforts to measure the noise, vibration and temperature of the transformer as there was a gap between housing and transformer.

5 Sensor A: MEMS Magnetometer

5.1 Theory

A magnetometer measures magnetic field in three directions (x,y and z). Typically these are in μT. The relationship between current and magnetic field comes from Amperes law. The magnetic flux density B (T) at a distance r (m) from the centre of a conductor can be calculated from Equation 5-1.

$$B = \frac{\mu I}{2\pi r} \qquad \text{Equation 5-1}$$

Where I is the current in the conductor (A) and $\mu = \mu_r \mu_o$ is the magnetic permeability (H/m).

The current is continually changing as a sine wave and therefore the measurement can be taken at any point in the sine wave. This forces the data to go through a post processing phase in order to capture a set of meaningful results. An additional issue with this data is that the sample rate of the controllers under test are not high enough to avoid aliasing issues. These can occur when the data is not sampled at a sufficient rate to be able to reconstruct the original signal as shown in Figure 8.

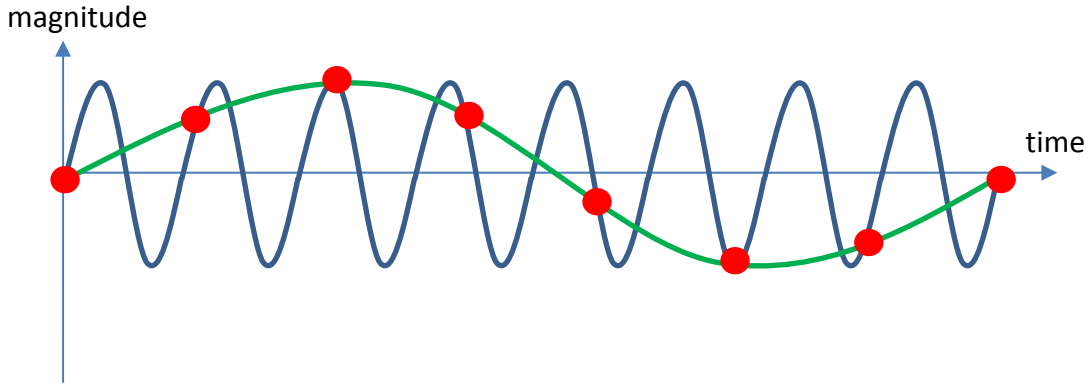

Figure 8: an example of aliasing showing two possible solutions to one set of data

In applications looking at load current this can be a problem if the peak of the sine wave is not reached as it then becomes difficult to accurately determine the rms of the values from a single set of data. Fortunately the magnetic field has more than one component. This can be used to help identify the peaks in the wave form by using elliptical theory.

Aligning the sensor vertically with the "y" axis pointing up the cable results in two components of magnetic field B_x and B_z. On a single core cable if the B_x could be perfectly aligned with the radial direction then this would be the only measured value. However, in reality a small component of field is present in the z axis. Plotting the B_x component against

the B_z component traces out an ellipse which may be offset (for example by the Earth's magnetic field) as shown in Figure 9. If the magnetic field due to the current can be measured then the current can be back calculated. The magnetic flux density related to the presence of a single core cables can consider only a single current assuming no other cables are close by. However, the field produced by multi-core cables needs to consider the impact of the current in all the phases on the flux density. The solution is to use Principle component analysis.

Suppose we have a large number N of magnetic field readings $B = (B_x, B_y)$,, and it is observed that they lie approximately on an ellipse similar to below:

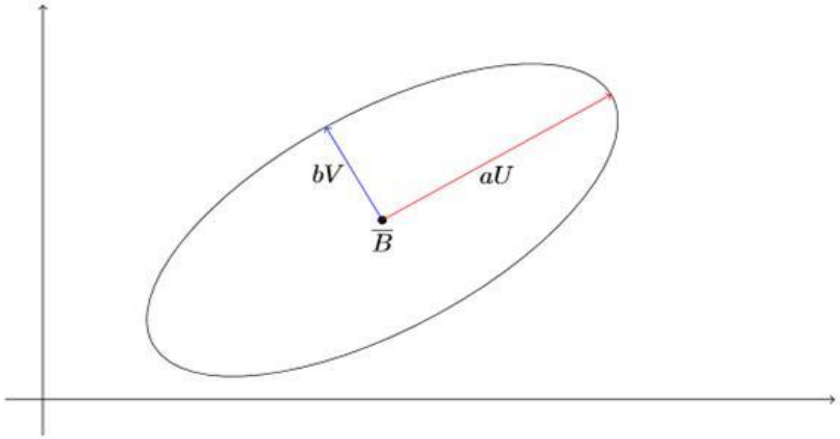

Figure 9: Magnetic field measurements

The center of the ellipse is $\bar{B}$. The longer radius (shown in red) has length a, in the direction of the unit vector U. The shorter radius (shown in blue) has length b, in the direction of the unit vector V. The relationship between the vectors and the measurements can be explained using Principal Component Analysis as follows.

Firstly, the vector $\bar{B}$ is just the average of the readings: $\overline{B} = \frac{1}{N}\sum B$.

For each reading $B = (B_x, B_y)$, consider the corresponding centered reading:

$$C = (C_x, C_z) = (B_x - \overline{B_x}, B_z - \overline{B_z}) \qquad \text{Equation 5-2}$$

In the form of the resulting matrix:

$$M = \begin{bmatrix} C_x^2 & C_x C_z \\ C_x C_z & C_z^2 \end{bmatrix} \qquad \text{Equation 5-3}$$

The average of these matrices is taken as $\overline{M} = \frac{1}{N}\sum M$. This will always be symmetric, so it has the form:

$$\bar{M} = \begin{bmatrix} P & Q \\ Q & R \end{bmatrix}$$ Equation 5-4

for some P, Q, R.
Putting $S = \sqrt{(P-R)^2+4Q^2}$. The lengths of the two elipse radii a and b are

$$a = \sqrt{P + R + S}$$ Equation 5-5

And

$$b = \sqrt{P + R - S}$$ Equation 5-6

The unit vectors U and V can be found as

$$U = (2Q, R - P + S) / \sqrt{4Q^2 + (R - P + S)^2}$$ Equation 5-7

$$V = (2Q, R - P - S) / \sqrt{4Q^2 + (R - P - S)^2}$$ Equation 5-8

Alternatively, U and V are the eigenvectors of $\bar{M}$, with eigenvalues $a^2/2$ and $b^2/2$. It is also useful to consider the matrix

$$T = \begin{bmatrix} U_x/a & U_z/a \\ V_x/b & V_z/b \end{bmatrix}$$ Equation 5-9

For each centered reading C, the vector TC should lie on the unit circle, so we should have $|TC| = 1$. In practice the original readings will not lie exactly on an ellipse so $|TC|$ will not be exactly equal to 1.

As the data is a continuous stream and the sampling period of the phone is asynchronous it is necessary to consider how the data is analysed and reported back to the user. In this project a faded average or exponential moving average (EMA) method was implemented as follows.

Consider a set of readings $x_1, x_2, x_3 \ldots\ldots x_n$
The average of these readings is $\bar{x} = \frac{1}{n}(x_1 + x_2 + x_3, \ldots\ldots x_n)$
The EMA is defined as

$$\overline{x_{exp}} = \frac{x_n + \theta x_{n-1} + \theta^2 x_{n-2} + \cdots}{1 + \theta + \theta^2 + \cdots}$$ Equation 5-10

For some $\theta = e^{-\tau}$ where τ is small and positive so $\theta \approx 1$ and equal to $\delta t/k$ where δt is the change in time and k a constant.
Adding a new reading x_{n+1} the new exponential moving average becomes

$$\overline{x_{exp,new}} = \theta \overline{x_{exp,old}} + (1 - \theta) x_{n+1}$$ Equation 5-11

This equation is computationally efficient, since it doesn't require a set or previous measurements to be stored in memory only the most recent raw measurement and the EMA calculated for the previous measurement.

Once the magnetic flux density is determined then the peak load current can be calculated. This is straightforward for a single core cable as

$$\hat{I} = \frac{2\pi r \hat{B}}{\mu}$$ Equation 5-12

Where $\hat{B}$ is the equivalent to "a" in Equation 5-5.

The measurement distance r, is taken as the estimated distance of the sensor location to the center of the conductor. This therefore varies with each installation as cable diameter changes depending on the substation design. This is also dependent on the location of the sensor and whether or not it is in a phone. If it is contained in the phone then this also changes with phone type.

In a 3 core cable this calculation is more complex. Consider a sectored 3 core cable as shown in Figure 10. The most straightforward case is when the sensor is aligned to the same axis as one of the conductors, in this case the red phase.

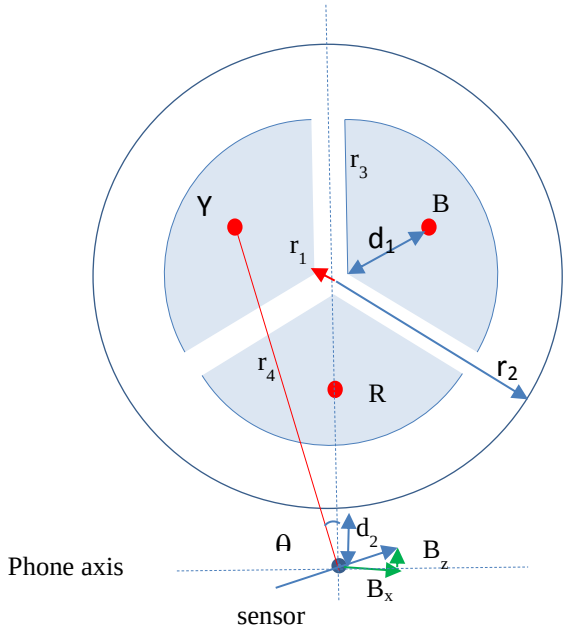

Figure 10: Pictorial representation of a 3 core sectored cable with the sensor location shown.

In this approximation, if it is assumed that each sector has a half angle α of 60°, then a 95mm^2 cable can be represented by a sector of radius r_3 of 9.5mm. The distance from the centre of the sector to the centroid of the sector, d_1, can be found from

$$d_1 = \frac{2r_3 \sin(\alpha)}{3\alpha}$$ Equation 5-13

The field at the sensor due to the current in conductor R can be assumed to be in the x direction only and can be calculated from:

$$B_x = \frac{\mu_o \hat{I} sin(\omega t)}{2\pi(d_2 + r_2 - d_1 - r_1)} = \frac{\mu_o \hat{I} sin(\omega t)}{2\pi d_3}$$ Equation 5-14

The distance from the centre of conductor Y and B to the sensor is then found from

$$r_4 = \sqrt{(r_2 + d_2)^2 + (r_1 + d_1)^2 + (r_2 + d_2)(r_1 + d_1)}$$ Equation 5-15

The magnetic flux density at the sensor due to the current in conductor Y, $I_Y = \hat{I}\sin(\omega t - 120^o)$ is given by Equation 5-16 and Equation 5-17.

$$B_x = \frac{\mu_o \hat{I} sin(\omega t - 2\pi/3)\cos(\theta)}{2\pi r_4}$$ Equation 5-16

$$B_z = -\frac{\mu_o \hat{I} sin(\omega t - 2\pi/3)\sin(\theta)}{2\pi r_4}$$ Equation 5-17

Where $\sin(\theta) = \frac{\sqrt{3}(d_1 + r_1)}{2r_4}$.

A similar equation for the field at the sensor due to the current in the B conductor can also be calculated If it is assumed that the currents in all three phases are balanced then the peak flux density can be related back to the peak current through Equation 5-18.

$$\hat{I} = \frac{2\pi \hat{B}}{g_f \mu_o}$$ Equation 5-18

Where g_f is a geometric factor relating to the back calculation and is equal to:

$$g_f = \frac{1}{d_3} - \frac{\cos(\theta)}{r_4}$$ Equation 5-19

In the event that the sensor doesn't directly align with the conductor this doesn't have too much of an impact on the calculation of current as the field at any point on the cable has a similar magnitude but is offset in phase and therefore the current magnitude can still be estimated. A similar analysis can be undertaken for cylindrical conductors (as per the 11kV substation cable).

As an aside –Figure 11 shows the traditional calculation of RMS (taking the square root of the mean squared) of the x-axis field. The changes in the magnitude are not really happening in the data as elliptical curves of the raw data do not show an amplitude change – that would have been visible on the scatter graph as a reduction in ellipse dimensions.

More intense averaging can iron out the RMS calculated offset but at the cost of a slower delay period and reduced clarity on current change boundaries as shown in Figure 12.

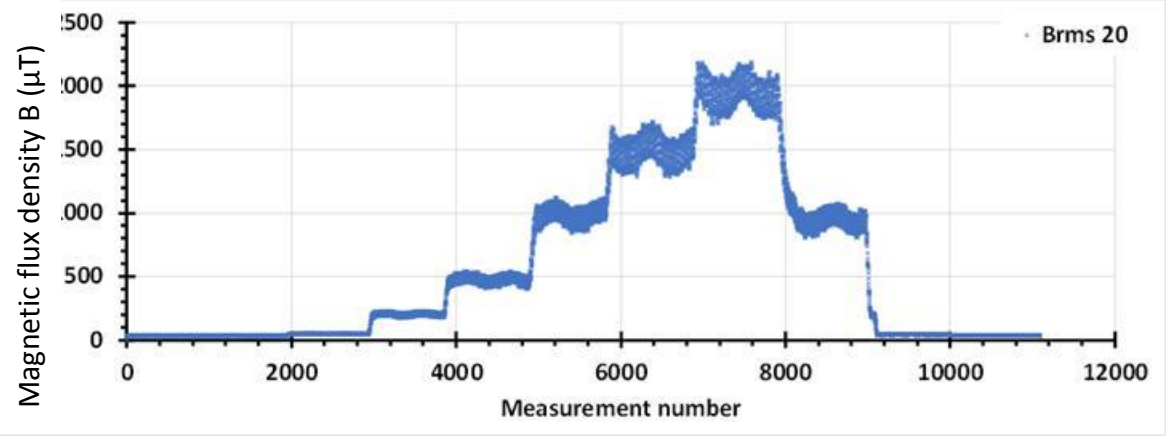

Figure 11 : RMS magnetic field based on RMS over 20 points

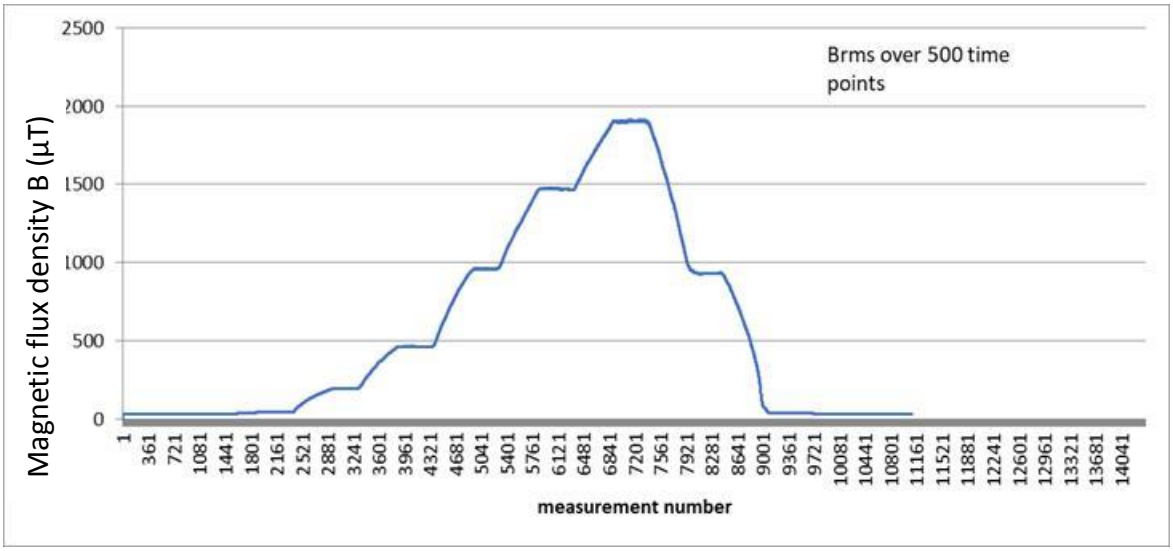

Figure 12 : RMS magnetic field based on RMS over 500 points

LP 2	Low cost control platforms for logging data operate at a time span that is comparable to the frequency of the supply. Care is therefore needed to deal with aliasing and post data processing. In particular, it is recommended that traditional calculation of RMS is not used on fast changing signals such as magnetic field..

An alternative method shown below relies on taking the peak measured value over 100 points (square root of Bx a squared and Bz squared) and then dividing by root 2. This is fine while there are not issues with data corruption.

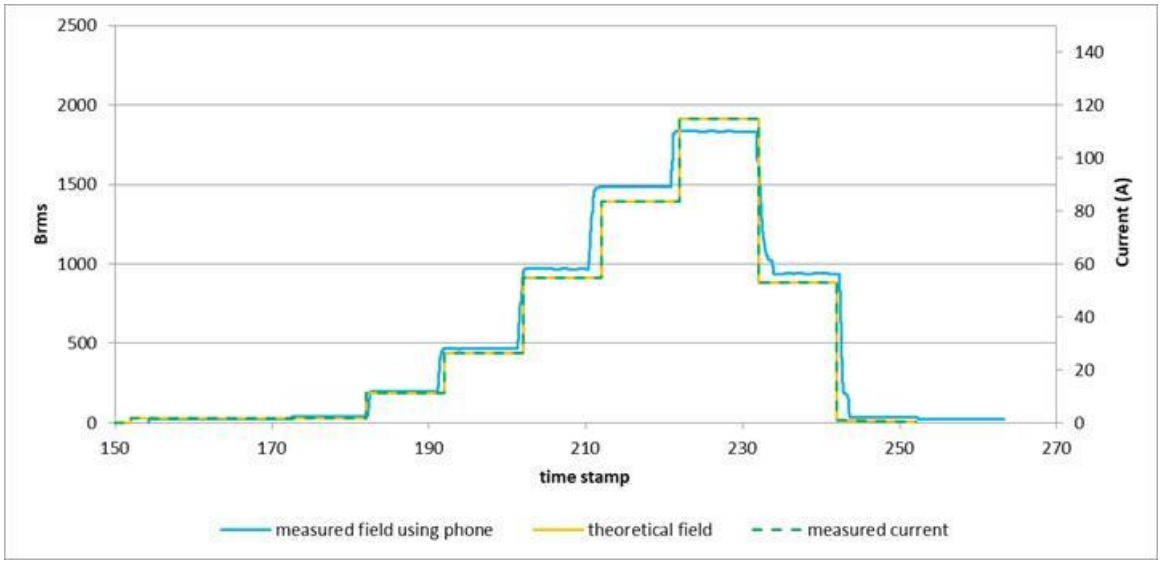

Figure 13 : RMS magnetic field based on RMS over 20 points

LP 3	Good RMS values can be obtained from looking for the peak values over a fixed time span (eg 1 second) and dividing by the square root of 2 if the data isn't corrupted. However this isn't guaranteed.

Due to the fact that a good RMS value is not guaranteed by calculation from the peak due to the impact of spurious signals, a more robust approach is suggested.

LP 4	Using an exponential moving average method with principle component analysis (calculating the "a" dimension of the magnetic field when plotted as an elliptical curve) is the most suitable method for removing the impact of aliasing and also ensuring that spurious data points do not disrupt the information while getting clean boundary changes when the current changes.

5.2 Hardware

There are many different magnetometer sensors. These are typically supplied in very small packages and come under the category of micro electro mechanical systems (MEMS) sensors. MEMS magnetometers generally measure the Lorentz force on a current carrying conductor rather than the hall effect. These can be challenging to solder onto circuit boards without automated soldering machines, however most MEMS sensors are available on prototyping or development PCBs with essential outboard components included. MEMS sensors are usually designed to communicate with a microcontroller or processor using the I^2C bus, which is used by the Arduino, Raspberry Pi and internally within smartphones. Therefore, one of these prototyping systems is a logical platform with which to test MEMS sensors.

Android smartphones often have separate magnetometers and accelerometer chips, whereas development boards aimed at the electronics market sometimes use combined magnetometer, accelerometer and gyroscope chips. These devices are described as 9-axis, since they measure the 3 parameters in X, Y and Z axes. A comparison of commonly used devices in smartphones and development boards is shown in Table 5-1.

A magnetometer will be tested as part of the Android phone testing (see Section 12) but also as an independent device with serial data connection to a controller.

Table 5-1 : Comparison of magnetometer chips in common use.

Sensor	Range	Sensitivity	Sample rate (max)	Application
Freescale MAG3110	+/-1000µT	0.1uT	80Hz	Prototype PCBs
Yamaha YAS537	2000µT	0.3uT	626Hz	Samsung S6 /S7
AKM AK8963	5000µT	0.15µT/LSB		LG Nexus 5
ST LSM9DS0	+/-12G = 120µT	0.48mGauss/LSB	400 kHz	Adafruit dev board
Bosch 3060102 MM150	+/- 1.3 (X,Y) +/-2.5 (Z) G	0.3uT	100Hz	Sony Xperia M4 Aqua E2303
AKM AK09911	4900µT	0.6uT	5Hz	OnePlus 5
TDK Invensense MPU 9250	4800µT	15µT/LSB	100Hz	Sparkfun dev board

Note: 1 Tesla = 10,000Gauss

This section will look at the independent device – two such devices have been chosen; the ST Microelectronics LSM9DSO device and the TDK Invensense MPU9250. As the magnetometer is a surface mount component it makes sense to trial this using a pre-fabricated development board. The development board then links into a hardware platform. In this instance an Arduino compatible controller as shown in Figure 14. The cost of the sensor and controller is shown below. The controller is shown in grey and listed as a LinkitOne Arduino compatible device, but this may be substituted later for any other such device. The LinkitOne is used because it incorporates communication by WIFI and GPRS.

Table 5-2 : Cost of sensor A hardware

	Vendor	Part	Qty	Unit cost	Line cost
Option A	RS	LSM9DSO magnetometer Dev PCB	1	£14.78	£14.78
Option B	Pimoroni	SparkFun IMU MPU-9250	1	11.67	£11.67
	Rapid	LinkitOne PCB (Arduino compatible)	1	£44.24	£44.24
	Amazon	Power supply	1	£4.99	£4.99
				System Total	£60.90

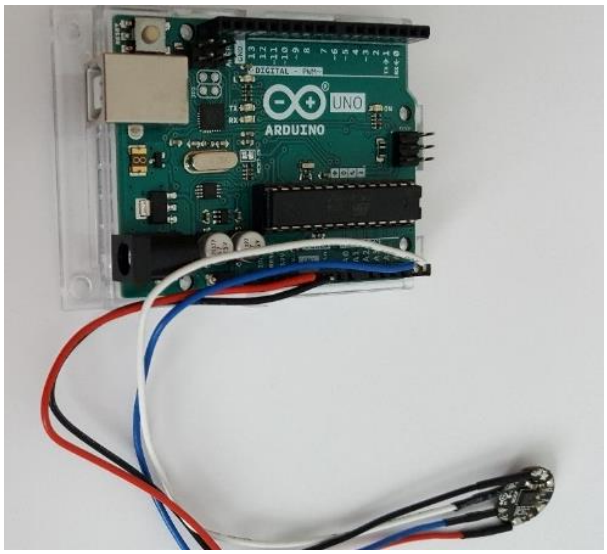

Figure 14: Photo of Arduino Uno with LSM9DSO magnetometer circuit

The magnetometer has two power pins (+3.3V and GND) and two I^2C pins (SCL and SDA) for communication. This is common across the digital MEMS sensors that were tested in this project. I^2C is only compatible with 3V logic signals. Pins A4 and A5 on many Arduino boards can be setup for I^2C or analogue connection. The circuit diagram is shown below.

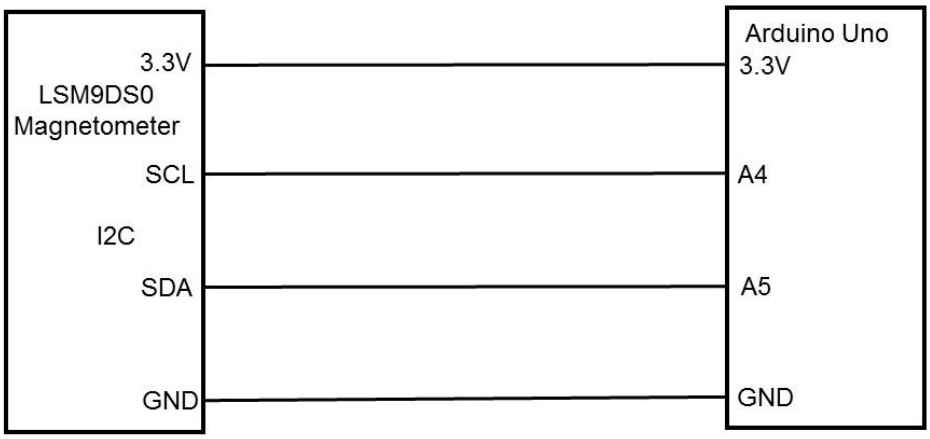

Figure 15: Circuit diagram of Arduino Uno and magnetometer

LP 5	Pre-fabricated MEMs sensor development boards help reduced time scales to development and are set up to easily interface through common platforms. These may also come with libraries which speed development on the coding.

5.3 Rig testing

5.3.1 LSM9DSO chip

The magnetometer PCBs were fixed to the 1-core waveform cable as shown in Figure 16.

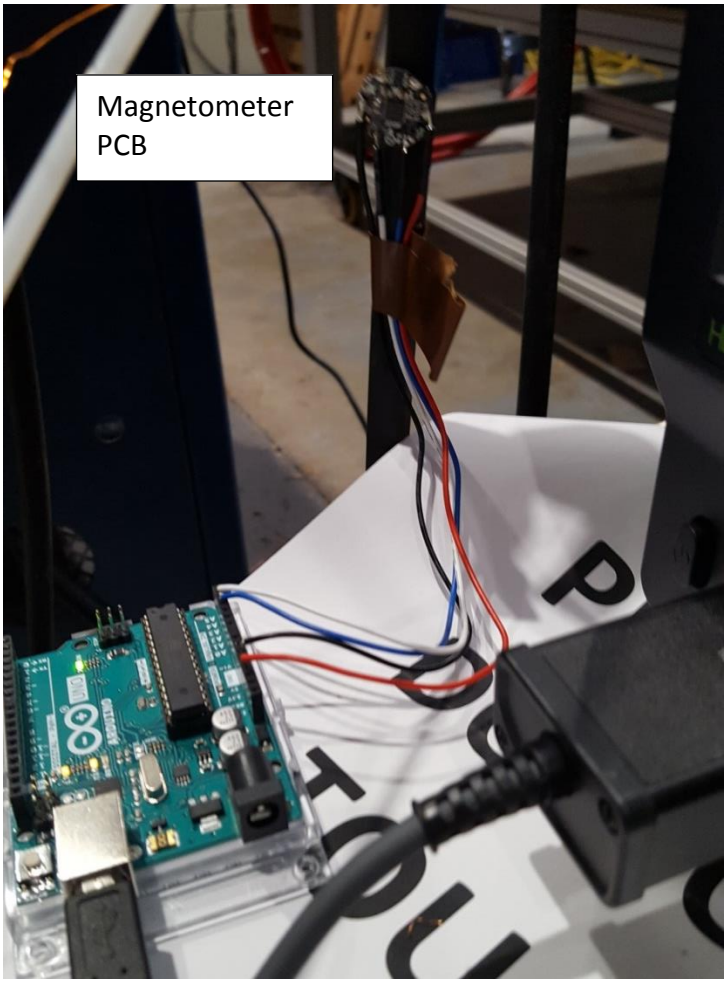

Figure 16: Photograph of the LSM9DSO magnetometer fixed to a single core 16mm^2 rubber sheathed welder cable

TT 1	Align the measurement devices such that the y axis is vertical against the cable. This then removes the need to monitor 3-axis so only 2-axis measurement is required.

The current in the test rig was taken to its highest value and then stepped back down to zero to look at the variation of recorded field against current as shown in Figure 17. The figure shows the x-axis field saturates at the highest value and doesn't change with time whereas the z axis field reduces in line with the reduction in current. The y axis field is showing signs of unexplained spurious behaviour. Another important oversite from this figure is the "apparent" changes in frequency of the Bx wave shown by the line space varying which is less visible in the Bz field. This is due to measurement aliasing issues.

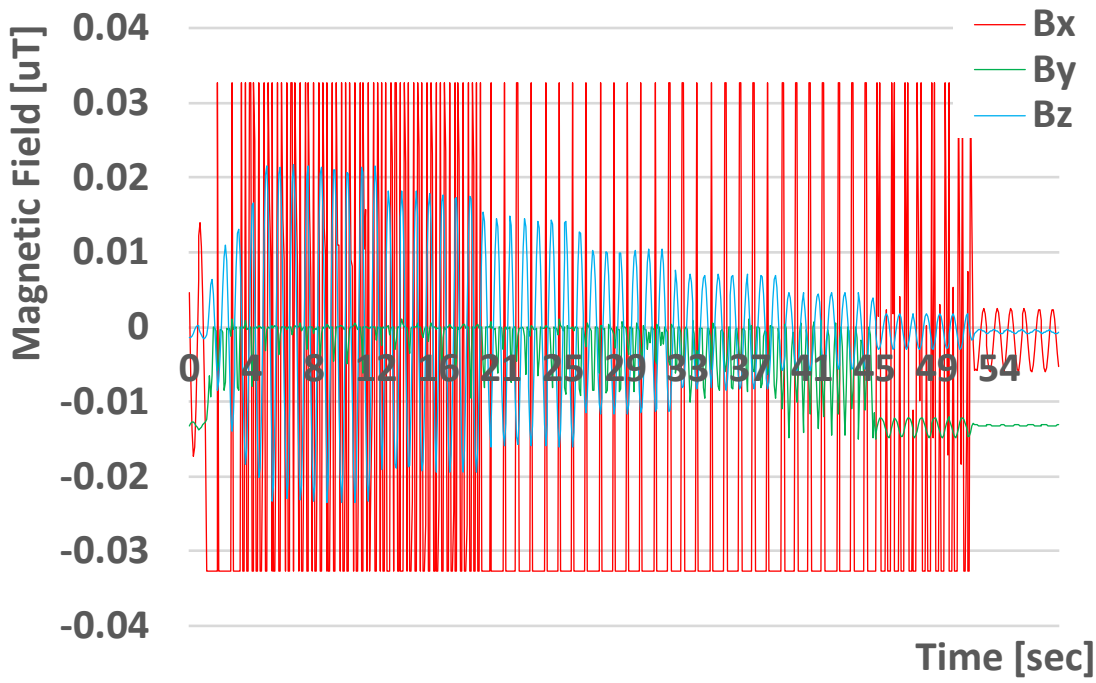

Figure 17: Testing of the LSM9DS0 magnetometer with current ramped up from zero to 100A then back down to zero

TT 2	In the first instance the raw data should be monitored so that specific sensor idiosyncrasies e.g. auto calibration can be identified

One of the best ways to make sense of the data is to plot the x-axis values against the z-axis values. This largely takes away the issues of the aliasing over longer time periods. In addition the offset of any other remnant field can be removed in the processing.

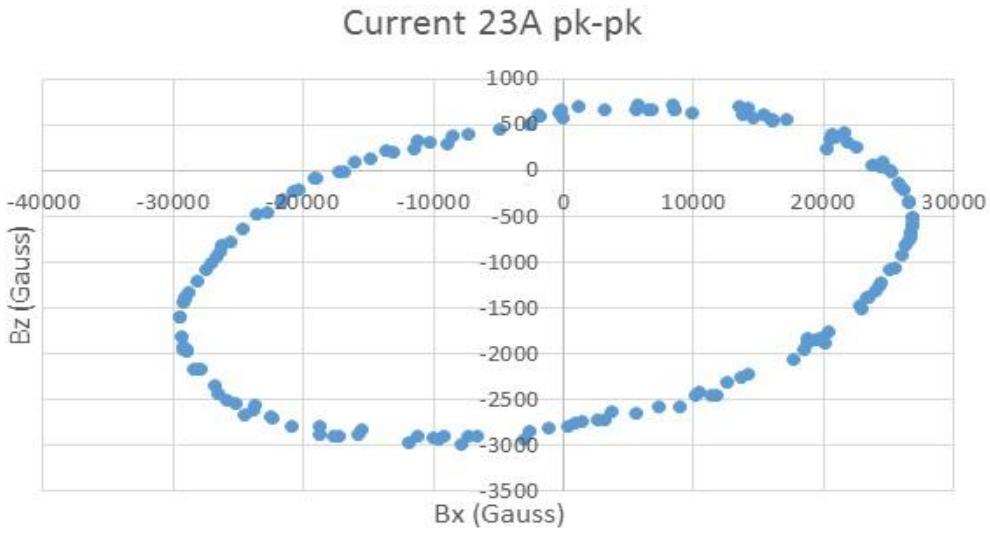

Figure 18: LSM9DSO plotted raw data (magnetic field in x and z directions for a low current)

At a higher current the x axes measurement value saturates, and it is not possible to see the elliptical shape as shown in Figure 19. However, there is no saturation in the z direction and Figure 20 shows that a linear relationship between current and detected field is present. It would be much harder to deduce the load current and this has not been attempted because the reported values of Gauss are way out from what is expected for this chip.

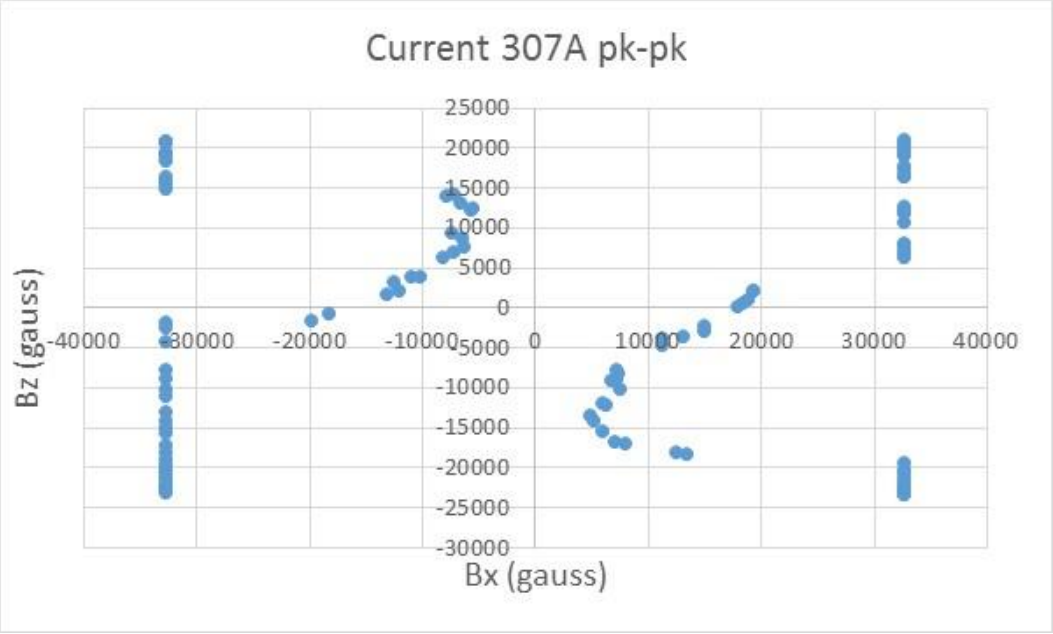

Figure 19: LSM9DSO plotted raw data (magnetic field in x and z directions for a higher current

TT 3	The Arduino Uno uses an 8-bit chipset but can handle 16-bit integer numbers (-32,768 to 32,767). Also, the Arduino is inefficient with floating point numbers, therefore measurement values must be carefully scaled to fit within the 16-bit range with optimal resolution.

TT 4	The measurement of the LSM9DS0 chip outputs measurements in Gauss – the equivalent in µT is much lower than many other sensors on the market. This would explain why it saturates at higher current.

TT 5	The sensitivity of the LSM9DS0 chip can be set in code between 2 and 12 Gauss. However, adjusting these settings had no impact on the clipping observed.

TT 6	The reported value of Gauss for the LSM9DS0 does not align with the chip's rated range so it is suspected that the scaling is dubious in the open source code.

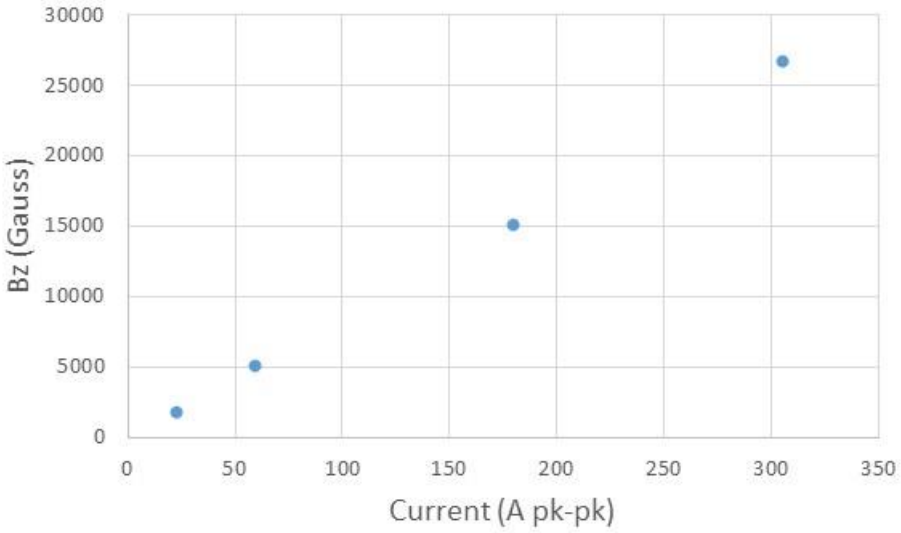

Figure 20: LSM9DSO plotting magnetic field Bz against conductor current

LP 6	A magnetometer detects magnetic field on three axes. Saturation on one sensor vector doesn't impact any of the other sensor axes and it's still possible to obtain meaningful relationships between load current and magnetic field – even if not all the chip's sensor axes are used.

LP 7	However, saturation of sensor output even on one axis of a magnetometer compromises the ability to accurately check measurements against theory using principle component analysis as this relies on a two-axis measurement. Determining the field from the peak value of field in any one direction is still possible.

5.3.2 MPU9250 chip

An alternative chip with the same interface signals was also tested. This is shown in Figure 21 connected to the single core cable. A plot of the Bx field against the Bz field in Figure 22 shows that there is no saturation effects at the highest current from the test rig. Figure 23 shows a plot of the measured field against current against the theoretical values. The magnetic field is related to current in a linear manner and the theoretical and experimental data align with reasonable accuracy.

On the strength of this data the magnetometer was taken forward for substation testing on one of the single core 400V feeder cables.

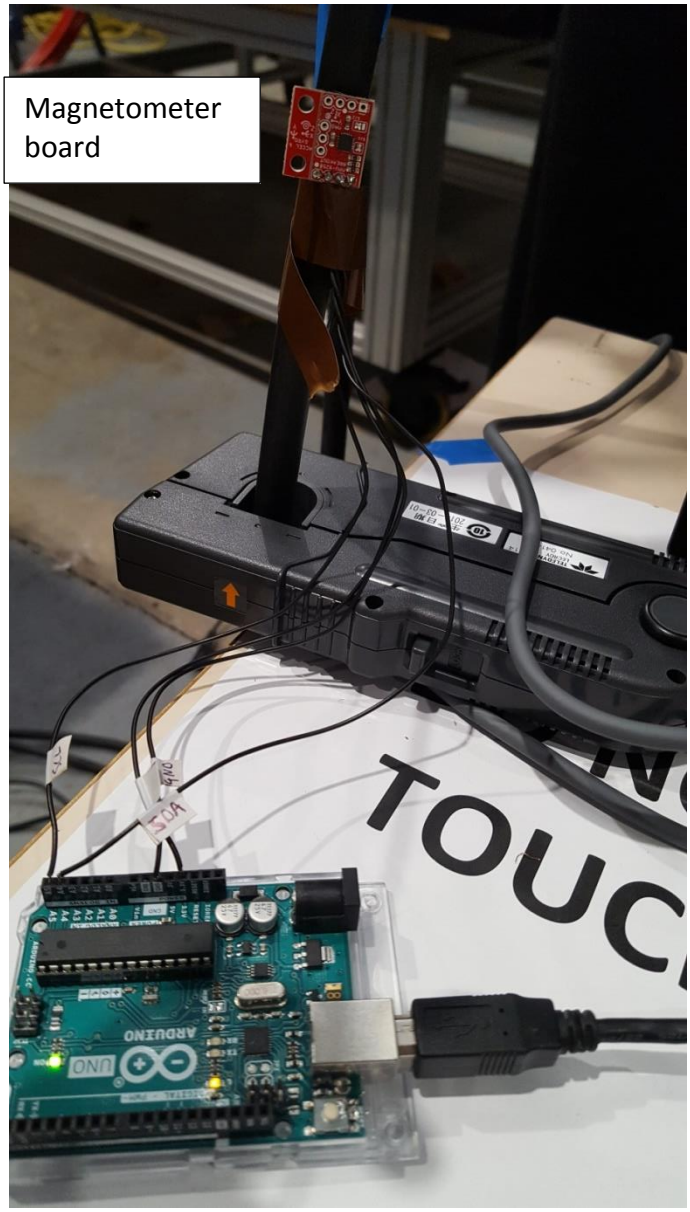

Figure 21: Photo of MPU9250 magnetometer connected to the test rig

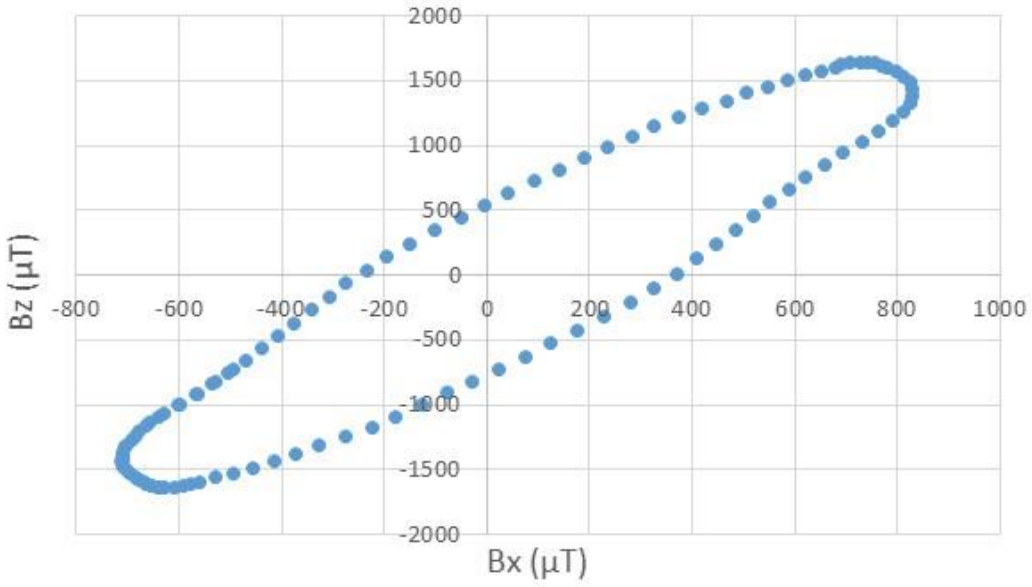

Figure 22: Raw data plotted from MPU9250 (magnetic field in x and z directions for a current of 308A pk-pk)

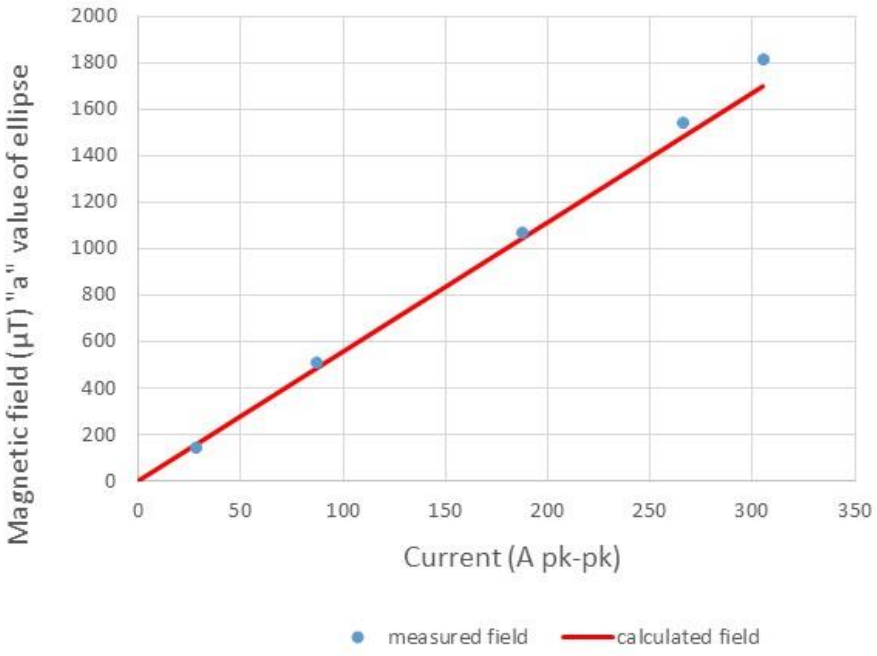

Figure 23: MPU9250 current (peak-peak) [A] against peak magnetic field (“a” of ellipse)

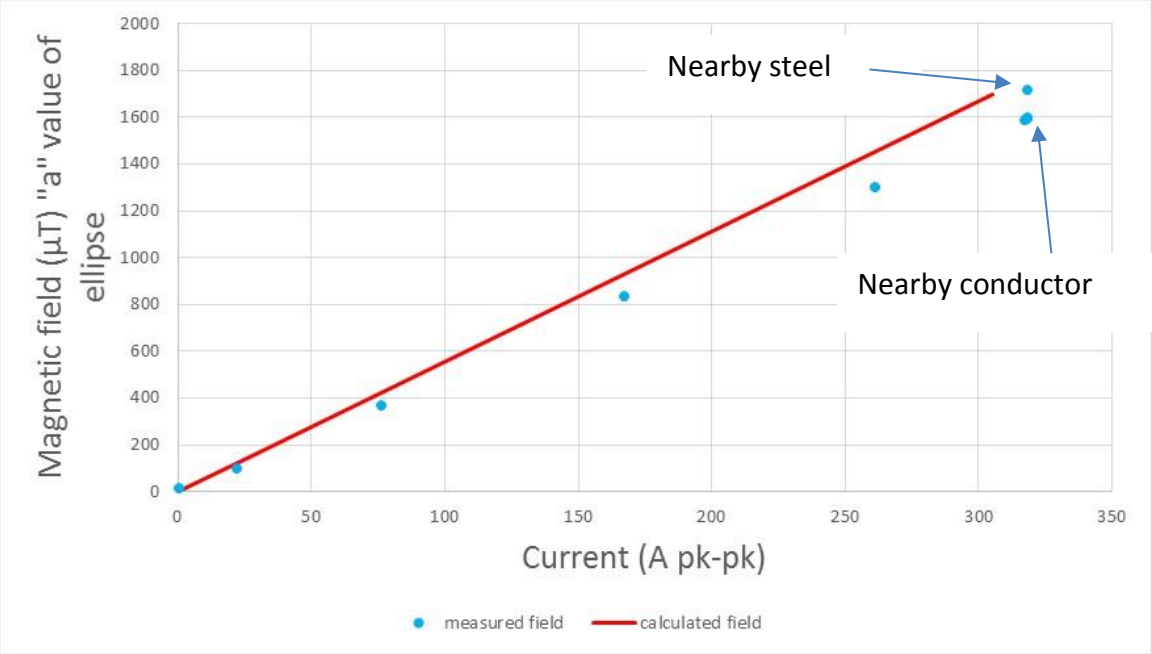

Figure 24: Repeat test MPU9250 current (peak-peak) [A] against peak magnetic field ("a" of ellipse)

LP 8	Not all magnetometers are equally useful for measuring field. Careful selection is needed to get a magnetometer fit for purpose.

LP 9	The magnetometer field appeared to increase slightly with temperature. This is in keeping with previously published work. In this application the impact is minimal.

This magnetometer was also tried on the three core trefoil cable as shown in Figure 25

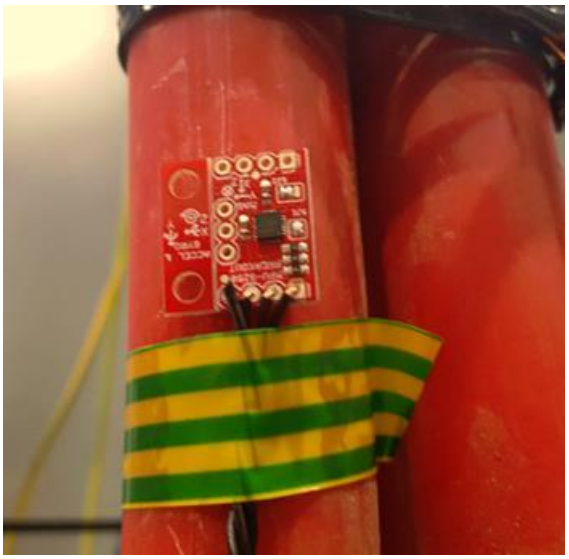

Figure 25: MPU9250 sensor on the trefoil cable

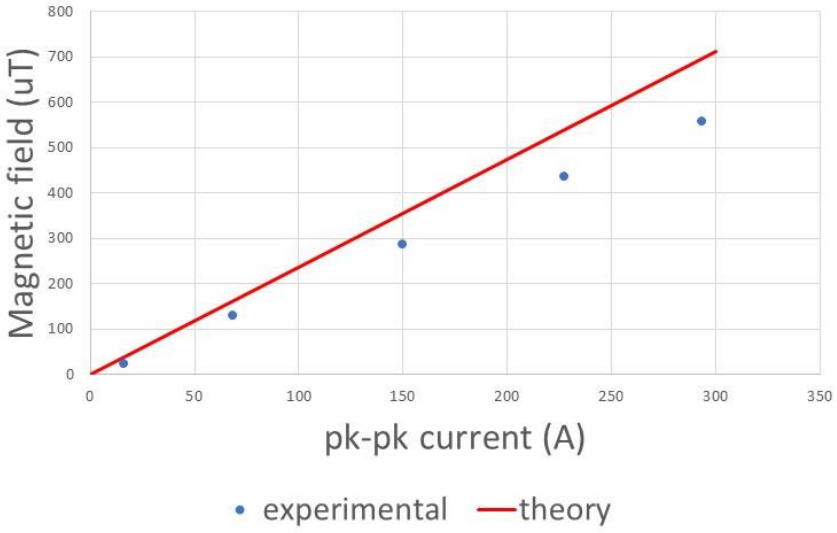

Figure 26: MPU9250 sensor experimental data vs theory

Further work is needed to look into the theory behind the magnetometer calculation on a trefoil cable to allow the accuracy to be assured. However, the correlation looks good.

5.4 Substation testing

The MPU9250 development board was taped to one of the single phase feeders which was also monitored with a Rogowski coil connected to a Fluke power quality meter set to 10s measuring interval as shown in Figure 27.

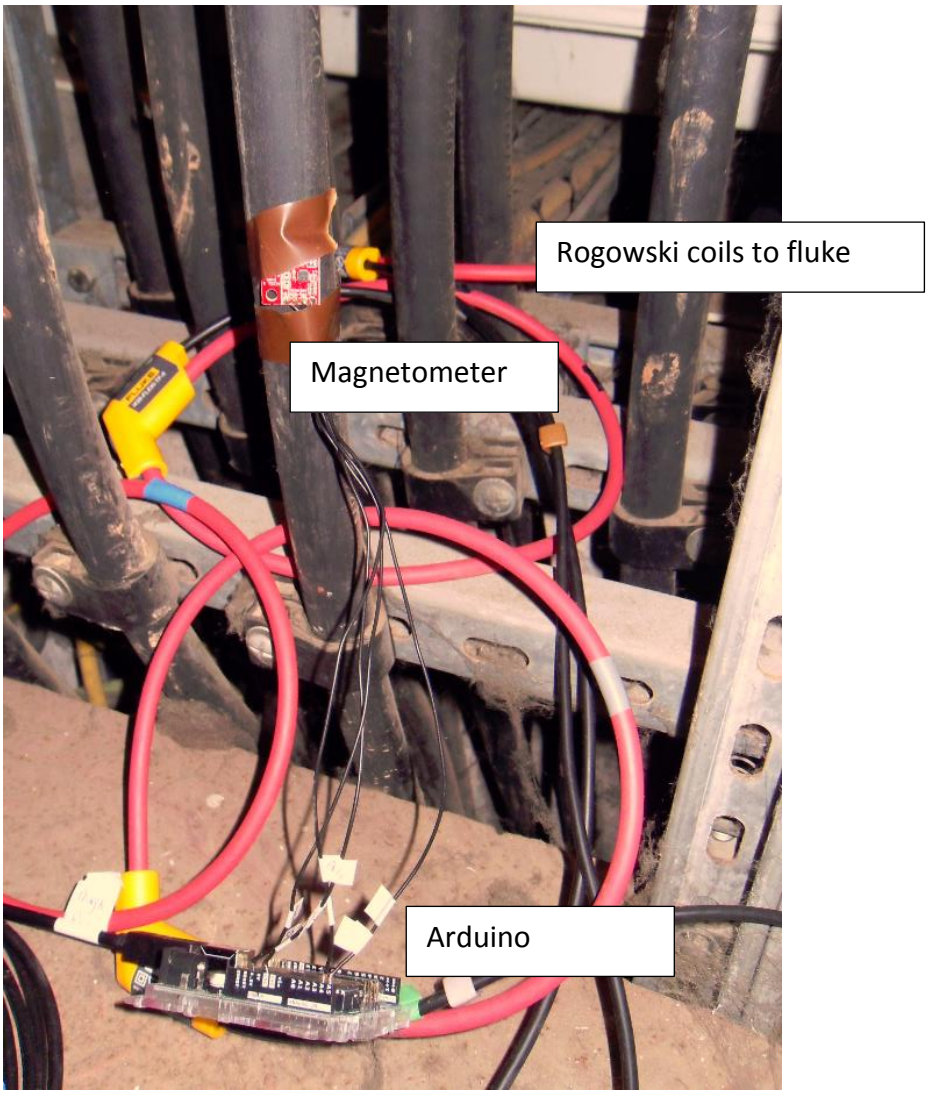

Figure 27: MPU9250 and Fluke in situ

A plot of the raw reported data in the x and z-axis against time is shown in Figure 28. It appears that there is some harmonics on the system which are even more apparent when the x-axis and z- axis fields are plotted against each other in Figure 29. This 7th harmonic component has also been picked up in other tests later in this report.

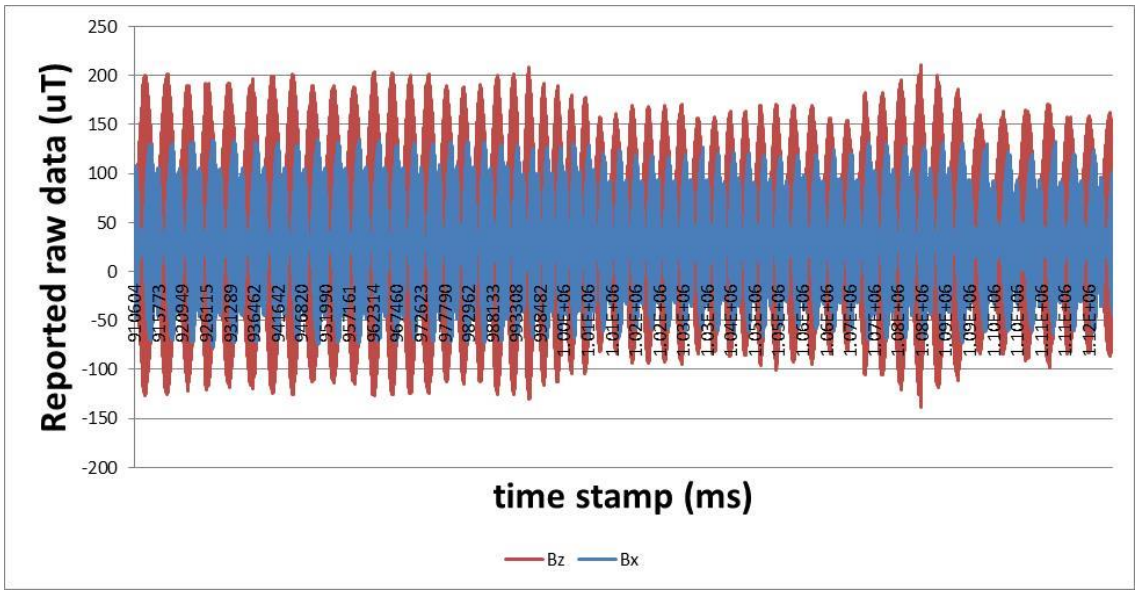

Figure 28: MPU9250 raw field data against time

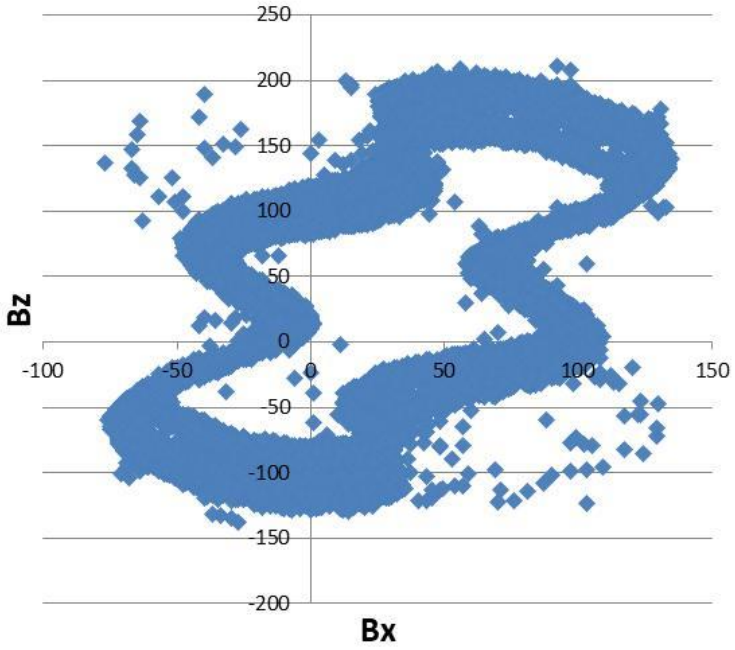

Figure 29: MPU9250 x-field against z-field

The processing of the data appears to work reasonably well and a plot of the ellipse “a” value reported by the Arduino against time compared to the reported current from the fluke shows good correlation over the test period as shown in Figure 30. However, the accuracy between the calculated current (rms) and reported current doesn’t tie up too well at these lower values. It is not clear why there is this discrepancy, but this may be due to the accuracy level at low currents as this point ties up with the lowest current that could be tested on the test rig. Testing later with a magnetometer in a phone shows much better accuracy.

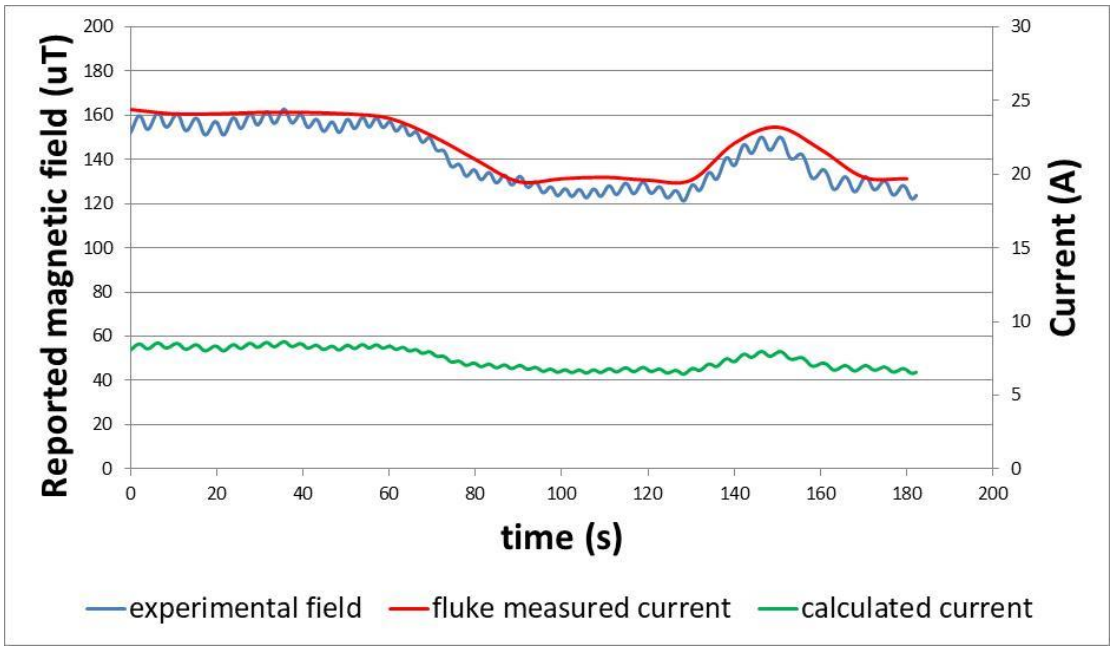

Figure 30: MPU9250 field against time and Fluke reading against time

LP 10	MEMs magnetometers are able to measure fields which can track the loading on a cable.

LP 11	Installing the MEMs magnetometers at a substation took less than 5 minutes – attach the device to the cable and provide power to the platform unit. Further work is needed on packaging this solution to give it an appropriate IP rating and allow the connectors to be better developed.

LP 12	The cost of the MEM's magnetometer is such that more than one may be applied to different cables (limited by the IO of the platform) and these may be daisy chained on the I^2C bus. The theoretical limit is 127 but this is lower in practice.

LP 13	It could be possible to pick up some harmonic content within the system, but the maths needs to be further developed. This is also limited by the processor of the platform device.

5.5 Summary

A magnetometer is a promising candidate for long scale testing.

	Comment
Functionality	Can be used • To provide single phase or three phase magnetic field measurements which can be used to back-calculate the load current (assuming balanced if 3 phase) • In time scales of 10ms upwards (limited by serial link to hardware)
Failure mode	Fail dead
Stability/reliability	No issues on test
Ease of deployment	Needs packaging and linking to hardware platform
Calibration	No obvious calibration needed – but substation calculation would need checking at higher currents

Test	Comments
Linearity	Linear up to saturation
Effect of adjacent steel work	Net field remains similar to that measured without steel due to calculation technique but raw data changes
Effect of adjacent conductors	<10cm away some impact. Very close nearby cables (touching) in this instance in a different phase reduces the field and therefore the measurement – would need appropriate calculation
Effect of temperature	Small impact
Accuracy	Better than 7.5% on the rig but much worse in the substation
Correlation of reading to load	0.9996
Sensitivity	Careful placement needed
Repeatability	Repeatable
Power/excitation	Linked to hardware platform and powered through 3.3V serial link

6 Sensor B: Hall effect chip

6.1 Theory

Hall effect transducer – A semiconductor material passes a constant current. When the device is placed in a magnetic field, the field deflects the holes and electrons sideways, generating a voltage as shown in Figure 31.

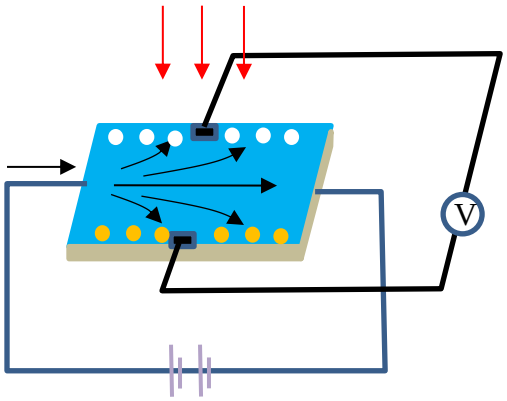

Figure 31: Hall effect transducer operation

6.2 Hardware

Hall effect devices can also be used to measure magnetic field and should therefore give a similar result to sensor A. These devices are generally configured in one of four types of package

1) Through-hole current sensors
2) PCB mounted current sensors with in & out terminals
3) Hall effect switches, with a logic output in response to a magnetic field, used for machine interlocking.
4) Linear hall effect devices which respond to magnetic field.

The fourth type are not commonly used for current sensing, but these offer the most flexibility for testing the magnetic field as they don't just provide on/off logic output signals. It was decided to test the 'open field' type of linear hall effect device. It should be noted that these are less common so there may be significant lead times for large orders.

One of the key issues with these is that they measure magnetic fields up to 500-700 Gauss. This is equivalent to 5000-7000μT.

Table 6-1 : Cost of sensor B hardware

Vendor	Part	Qty	Unit cost	Line cost
RS	A1319LUA-5-T LHE chip	1	£1.75	£1.75
Farnell	0.1uF Capacitor	1	£0.14	£0.14
Farnell	10nF Capacitor	1	£0.12	£0.12
Farnell	47kR Resistor	1	£0.09	£0.09
Amazon	Power supply	1	£4.99	£4.99
Rapid	LinkitOne PCB (Arduino compatible)	1	£44.24	£44.24
			System Total	£51.33

The A1319LUA-5-T LHE chip looks like a transistor, has 3 legs and is supplied at 3- 3.6V. the device is stable with temperature and the claim is it provides an output voltage proportional to magnetic field. It is therefore suitable for connection with an Arduino board.

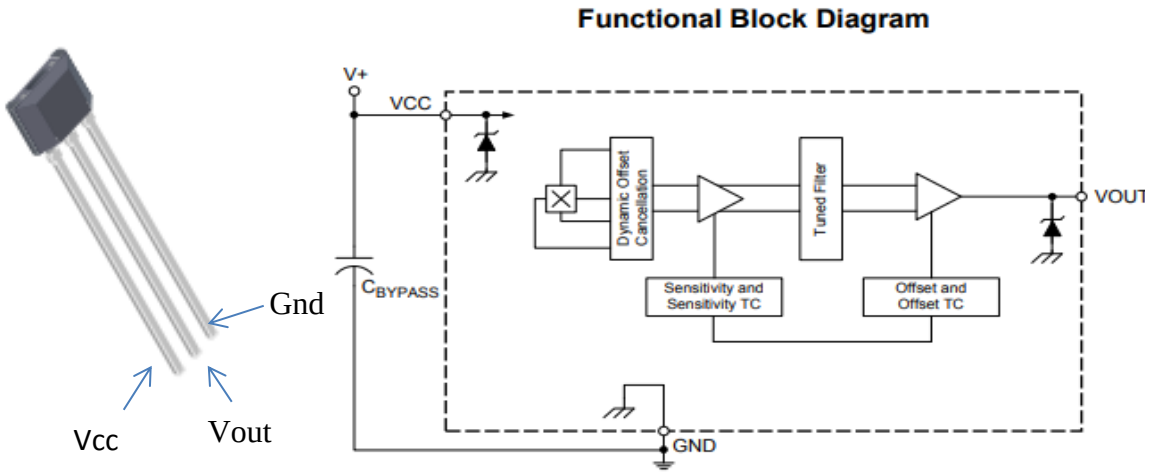

Figure 32: Photo of hall effect chip and its functional diagram

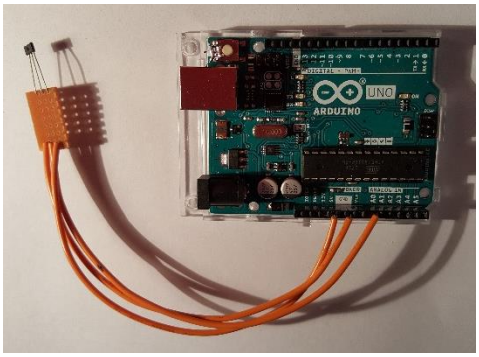

Figure 33: Photo of the linear hall effect device to the analogue input on an Arduino Uno

The circuit diagram for connection of the Hall Effect device is shown in Figure 34.

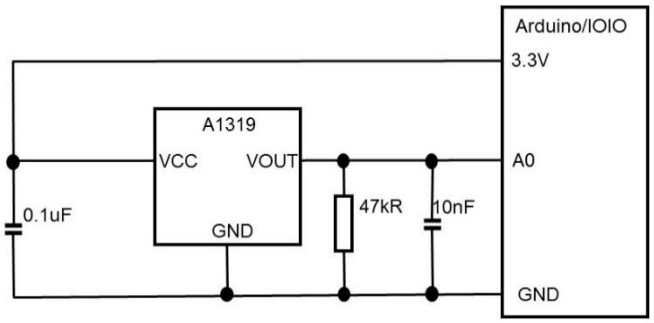

Figure 34: Circuit diagram Arduino Uno with Hall effect chip

6.3 Rig testing

The hall effect sensor was connected to the single phase cable on the rig as shown in Figure 35. Unfortunately no change in voltage was recorded with current variation. Three different devices were tested and there was no variation in any of the devices. The recorded output waveform at two values of load current 260A and 110A is shown in Figure 36.

Figure 35: Photo of hall effect chip on the rig

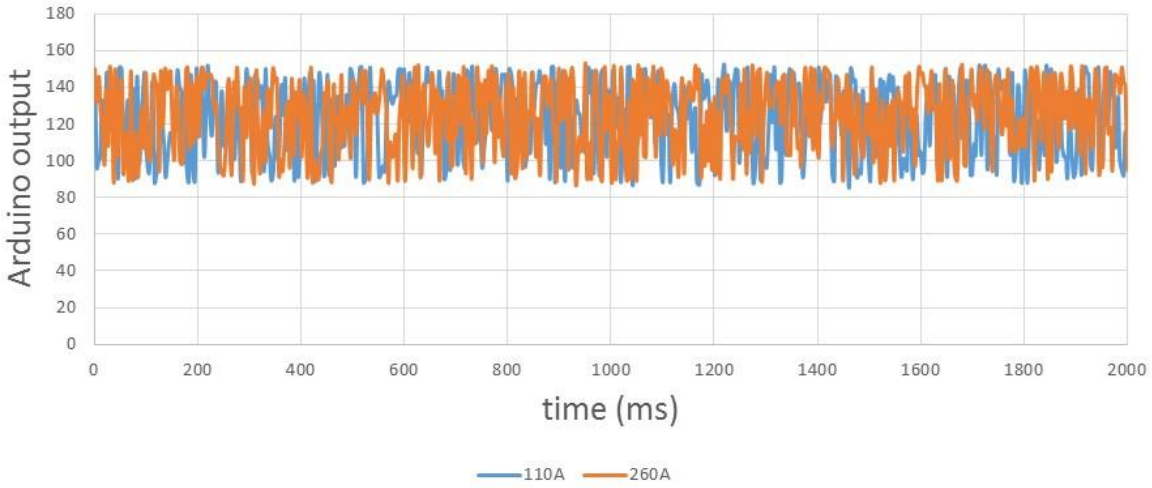

Figure 36: Arduino output of hall effect sensor against time at two different currents

LP 14	A hall effect measurement device did not provide a suitable measurement reading to allow output to be correlated to load current. It is not clear why there this did not work as suggested in the data sheet, but three different devices were trialled.

Three different chips were tried to compensate for possible issues with a dud. The chips were wired and cross checked against the data sheet by different researchers. The recorded value of the chip at around “120” shows that a dc offset is present as expected. However, this value is lower than expected for a 3.3V AI and suggests that accuracy and scaling are an issue.

6.4 Summary

A hall effect chip is not a candidate for long scale testing.

	Comment
Functionality	Unable to get working properly. It is not clear why the hall effect device did not work as expected.
Failure mode	Fail dead
Stability/reliability	Unable to get working properly
Ease of deployment	Needs packaging and linking to hardware platform
Calibration	Unable to get working properly

Test	Comments
Linearity	Unable to get working properly
Effect of adjacent steel work	Unable to get working properly
Effect of adjacent conductors	Unable to get working properly
Effect of temperature	Unable to get working properly
Accuracy	Unable to get working properly
Correlation with load	Unable to get working properly
Sensitivity	Unable to get working properly
Repeatability	Unable to get working properly
Power/excitation	Linked to hardware platform and powered through 3.3V serial link

7 Sensor C: i2m sensor

7.1 Theory

The magnetic field generated in a 3-phase cable looks very similar to a 2-pole field. As the current changes in the cable the field appears to rotate. This time varying change in magnetic field can be detected by a coil and the induced EMF measured. The time-varying dynamic magnetic field around a 3-phase cable was modelled using FEM (finite element modelling).

A 3-core cable of outside diameter 33.84 mm carrying 150 A peak was modelled with three phases carrying current offset by 120° as shown Figure 37

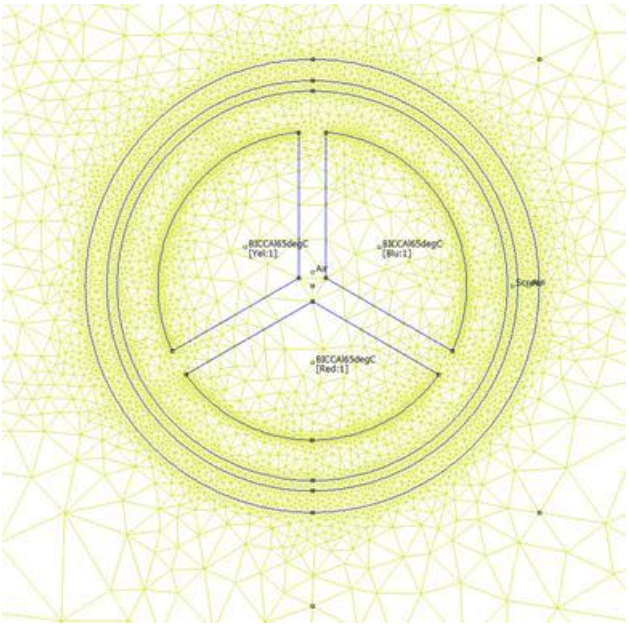

Figure 37 Finite Element Model of the three-core cable

The rotating magnetic field has similarities with that in the stator of an induction motor as shown in Figure 38. This time varying magnetic field can be used to induce an EMF in a coil attached to the cable which can then be measured to infer the current. It was decided to design a coil which acts loosely like a locked rotor of an induction machine (but located outside of the 3-core cable) as shown in Figure 39.

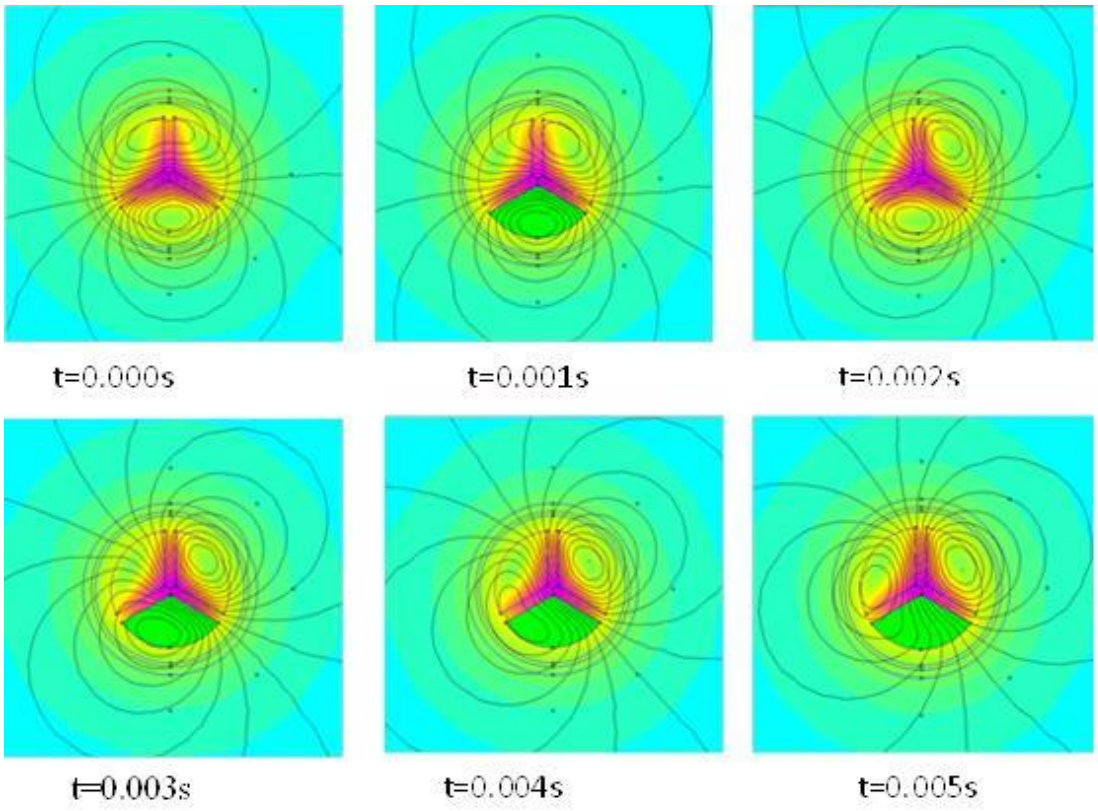

Figure 38: Magnetic flux plot showing rotation of magnetic field with time.

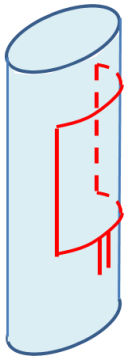

Figure 39 : Coil for detecting changing magnetic field

Although the principle of induction is used, the coil works differently to a Rogowski coil and can only be used on a 3-coil winding where the magnetic field is changing in space as well as time. The Rogowski coil only works on a single-phase system where the magnetic field is changing in time as the change in magnetic field with space is not detected.
The difference in operating principle is illustrated below.

3 core cable with i2m coil - works

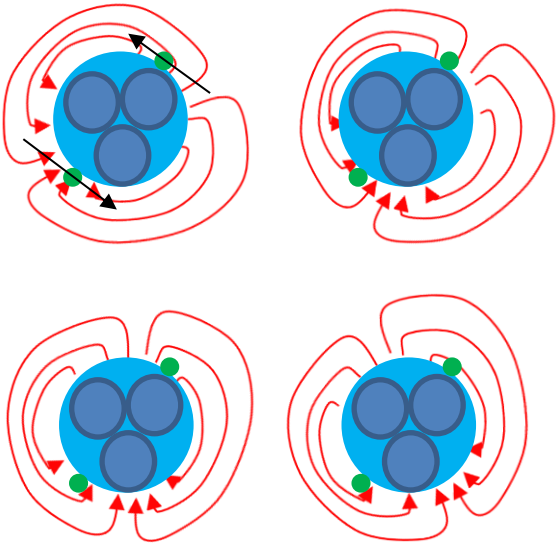

As the normal magnetic field (red) rotates in space due to the time varying currents, the flux cuts tangentially across the coils (green) as shown by the black arrow with velocity ωr, this induces an emf axially in the coil. The two emfs are induced in opposite directions so add

3 core cable with Rogowski coil – doesn't work

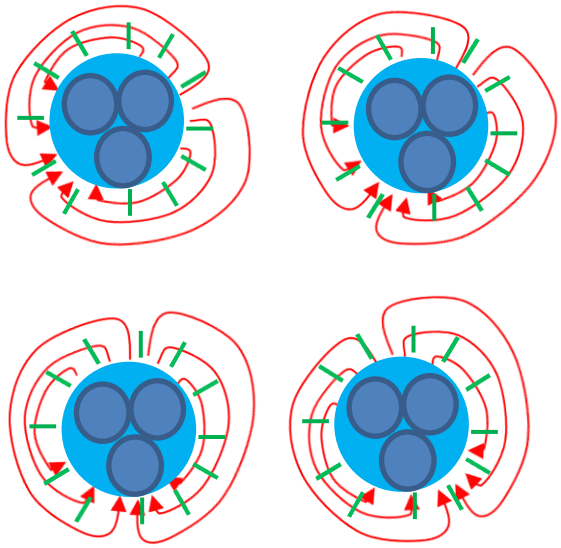

As the normal magnetic field (red) rotates in space due to the time varying currents, the flux cuts tangentially across the Rogowski coils (green) this induces an emf axially in each coil. However, because the coils are distributed round the cable equally the induced emfs in each coil add together to cancel each other out

1 core cable with i2m coil – doesn't work

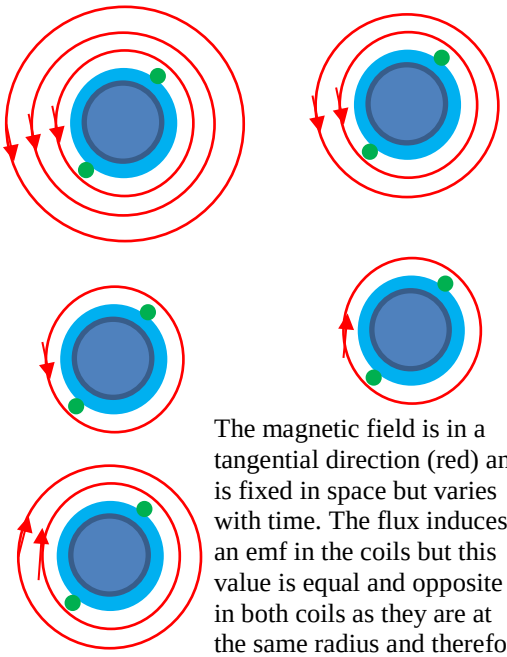

The magnetic field is in a tangential direction (red) and is fixed in space but varies with time. The flux induces an emf in the coils but this value is equal and opposite in both coils as they are at the same radius and therefore the emf cancels out.

1 core cable with Rogowski coil –works

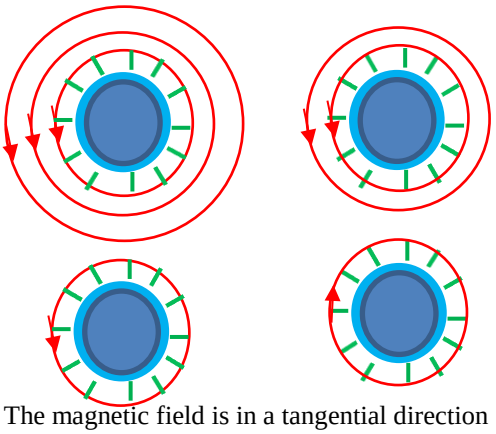

The magnetic field is in a tangential direction (red) and is fixed in space but varies with time. The flux changes in time in each Rogowski coils (green) inducing an emf at both ends of each coil. However, the emf reduces with distance from the conductor, The emf at the furthest part of the coil is less than at the part closest to the coil. Each coil produces a small emf. Many coils connected in series produce a measurable emf.

Figure 40: Operating principle of coil design compared to Rogowski coil

The induced EMF in the i2m coil with around a 3-core cable (or 3 single cores in a trefoil arrangement) can be estimated using Faraday's Law directly (Equation 7-1) or through derivations from the integral form of the Maxwell-Faraday equation. Both yield the same answer, however itis useful to derive from first principles to aid understanding.

Deriving through Faraday's equation; e is the induced voltage [volts], N is the number of turns in the coil and φ is the flux [Wb].

$$e = -N\frac{d\varphi}{dt}$$ **Equation 7-1**

If it is assumed that the flux density, B is changing sinusoidally around the conductor as per (Equation 7-2), then the induced EMF in the coil can be calculated from (Equation 7-3)

$$B = \hat{B}sin(\omega t + \theta)$$ **Equation 7-2**

Where $\omega = 2\pi f$ (rad).

$$e = -2N\omega rl\hat{B}cos(\omega t + \theta)$$ **Equation 7-3**

The radius of the cable, r [m] is assumed as the coil is attached to the outside of the cable and l is the length of the coil [m].

Deriving from first principles through Maxwell's equation

Consider a single coil as shown in Figure 41.

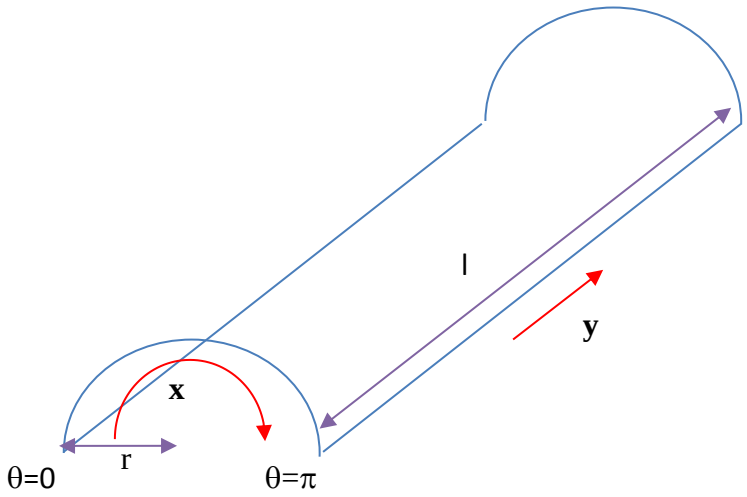

Figure 41 : Coil variables

Consider **x** and **y** as vectors in the radial and axial directions.
A small change in the **x** direction, *dx*, can be rewritten in cylindrical form as $dx = rd\theta$

The integral form of Maxwell-Faraday for each coil is:

$$V = \oint E \cdot dl = -\frac{d}{dt}\iint_S B \cdot dS$$ Equation 7-4

Substituting for B from Equation 7-2

$$V = -\frac{d}{dt}\int_{x=0}^{x=r\theta}\int_{y=0}^{y=l} \hat{B}sin(\omega t + \theta)\, dy\, dx$$ Equation 7-5

Substituting for dx

$$V = -\frac{d}{dt}\int_{\theta=0}^{\theta=\pi}\int_{y=0}^{y=l} r\hat{B}sin(\omega t + \theta)\, dy\, d\theta$$ Equation 7-6

Integrating gives

$$V = -\frac{d}{dt}\left(-2rl\hat{B}cos(\omega t)\right)$$ Equation 7-7

Then taking the time differential gives

$$V = -\frac{d}{dt}\left(-2rl\hat{B}cos(\omega t)\right)$$ Equation 7-8

$$V = -2\omega rl\hat{B}sin(\omega t)$$ Equation 7-9

This is the same as Equation 7-3, where $\theta=\pi$ and the number of turns of coil =N.

To achieve a sufficiently high induced EMF and an acceptable signal to noise ratio (SNR), the coils were designed to be 200 mm long and have 15 turns. As the magnetic field from the 3 coils rotates like a 2-pole machine, the coil is designed to go 180° around the cable as shown. Having additional coils offset by 120° allows the rotating field to be observed in each of the coils. While it is desirable to have this information (and it could give indication of unbalance and current direction if a reference voltage is present) this is not essential. Using these values in Equation 7-3 with a peak magnetic field (from the FEM) gives an induced EMF in each coil of approximately 60 mV. The output from the coils can then sent to an isolating level shift and amplifier circuit before being connected through to a GPRS Arduino platform for sending the readings to a server.

The main purpose of detecting the voltage is to derive the current in the cable. As this research is in preliminary stages, it is assumed, in this case, that the currents in the cable are balanced. Under this scenario, an estimate of current can be made by assuming the current as a point source at the center of each sector and using the geometrical parameters in Figure 42 with reference to and using the following equations to back calculate the

current. Using multiple coils located around the outside of the cable could allow unbalanced currents to be calculated. However, the mathematics in determining this is involved and outside of the scope of the current project.

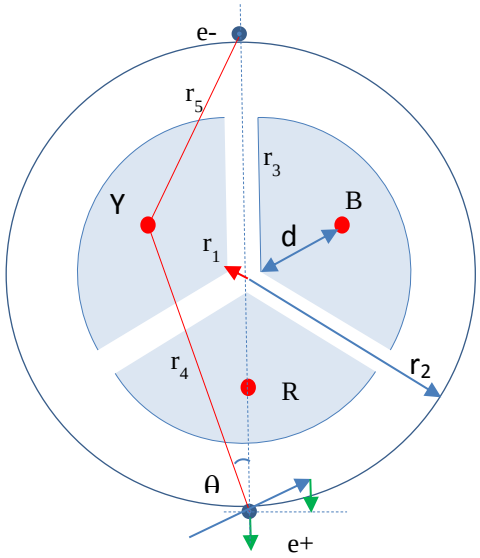

Figure 42: Simplified model of 3 core sectored cable and location of coil

The distance from the center of a sector to its centroid is found from Equation 7-10.

$$d = \frac{2r_3 \sin(\alpha)}{3\alpha}$$ **Equation 7-10**

Where α is the half angle of the sector (60^o). While the distance from the center of conductor Y to one end of the coil is found from Equation 7-11 and a similar expression can be found between the center of Y and the other side of the coil:

$$r_4 = \sqrt{r_2^2 + (r_1 + d)^2 - 2r_2(r_1 + d)cos(120^o)}$$ **Equation 7-11**

It is necessary to calculate the normal component of flux density at each end of the coil due to the currents in each of the three phases. As this has been aligned specifically with the R phase so normal component exists, the maths may be simplified. An example of the normal field in the bottom part of the coil due to the current in Y, is shown by the green arrow in Fig. 5 and can be calculated from Equation 7-12.

$$B_n = \frac{\mu_o I_Y}{2\pi r_4} . \frac{(r_1 + d)}{r_4} \sin(120^o)$$ **Equation 7-12**

With balanced currents, the peak emf can be found from the magnetic field through Equation 7-9 and Equation 7-12 as

$$\hat{e} = 3N{r_2}^2 lf \frac{\mu_o \hat{I}}{2}\left(\frac{1}{{r_4}^2} + \frac{1}{{r_5}^2}\right)$$ **Equation 7-13**

Rearranging gives an estimate of peak current in each phase as

$$\hat{I} = \frac{\hat{e}}{3Nf(d + r_1)r_2 l\mu_o \left(\frac{1}{{r_4}^2} + \frac{1}{{r_5}^2}\right)}$$ **Equation 7-14**

7.2 Hardware

There are a number of methods of producing a suitable coil. For example, the coil can be made traditionally using insulated wire. As the coils are positioned in air rather than laminated steel (which would be too expensive and complex) the induced voltage in the coils is around 60 mV per 100 A of primary cable current. The coil can be wound round a former as shown in Figure 43 and then taped together before being fixed to the cable with cable ties linking each corner. This is a low cost and effective means of installation. The coil must be sufficiently rigid to install in this means which is why the thinnest transformer wire was not used. The coils are manufactured on a former from varnish insulated 'enamel' copper transformer wire (0.5 mm diameter). There is an additional design trade-off between the number of turns and the length of the coil. Coiling hundreds of turns similar to a Rogowski coil is time consuming and impacts the radius that the coil is located at. The coil is shown in Figure 44.

A coil design is not an exact solution, so an alternative design was also manufactured using copper printing on flexible PCB material. It was more straightforward to get exact coils in a suitable location, but the width of the tracks was fine in places and the track broke when the tracks were too fine. Several tries were needed to arrive at 1mm track width. It was difficult to solder the connections to the coil and great care was needed to provide support for the connection wires so these could not be pulled loose. This makes it unsuitable in its present form for a rugged substation environment. The alternative PCB based design had copper tracks of 1 mm and was 16 turns with 8 turns printed on each side and a common connector as shown in Figure 44.

A third alternative is to use conductive thread on material. Two types of thread were trialled steel covered nylon and silver coated copper. The former is easier to sew with while the latter is easier to solder onto. Figure 45 shows early attempts at machine sewing the conductive thread. Tension is an issue and therefore it is recommended the thread is sewn as the bobbin rather than the spool. Even once the tension is sorted, it is necessary to keep an eye on the sewing as loops which can be caught by other wires are all to easy to create as shown in Figure 46. This isn't an issue with hand sewn – but this was add cost and is not as exact a solution and less turns will be present in the available space.

It is necessary to amplify the coil output to achieve a voltage above the noise floor of the controller board. A bespoke signal amplifier circuit based on an MCP6231 op-amp is used to amplify the voltage signal from the sensor for compatibility with analogue inputs on an

Arduino device. The circuit board was manufactured at the University on a CNC milling machine which is used to manufacture prototype PCBs for student projects.

Table 7-1 : Cost of sensor C hardware

Vendor	Part	Qty	Unit cost	Line cost	System Total
University stores	Transformer wire	9m	£5 00	£5 00	
GTS	Flexible PCB	1m^2	£6.50	£6.50	
Amazon	Stainless steel conductive thread	5m	£3.00	£3.00	
Farnell	IL300 optocoupler	1	£1.81	£1.81	
Farnell	Green LED	1	£0.09	£0.09	
Farnell	Terminal Block	1	£0.30	£0.30	
Farnell	Ceramic Cap 0.1uf	1	£0.14	£0.14	
Farnell	OP-Amp OP07	1	£0.68	£0.68	
Farnell	Trimmer potentiometer 10k	1	£1.05	£1.05	
Farnell	DIP socket	1	£0.37	£0.37	
University technicians	Bespoke PCB	1	£2.00	£2.00	
RS	MCP6231T-E/OT Op Amp	1	£0.19	£0.19	
£4.99	Power supply	1	£4.99	£4.99	
Rapid	LinkitOne PCB (Arduino compatible)	1	£44.24	£44.24	
					£59.85

Figure 43: Former for winding

LP 15	There are many different methods to produce turns or wire onto something suitable to go round a cable. Material with conductive thread could be best for large scale implementation as the coils may be made to tighter specifications in a manufacturing environment (eg straight sides) and these can be easily overlapped for multi-coil designs and stacked to increase the number of turns. In addition waterproofing and adding suitable fastenings eg Velcro could ensure fast installation.

Figure 44: Photograph of one of the coils, a set of 3 coils and the PCB based coil

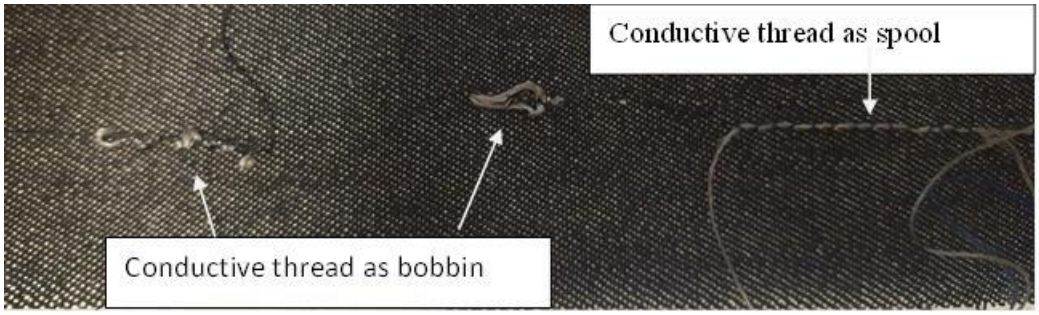

Figure 45: Conductive thread effect of sewing location

Figure 46: Conductive thread hand sewn and machine sewn

The following Figures show the sewn and machine coils attached to the three core cable with tape. It is anticipated in the next evolution of this design that woven material will be used to get straight lines and also waterproofing the material, multi-layering and adding Velcro as a fastening are all envisioned. Figure 48 shows the silver covered copper thread and an example of research into material based “pcb” design for future consideration.

LP 16	The new coil designs were all easily installed either by tape or cable ties. These were then plugged into an amplifier and level shift circuit before connection to a raspberry pi.

Figure 47: Conductive thread mounted on cable (hand sewn and machine sewn)

Figure 48: Solderable thread and an example of material based “pcb” design

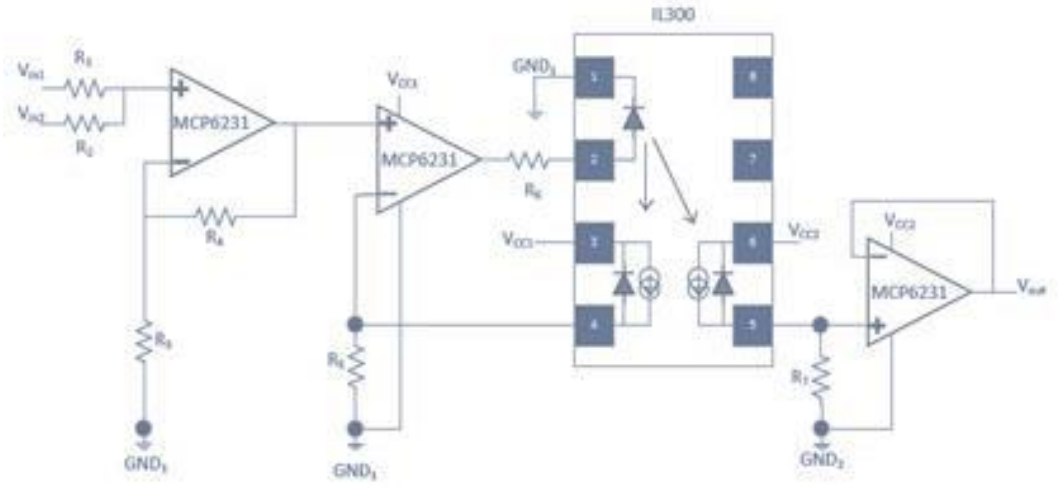

Figure 49: Circuit diagram of the CREST signal amplifier circuit

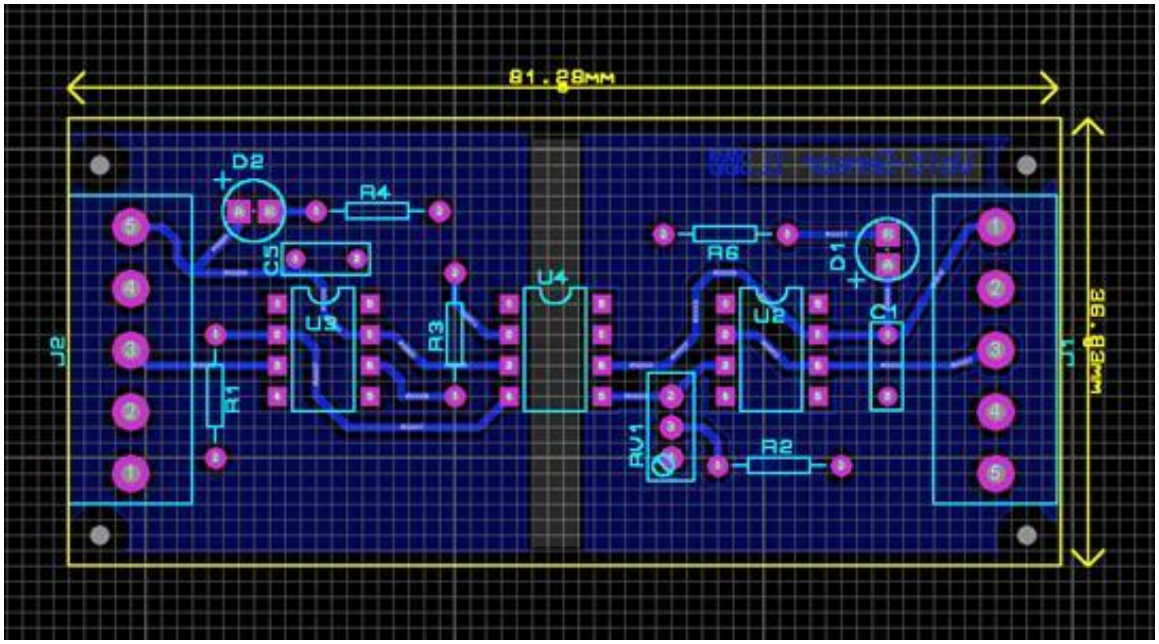

Figure 50: PCB Layout of the CREST signal amplifier circuit

7.3 Rig testing

7.3.1 Wired coil

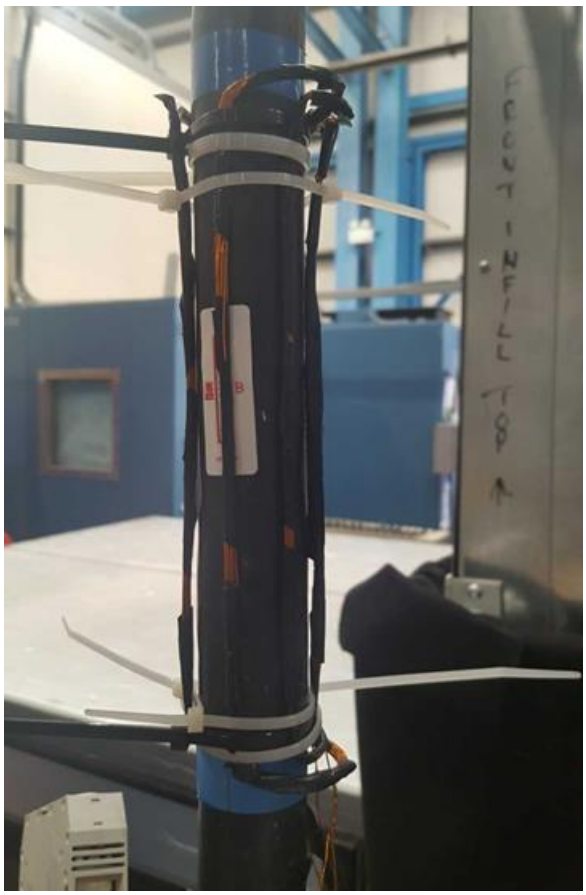

Figure 51: 3 coils in arrangement, sensor G2 the white temperature sensitive label can also be seen behind a coil.

The coils were placed around the three core cable with cable ties and the trailing threads connected to the amplifier circuit via twisted pair leads. (This added some noise to the measurement, but was considered acceptable for the testing underway). Three coils were placed at 120^{o} apart so that a three phase measurement with time could be obtained to check for consistency in reading around the coil.

The results for this are shown in Figure 52. These are the raw results at the terminals of the coil prior to going through the amplifier circuit as recorded by the LeCroy scope. The variation of this recorded voltage with current magnitude is shown in Figure 53. At higher values of current there is clearly correlation between measurement and load. However at low voltage levels noise pick up becomes an issue.

To assist with noise the output of the coils was sent through an amplifier circuit with a designed gain of 9. The initial results only showed a value for each half cycle as shown in Figure 54. The red amplifier voltage waveform is therefore only visible as a half sine wave.To allow the whole signal to be visible the signal was level shifted and then amplified as shown in Figure 55. Any drift in the level shift is removed through the calculation process.

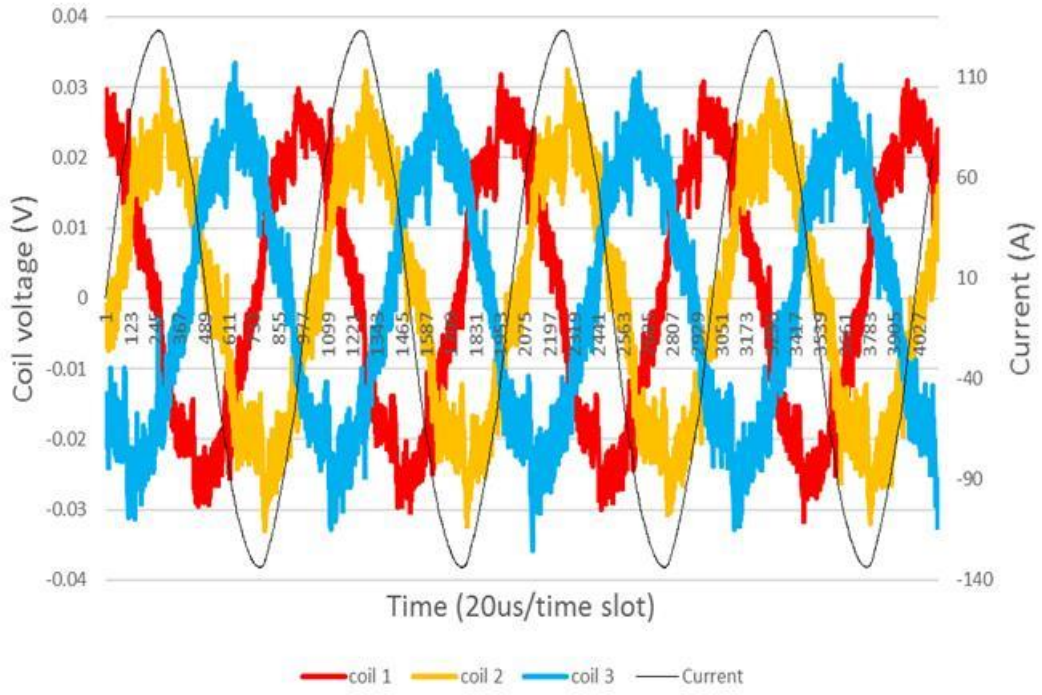

Figure 52: coil voltages [mV] against time [mSec] with a current of 260A peak-peak in the multicore cable

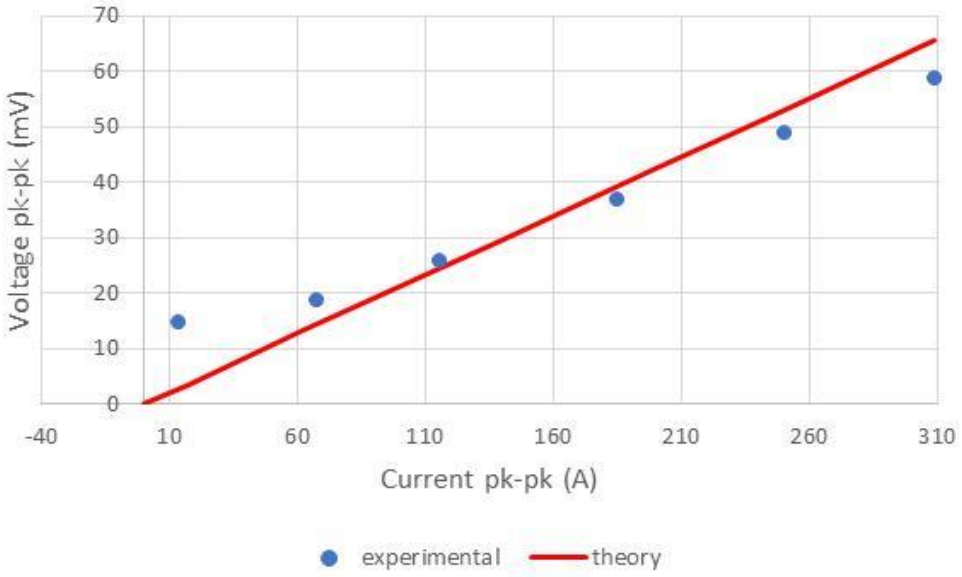

Figure 53: Measured and calculated coil voltage against cable current. The calculated value is estimated from theory using the dimensions of the coil and cable.

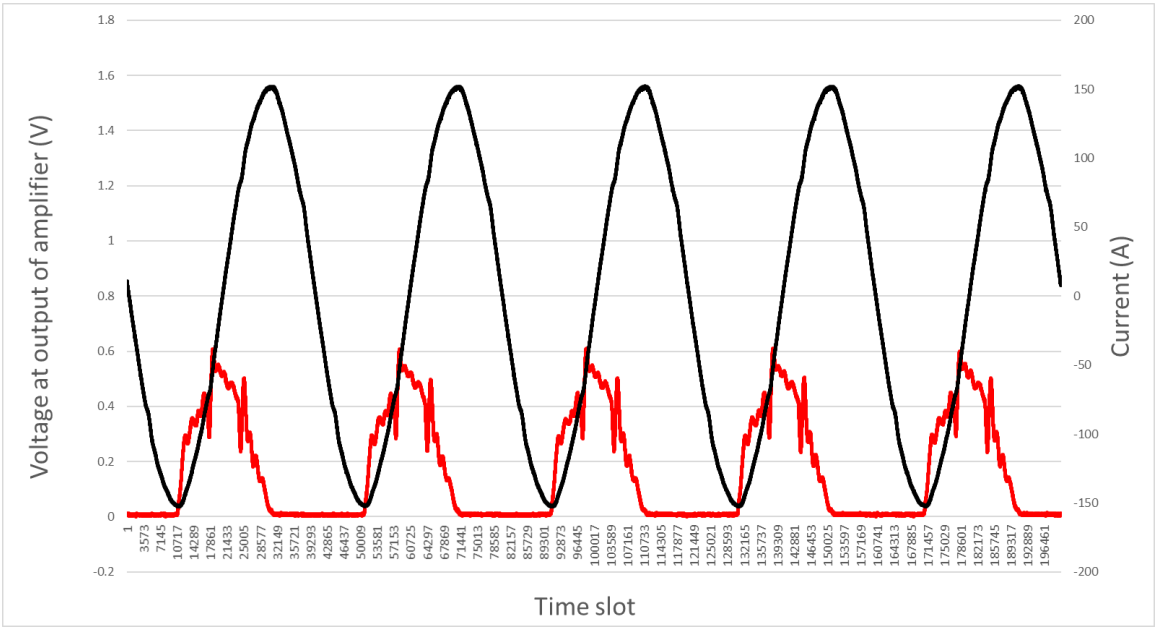

Figure 54: amplifier voltages [mV] against time with a current of 300A peak-peak in the multicore cable with no amplifier offset. The voltage is only visible when it is in the positive cycle.

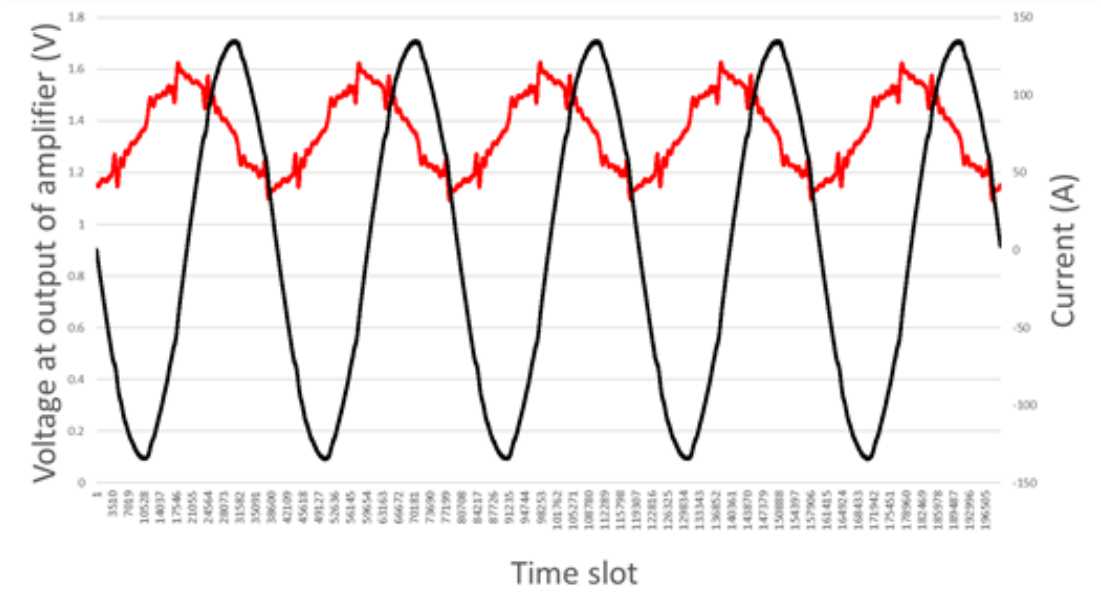

Figure 55: coil voltage at output of the amplifier

The variation of amplifier output with current was recorded and is shown in Figure 56. The difference between theoretical and experimental values is good with excellent accuracy across the range. However, there are spikes in the voltage causing a higher than theoretical value of peak to peak voltage. RMS values show a reverse trend with theory being about 10% higher than experimental values in Figure 57.

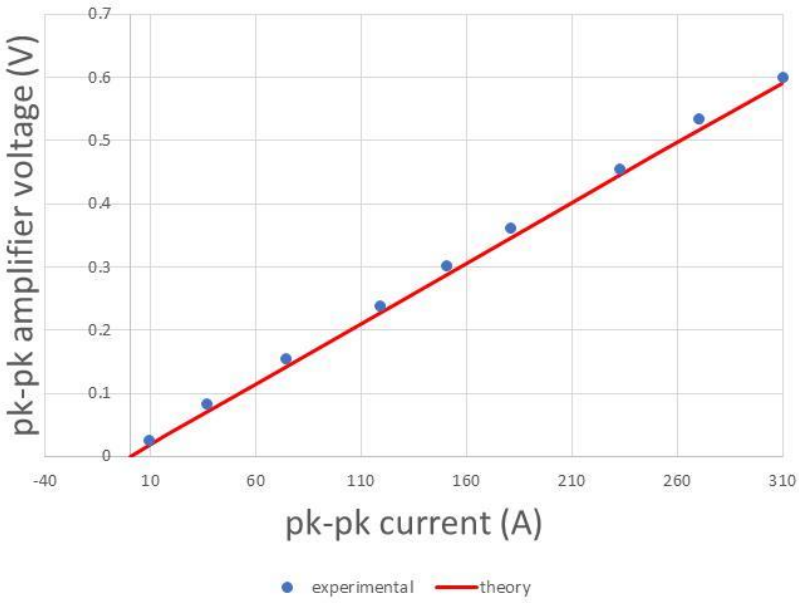

Figure 56: Measured and calculated coil voltage against cable current using pk-pk values

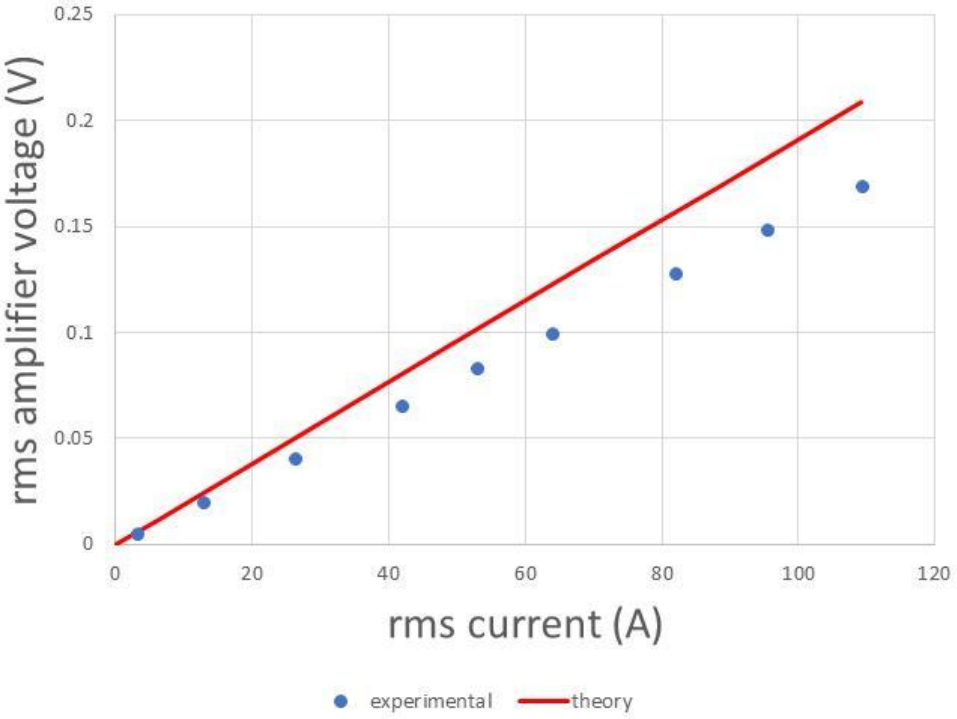

Figure 57: Measured and calculated coil voltage against cable current using rms values

It is not surprising that the theory is higher than the calculated as this research is at an early stage and an approximation of the coil location has been used as a point source. The bundle for these coils is around 5mm in thickness and this will impact the calculated value as some of the coils will be further distance from the cable.

Another change was to try the coils with a Raspberry pi as opposed to an Arduino. The key reason behind this is that the Raspberry pi logs quicker that the Arduino and is therefore less likely to be susceptible to aliasing.

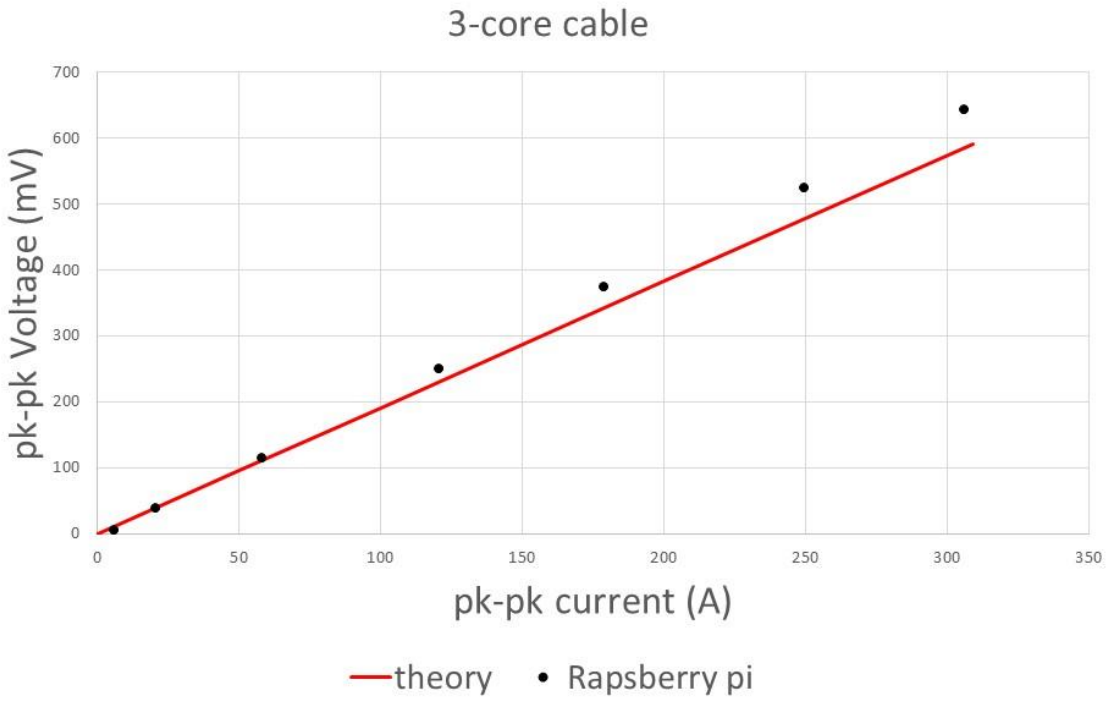

Figure 58: Measured and calculated coil voltage against cable current using a raspberry pi, 2 coils at 90° and the ellipse method of calculation

7.3.2 PCB coil

A similar set of graphs was obtained for the PCB coil as shown in Figure 59 and Figure 60.

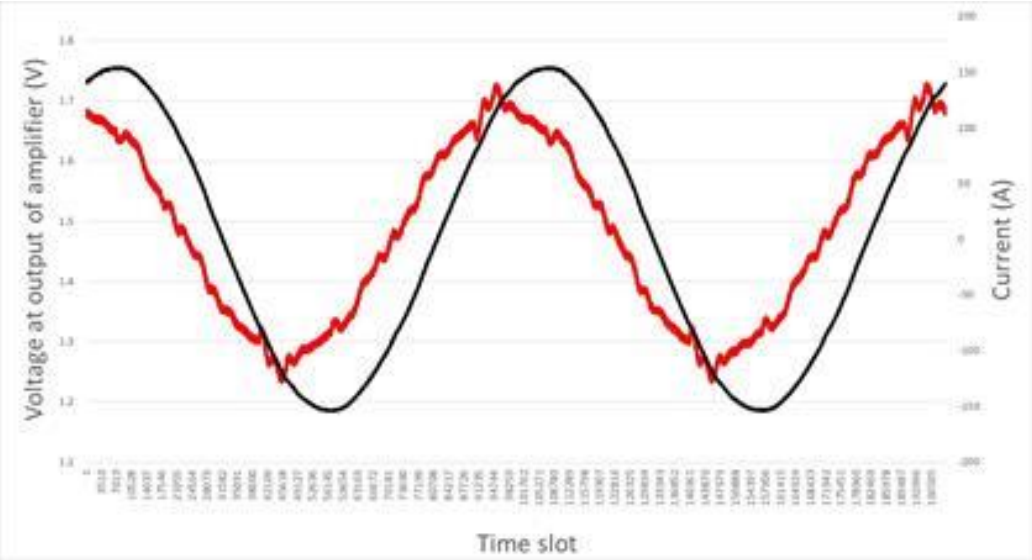

Figure 59: Measured pcb coil amplifier voltage and current against time

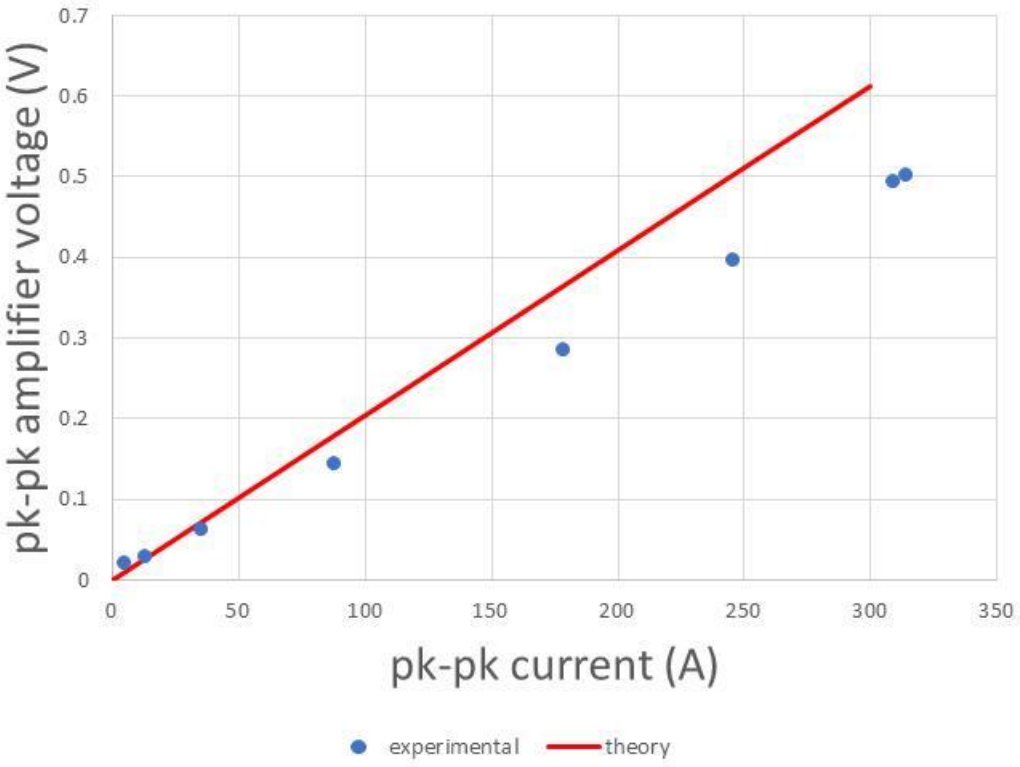

Figure 60: Variation of voltage against current for pcb coil with amplifier

7.3.3 Sewn coil

Results were also obtained for the sewn coil. These had half the number of turns so about half the value of induced voltage. Graphs are shown in Figure 61 and Figure 62.

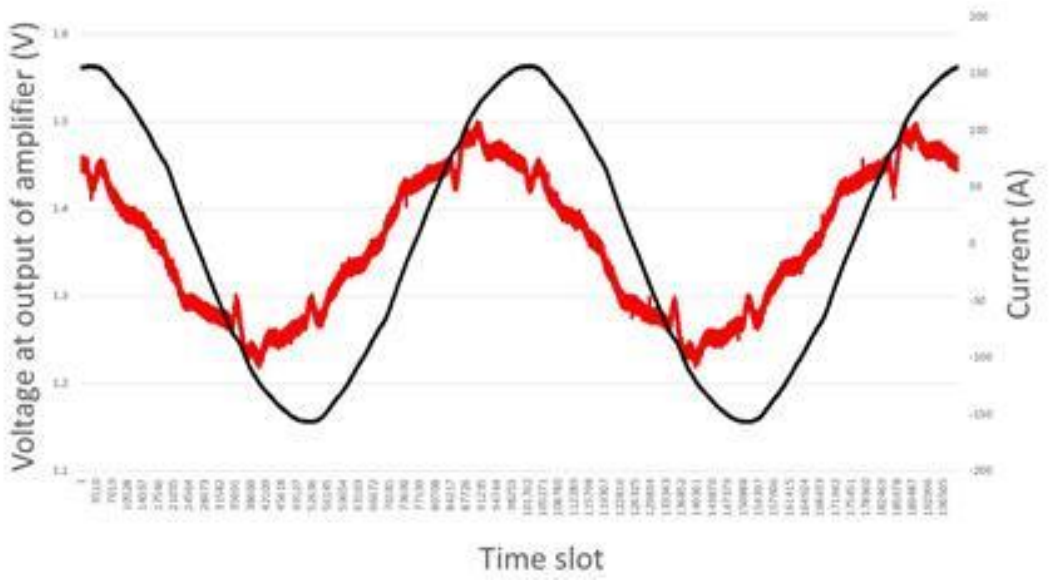

Figure 61: sewn conducting coil voltages [mV] against time [mSec] with a current of 300A peak-peak in the multicore cable

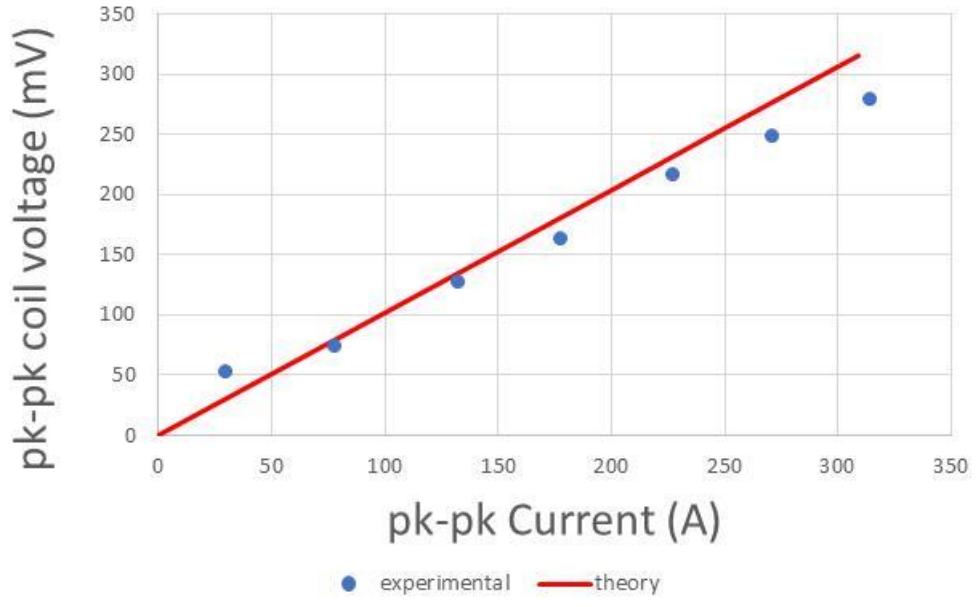

Figure 62: sewn conducting coil voltages [mV] against current in the multicore cable

7.3.4 Trefoil cable

In addition to the 3 core cable there was also the opportunity to test this measurement against a trefoil cable. As the results are fairly similar it was decided to use the wired coil to

test this as the current coils could be moulded to the new shape without too many problems – with a slight reduction in length.

To get a good connection across 180°, some stiff plastic from a file divider was used to create a circular shape from which the coil could be mounted as shown in Figure 63. Two sets of coils placed 90° apart were used. This was done so that the maths technique described for the magnetometer looking at the calculation of an ellipse can also be used to understand if this offers a better calculation for this method. Results are shown in Figure 65.

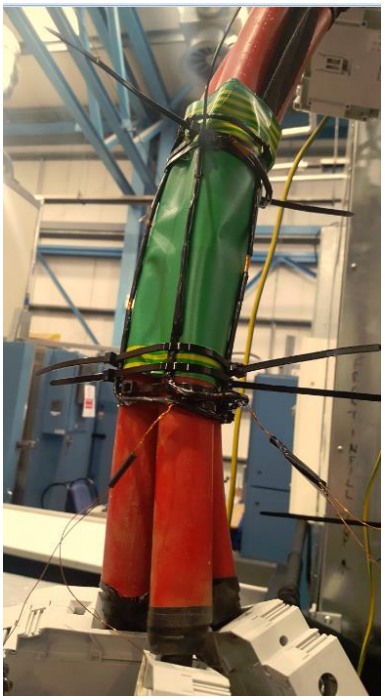

Figure 63: Wire coils on trefoil cable over plastic sheet

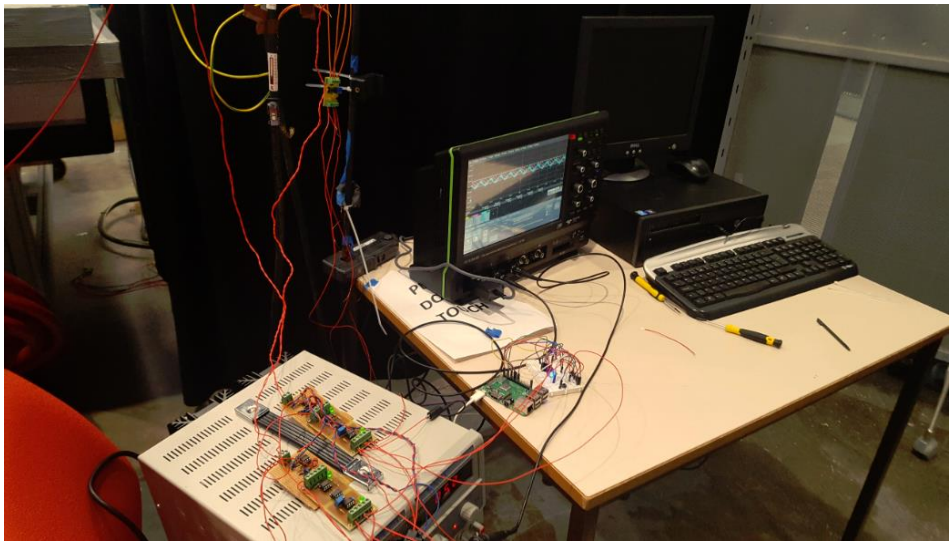

Figure 64: Coils connected to PCB and then onto Raspberry Pi with internal server logging

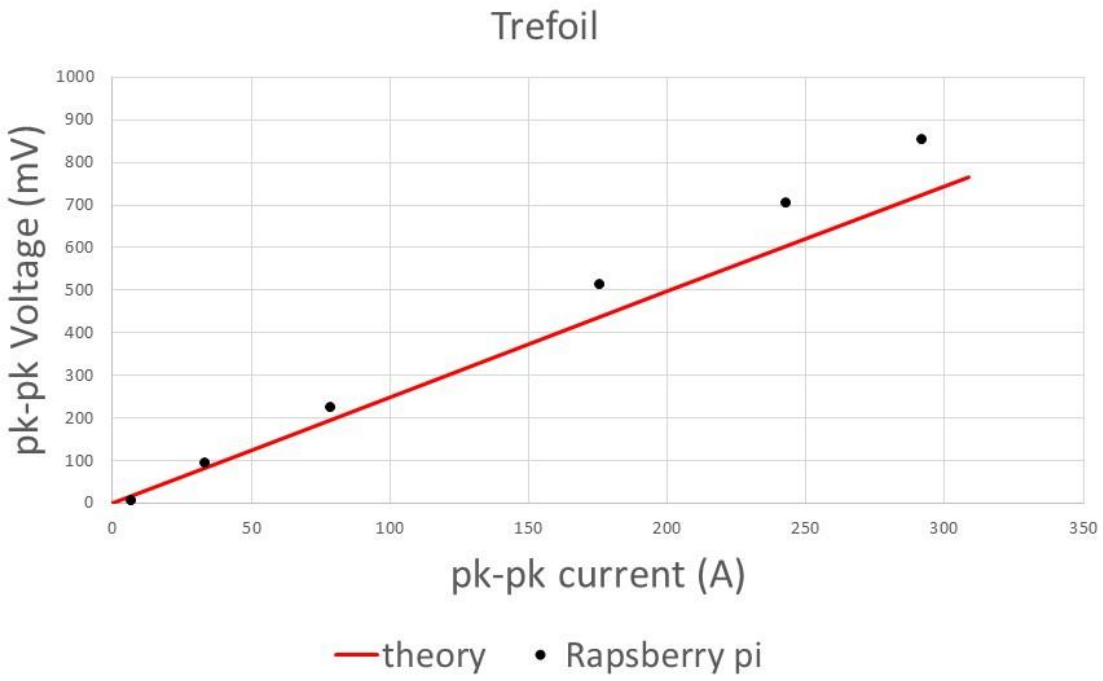

Figure 65: experimental and theoretical results of two coils at 90° with field calculated through ellipse theory.

7.3.5 Comparison of all types

Each of the three coils gave a good degree of correlation between load current and measured voltage signal as shown in Table 7-2. The comparison with theory showed around a 10% underestimate of load current based on measurement. However, it is fairly clear that this is due to two factors;

1. The bundling of the wire coil which results in distances changing between coils of wire.
2. The PCB and sewn coil have distributed windings and this will act to lower the field in the bundled set. Resulting in an underestimate.

Further work is needed to go through the maths and modify the back calculation to adjust for these.

Table 7-2 : correlation of sensor measurement and theory with current

Coil	Correlation co-efficient
Wound coil	0.999
PCB	0.999
Sewn coil	0.996

LP 17	The new coil designs showed good correlation between measurement and load current in a balanced system.

LP 18	At this stage the maths behind the i2m coil needs further development to take into account factors such as the distributed nature of the windings or the lumping together of the windings and also to look at imbalance.

LP 19	There was no impact on the readings in the presence of a thermal source (heat gun) and only a very small change in value with close by metal work.

7.4 Substation testing

The three coils were installed on the 11kV cable between the RMU and the transformer. Installation can be seen in Figure 66.

The results were firstly captured on the LeCroy scope and then on the Arduino through the analogue input channels A0, A1 and A2. The sewn and PCB coils were directly above each other and the vertical axis was carefully aligned. This meant that the captured data could be more easily compared as shown in Figure 67. There isn't a large variation in value but these are clearly changing at the same time. The sewn coil is very noisy because it was connected up on site and it was difficult to get a good connection on one of the wires. Pre-installation of the coil to cable is necessary to avoid this issue. The coils are then connected to the amplifier before being connected to the scope.

A close up on the AC coupled waveforms of the three coils is shown in Figure 68 and Figure 69. The sewn thread output has been multiplied by a factor of 2 to show the similarity against the PCB value. This latter curve also clearly shows a 7^{th} harmonic ripple on the current measurement value.

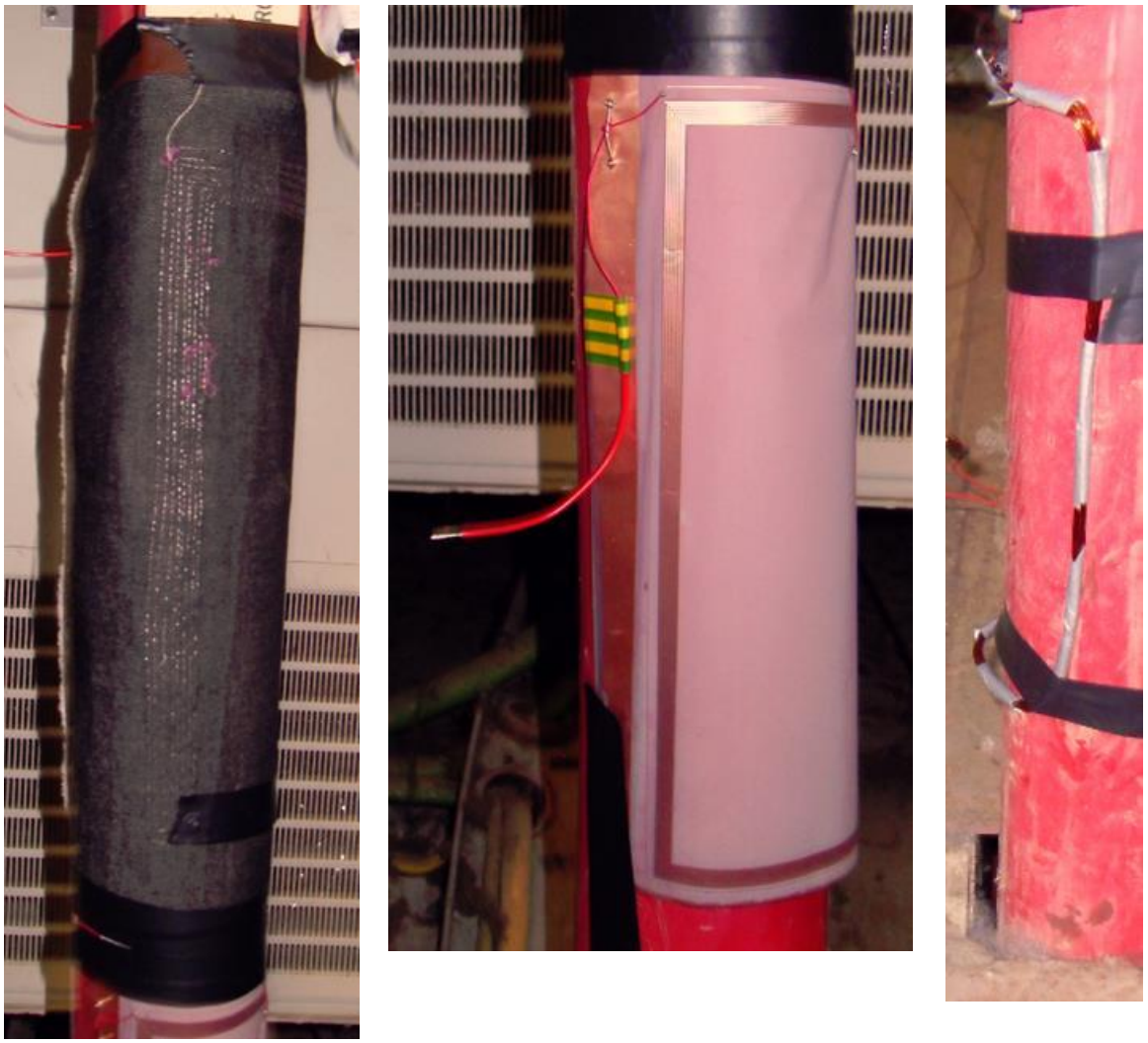

Figure 66: sewn , pcb and coil on substation cable

LP 20	The coils have to fit 180° around the cable these mean the coils sides have to be a set distance apart. The sewn coil offers the best opportunity for a single design as it can be folded to give the straight edges 180° apart. The PCB and wired coil would need to be made in different sizes for large scale roll out.

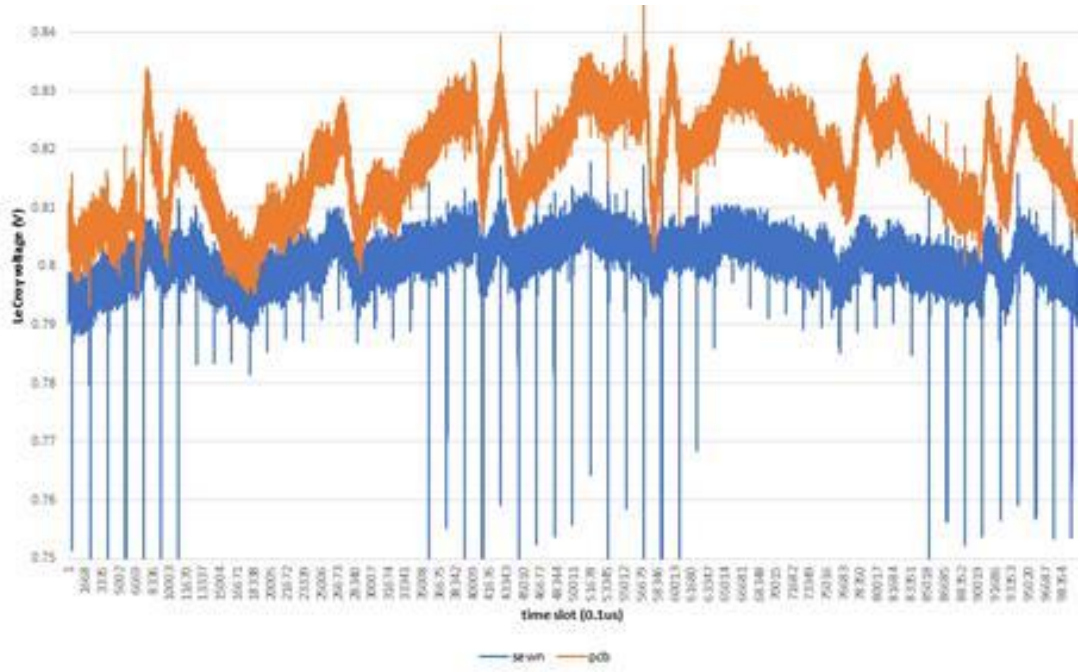

Figure 67: sewn , pcb scope readings

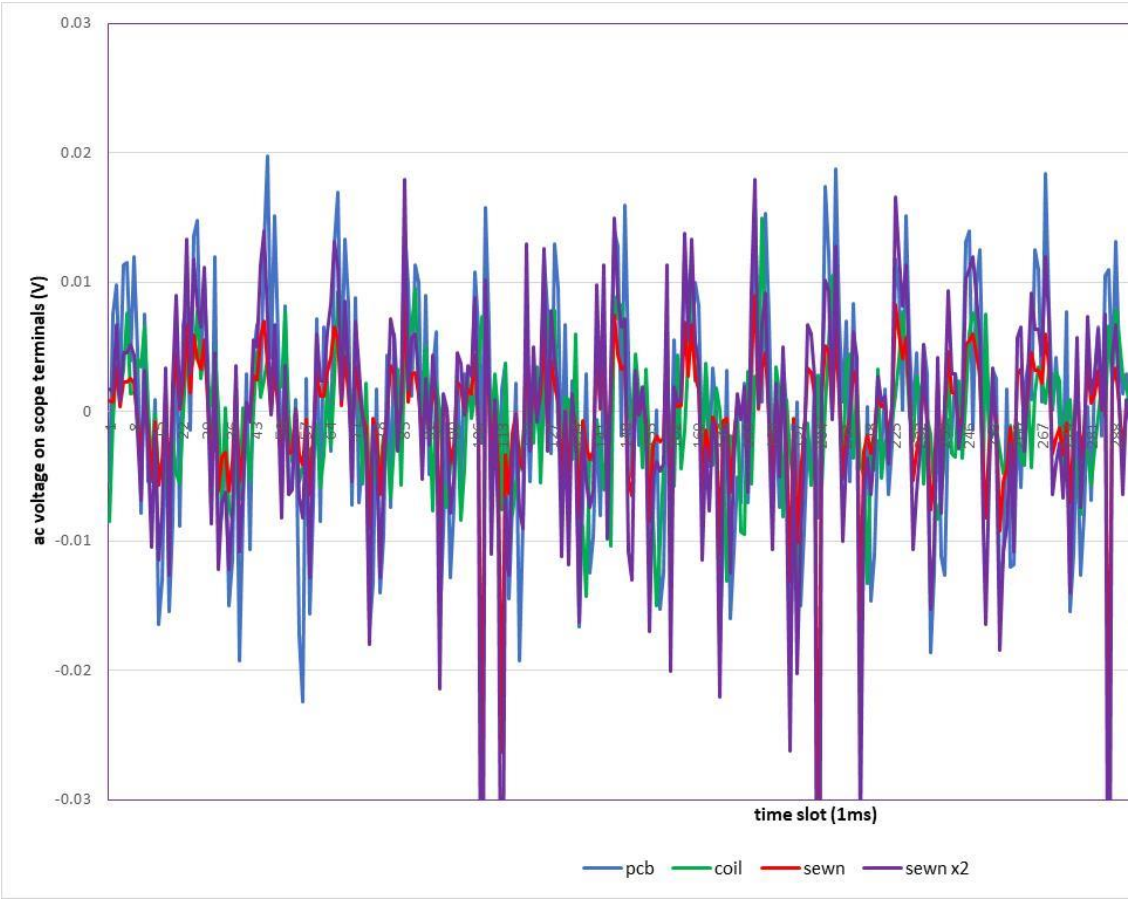

Figure 68: The induced ac voltage on the three different coils with time

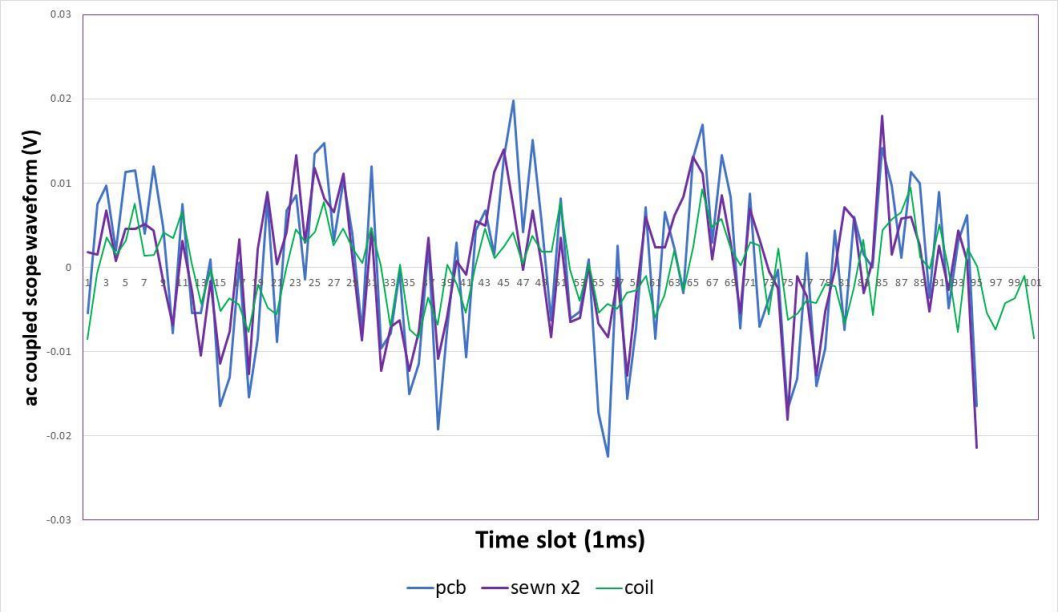

Figure 69: Close up of the induced voltages on the coil and the sewn sensor

As already explained it is difficult to estimate the loading on the 11kV transformer. Figure 70 shows the output from the pcb coil averaged over 1s compared to the recorded sum of the currents on the LV. There is no obvious correlation but this is not unexpected considering the low values.

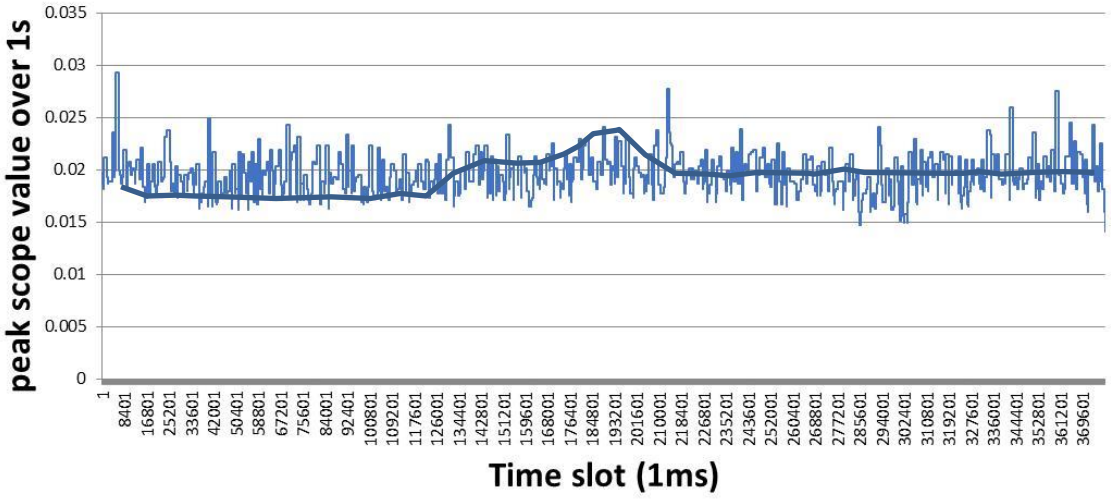

Figure 70: pcb scope readings

This level of detail is further reduced when the coil is plugged into the Arduino as opposed to a scope as shown in Figure 71

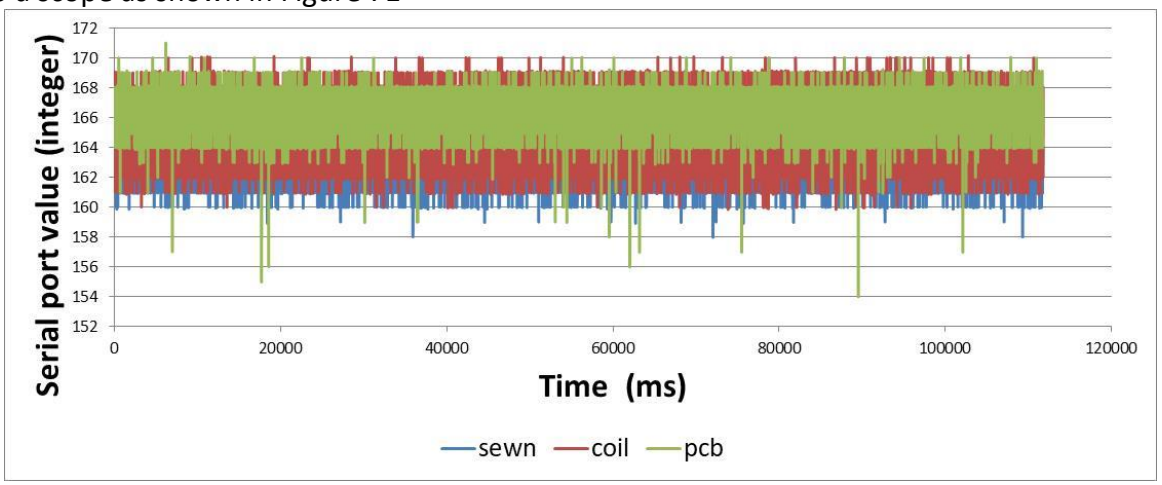

Figure 71: arduino readings

The Arduino has a 10bit analogue input. This means it can accept a reading on a scale between 0 and 1022 bits on the analogue input. These 10bits corresponds to 0-5V analogue input. Therefore, an analogue input of 2.5V corresponds to 511 and each volt is approximately 204 bits. Each byte is therefore close to 5mV

The analogue input bytes of coil voltage range are slightly different for each type and range from:

- 160-166 sewn
- 160V to 170 coil
- 154-171 pcb

That is a range of around 50mV.The 50mV is of comparable order of magnitude to the 40mV pk-pk values captured on the scope. The raw signal coming from the coil pre-amplifier is therefore around 4mV which is very low and close to the noise limit.

The current in all the red phases is around 60A on the secondary of the transformer from the Fluke. Assuming 433V on the secondary (as per transformer rating plate) the power in the secondary is around 45kVA. Therefore the current in the primary is about 2.4A. This is very difficult to measure accurately.

The coil was retested on a substation with a higher loading so that more sensible currents could be monitored. The coil was connected to a raspberry pi as opposed to an Arduino with a 10bit a to d converter. The results of testing are shown in

LP 21	Although the coil itself can pick up the harmonics. The platform it is connected to may limit the use of this information through the data logging resolution and also timing.

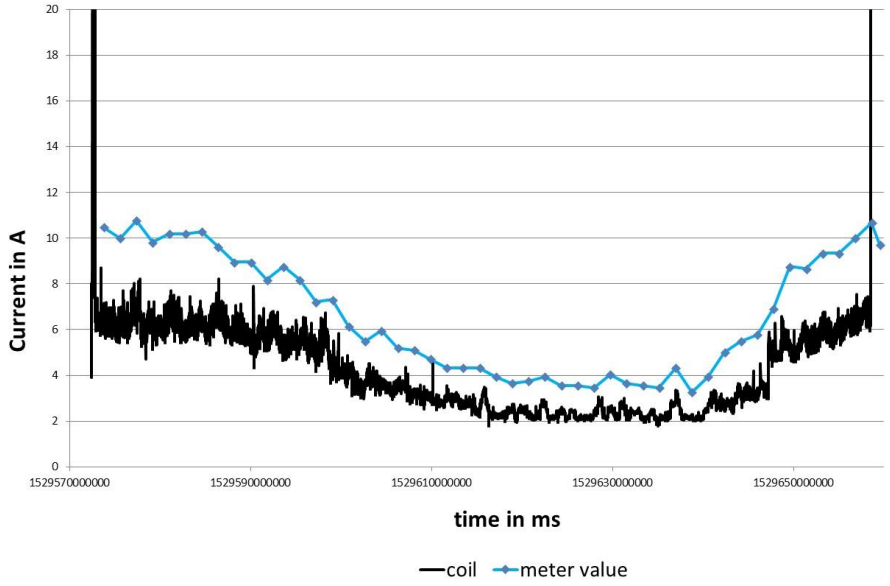

Figure 72: substation re-test showing the coil values compared to half hourly metered data

7.5 Summary

An i2m coil is a promising candidate for long scale testing.

	Comment
Functionality	Can be used • To provide three phase magnetic field measurements which can be used to back-calculate the load current (assuming balanced if 3 phase – but may be able to deal with unbalanced) • In real time as limited by hardware platform
Failure mode	Fail dead
Stability/reliability	No issues on test
Ease of deployment	Needs packaging and linking to amplifier on pcb then linking to hardware platform
Calibration	No obvious calibration needed – In theory the circuit should cope with OpAmp drift over time through the methodology – However, if this is an issue at field trial then further design of the OpAmp circuit may be necessary

Test	Comments
Linearity	Linear – no iron so no saturation (However, iron could be used in future designs to concentrate the flux). Readings only as high as 3.3V so some scope for higher currents. If fault current recording desired then the amplifier can be removed altogether.
Effect of adjacent steel work	No obvious change as the coil lies flush to the exterior of the cable and therefore the steel doesn't impact that part of the flux path
Effect of adjacent conductors	Unable to test
Effect of temperature	No obvious impact
Accuracy	Around 10% but work can be done to significantly improve
Correlation	>0.996
Sensitivity	At present due to hardware setups there are some long leads and these do suffer from noise pick up which is largely filtered out. A product solution would only have short cables between coil and amplifier – so this wouldn't be an issue.
Repeatability	Repeatable
Power/excitation	A single power supply could be used to power hardware platform and additional feed from this needed to power OpAmp circuits and offset voltage. Ideally isolated power supplies as the OpAmps have inbuilt isolation.

8 Sensor D: Accelerometer

8.1 Hardware

Android smartphones often incorporate separate magnetometers and accelerometers, whereas development boards aimed at the electronics market may use combined magnetometer, accelerometer and gyroscope chips. The TDK Invensense MPU-9250 device was used in this CREST prototype for vibration testing as an alternative to sensor A as this did not have the magnetometer present and provides a useful comparison.

Table 8-1 : Cost of sensor D hardware

Vendor	Part	Qty	Unit cost	Line cost	System Total
Amazon	Silverline 427714 Magnetic Mount	1	£7.27	£7.27	
pimoroni.com	SparkFun IMU MPU-9250	1	£11.67	£11.67	
Amazon	Power supply unit	1	£4.99	£4.99	
Rapid	LinkitOne PCB (Arduino compatible)	1	£44.24	£44.24	
					£68.07

As this device is to be used to test vibration it was planned to locate on the transformer rather than near a cable. A photo of the device and the circuit diagram are shown below. A magnetic mount designed as a welding earth block could be used to securely attach the device to the transformer.

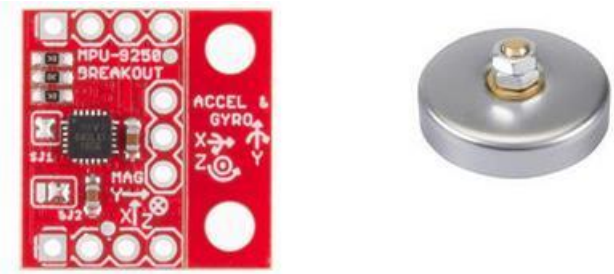

Figure 73: Photo of accelerometer and magnetic mounting clamp

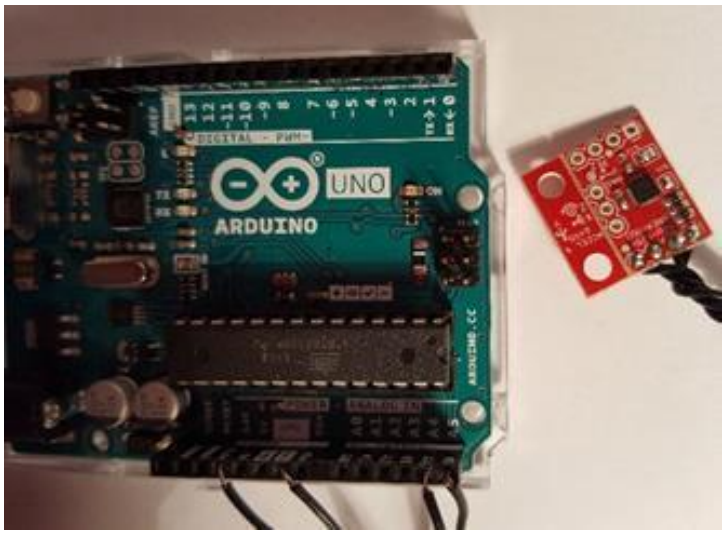

Figure 74: Photo of Arduino Uno with MPU 9250 accelerometer circuit

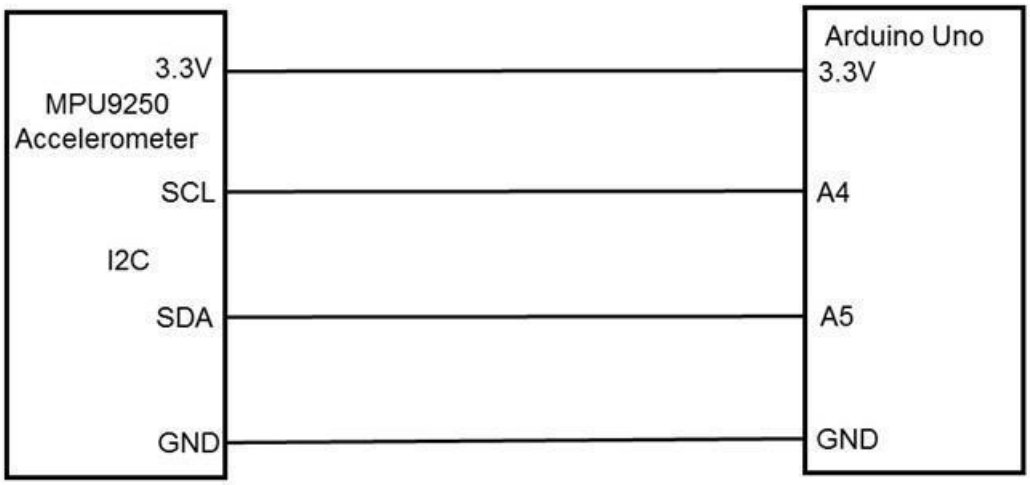

Figure 75: Wiring diagram for accelerometer and Arduino Uno

8.2 Rig testing

The power supplies that give the rig power at low voltage are all enclosed and there is no mechanism for testing vibration on a transformer. There was some vibration on the cable when cable was brought in close proximity to another cable. An example of this is shown in Figure 76. The X-axis value clearly increases while the other values stay approximately the same.

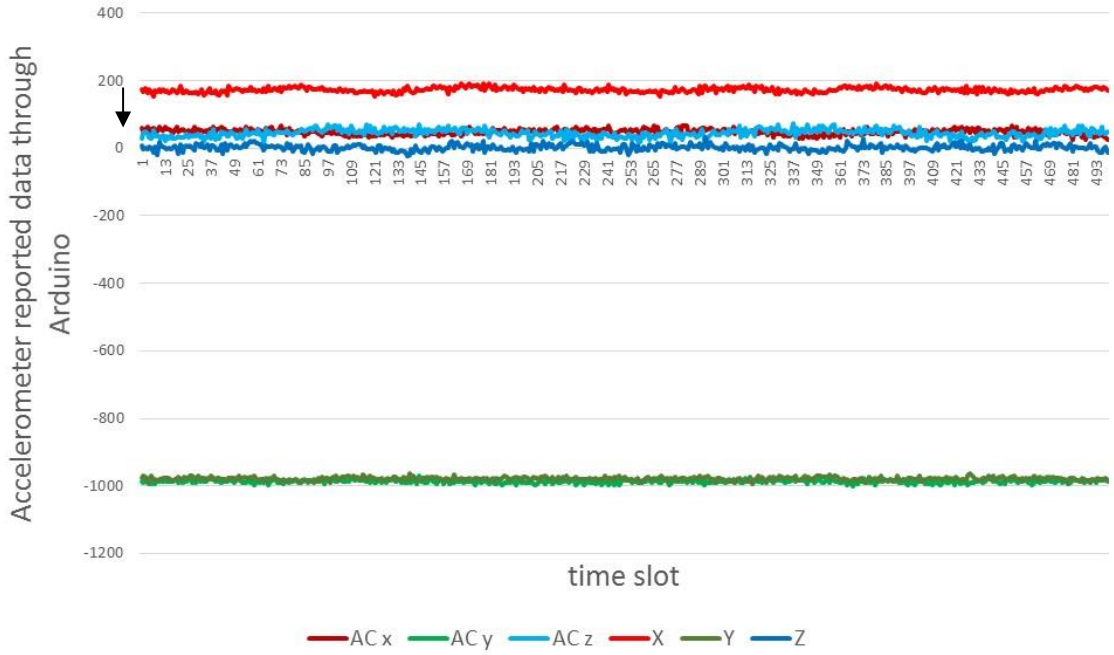

Figure 76: Acceleromter X-Y and Z measurement at 272 A pk-pk Current adjacent to another cable (AC - X,Y,Z) and away from other cables (X,Y,Z)

Changing the load current while keeping the cables in close proximity, allows the change in x-axis vibration to be plotted against current as shown below. The correlation between load current and change in accelerometer reading is 0.345 – a weak positive correlation.

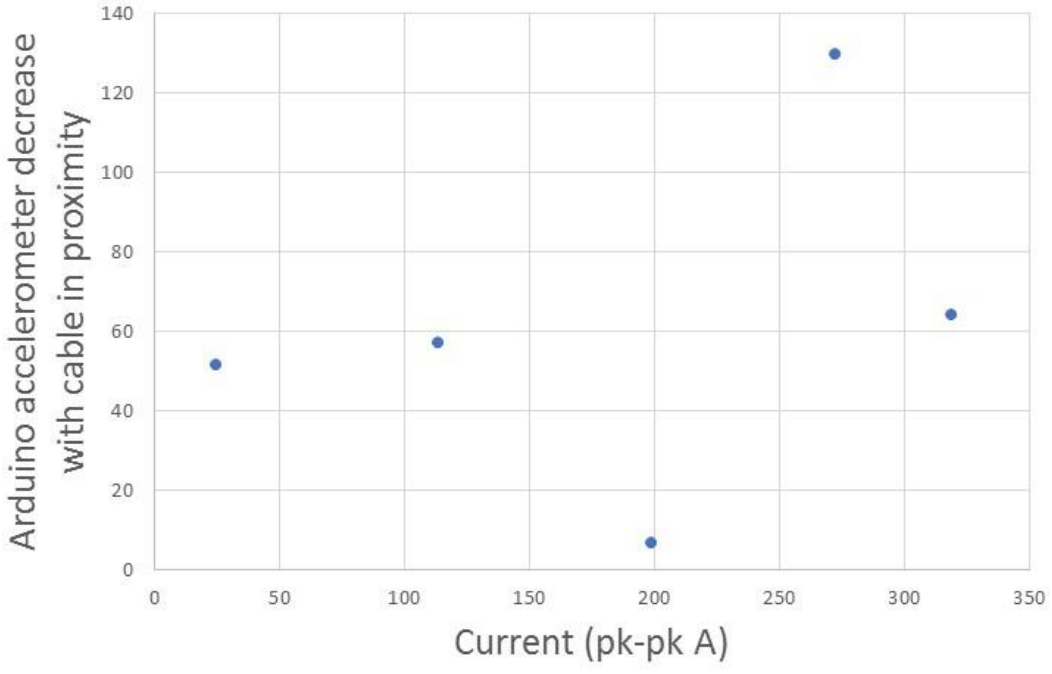

Figure 77: Acceleromter X-axis increase in reading for close to far away cable compared to load current

8.3 Substation testing

The substation was not an ideal location either. The transformer was located within a thin steel casing which was not directly touching. There was audible transformer hum and this casing was vibrating so an accelerometer was placed on the transformer casing and hooked to an Arduino through the I^2C Serial link.

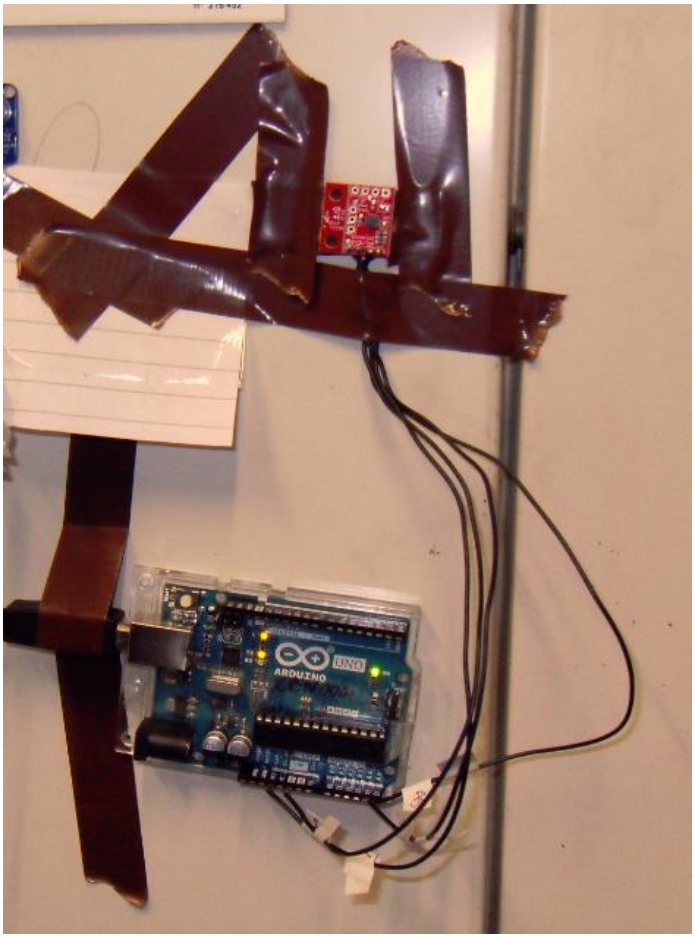

Figure 78: Accelerometer taped to transformer casing going to arduino

This is a three axis device and the values recorded on each axis are shown in Figure 79-Figure 82. The sum of the red phase currents on the LV side of the transformer are shown as a blue line with values on the right hand axis of the graphs in Amps.

There is no immediate and obvious correlation between the vibration and the load current. This could be due to several reasons – the load current over the test is only varying by 8A (or 6kVA) on a transformer rated at 800kVA. This is less than 1% of rating at a value of 49kVA or 6% of the transformer rating.
The vibration would be occurring at around the frequency of the transformer hum and this is difficult to pick up with the controller measuring at <80Hz. The signals show a clear sign of aliasing ripple which indicates this is an issue.

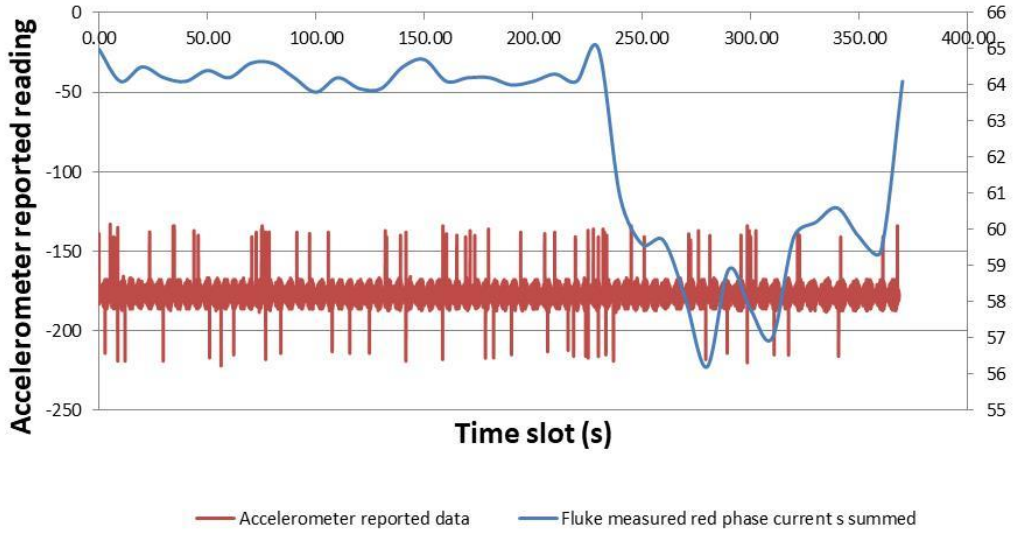

Figure 79: Acceleromter X-axis measurement and fluke estimated current with time

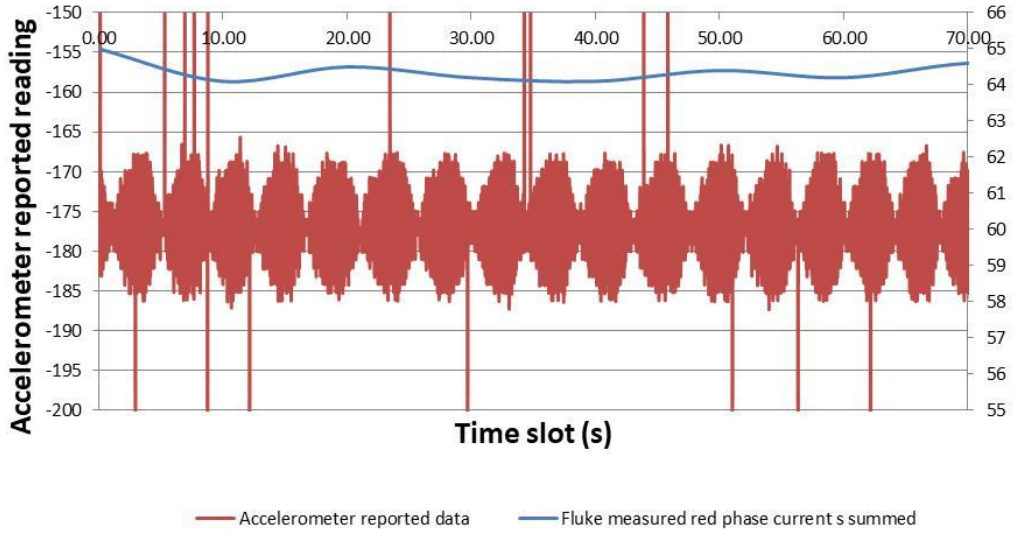

Figure 80: Acceleromter X-axis measurement and fluke estimated current with time

Other issues with this measurement include the spikes in the signals due to noise pick up – this is most noticeable on the x-axis in Figure 80. It is suggested that this test is re-run on a more heavily loaded transformer where there is direct axis to the transformer. Ideally this should be run with a device which doesn't report back through a serial link so that the raw data can be captured and analysed with an oscilloscope in the first instance.

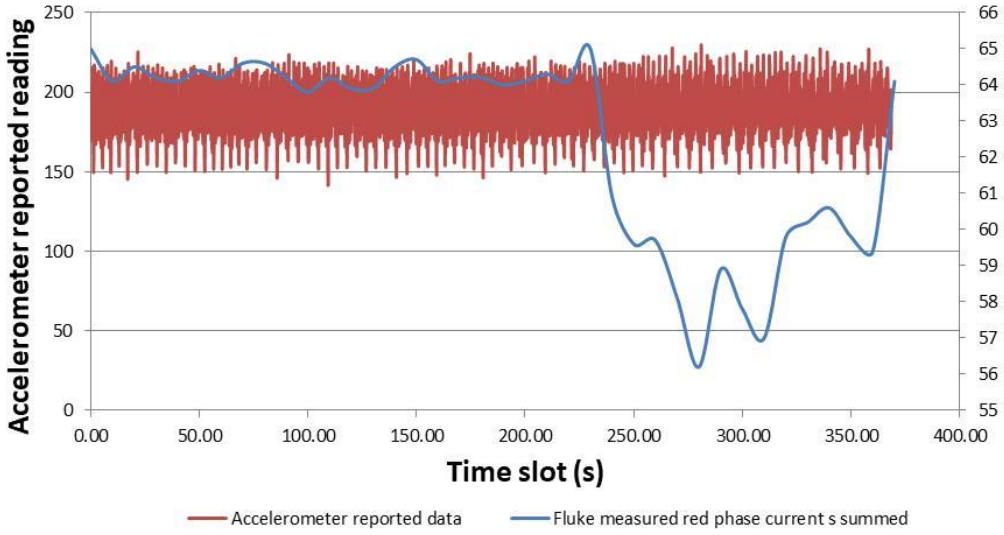

Figure 81: Acceleromter Y-axis measurement and fluke estimated current with time

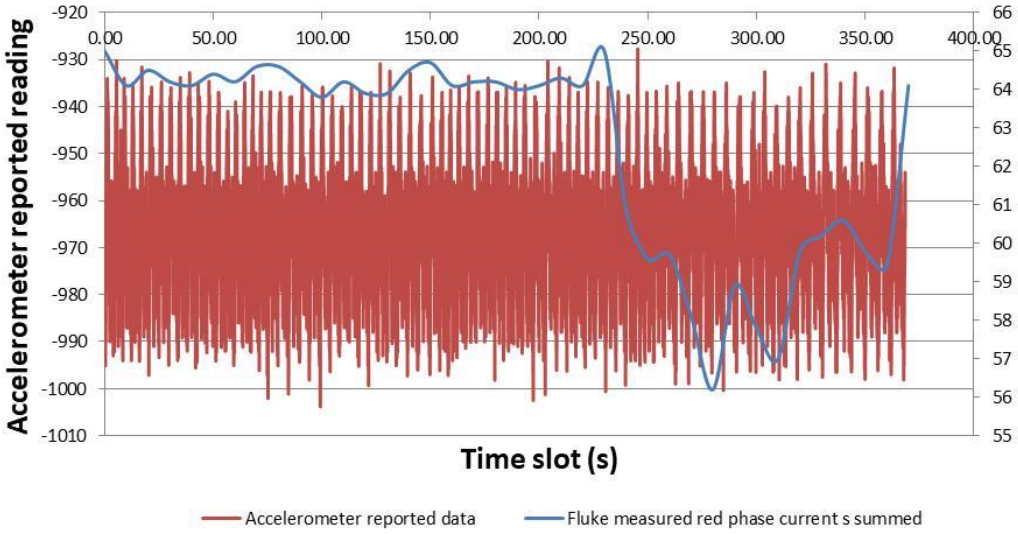

Figure 82: Accelerometer z-axis measurement and fluke estimated current with time

LP 22	The testing undertaken indicated that it was not going to be possible to relate vibration with loading.

LP 23	Even if further testing proved there to be a relationship between loading and vibration under more highly loaded transformers it would require a significant amount of work to develop the maths and calibration process required for large scale roll out. It is unlikely that the calibration procedure could be achieved in a low enough time scale to keep the costs of installation below £50.

8.4 Summary

An accelerometer is not a promising candidate for long scale testing as the signals back are not obviously related to loading. Even if this were to be proven to be suitable on a high loaded transformer – there would be issues with calibration of load current against reading which would need to be tuned on-site and could drift with time.

	Comment
Functionality	Unable to gather meaningful results
Failure mode	Fail dead
Stability/reliability	No issues on test
Ease of deployment	Needs packaging and linking to hardware platform
Calibration	Unable to gather meaningful results

Test	Comments
Linearity	Unable to gather meaningful results
Effect of adjacent steel work	Unable to gather meaningful results
Effect of adjacent conductors	Unable to gather meaningful results
Effect of temperature	Unable to gather meaningful results
Accuracy	Unable to gather meaningful results
Correlation with load	0.34
Sensitivity	Evidence of sensitivity
Repeatability	Unable to gather meaningful results
Power/excitation	Linked to hardware platform and powered through 3.3V serial link

9 Sensor E: Audio microphone

9.1 Hardware

It is planned to use a microphone to pick up transformer noise to try and detect loading. It is possible to record sound in MP3 format with a packaged device such as a smartphone, dictaphone or professional audio recorder. However, the process of converting MP3 into analogue data for analysis would have required a time consuming bespoke conversion program to be coded for example in Matlab or Labview. Therefore, for proof of concept testing it was decided to use an ADAFRUIT microphone and pre-amplifier development PCB in conjunction with an Arduino board to read the analogue signal.

Table 9-1 : Cost of sensor E hardware

Vendor	Part	Qty	Unit cost	Line cost	System Total
Rapid	Adafruit microphone + amplifier	1	£8.53	£8.53	
Amazon	Power supply	1	£4.99	£4.99	
Rapid	LinkitOne PCB (Arduino compatible)	1	£44.24	£44.24	
					£57.76

The microphone PCB and functional diagram are shown in Figure 83 and the circuit connected to a LinkitOne PCB in Figure 84.

There was no obvious noise present in the rig setup and therefore it was decided that this should be tested on the substation. Initial testing involved connecting the mico-phone to an oscilloscope to first determine if there was any signal worth recording before adding in the complexities associated with measuring 100Hz hum with a sensor platform.

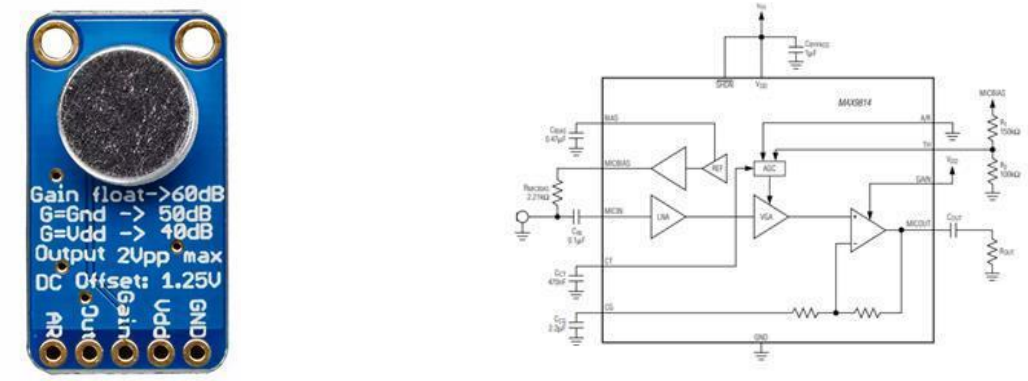

Figure 83: Photo of micro-phone and its functional diagram

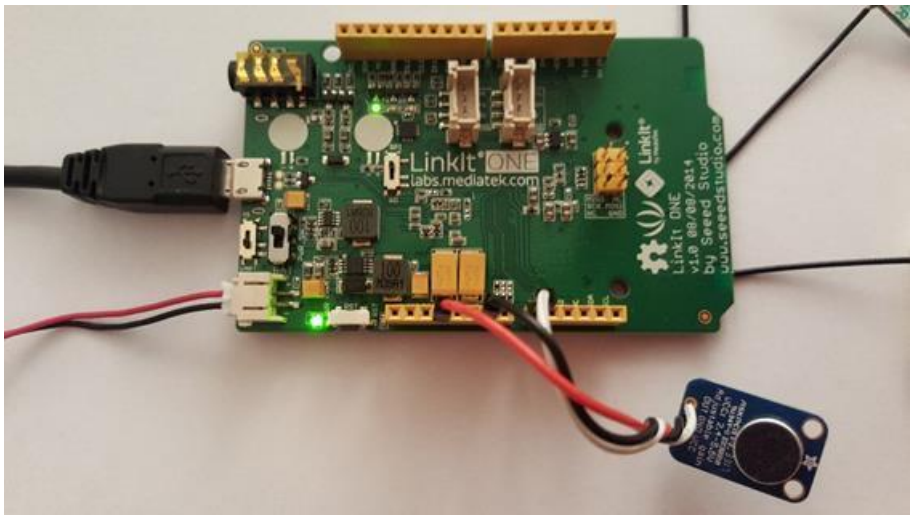

Figure 84: Photograph of microphone connected to LinkitOne board

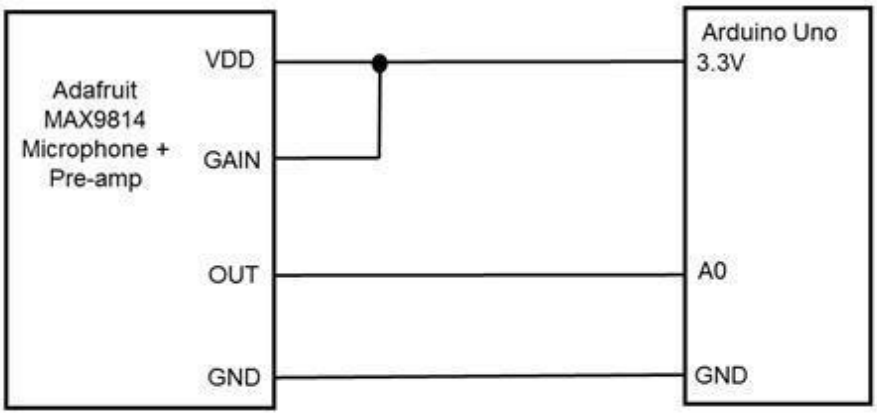

Figure 85: Wiring diagram of Adafruit MAX 9814 development board and Arduino

9.2 Substation testing

This sensor was tested straight onto an active substation where there was a human audible hum from the transformer. The sensor data was recorded on an oscilloscope in the first instance and the noise recorded and then filtered. Figure 87 shows the raw data and then this data filtered through a low pass filter and a band pass filter. The colours are as follows: Blue : origin signal, Red: LP filtered signal and Greed: BP filtered signal .

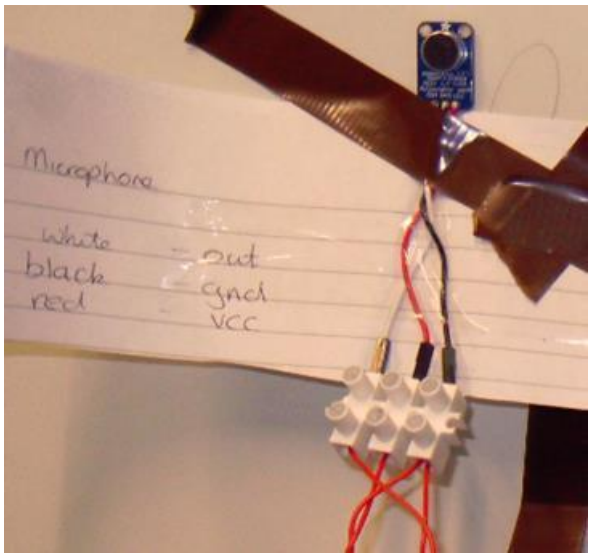

Figure 86: Micro-phone taped to transformer casing

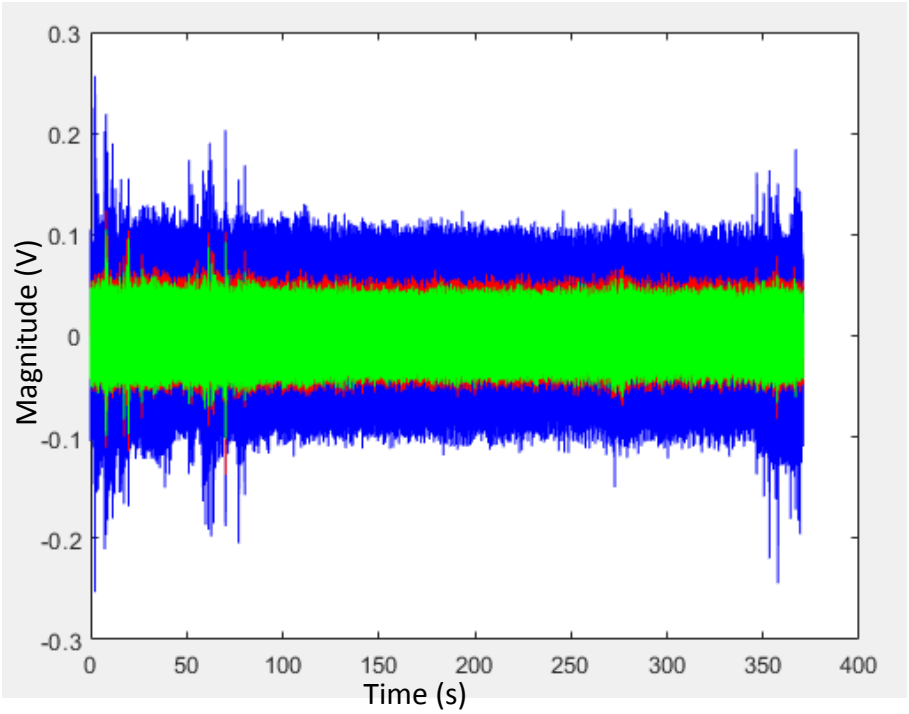

Figure 87: Micro-phone noise captured on the scope and passed through filtering (x-axis is time and y-axis magnitude)

To allow a more meaningful analysis a fast fourier transform of the signal was undertaken in Matlab in order to understand the frequencies of the noise source. This is shown in Figure 88 and Figure 89 is the equivalent plot that has been filtered. There is a clear 100Hz noise signal.

To determine if there is any relationship between this and the loading, an rolling 10s average of the 100Hz component of the noise was plotted against the load current in Figure 90.

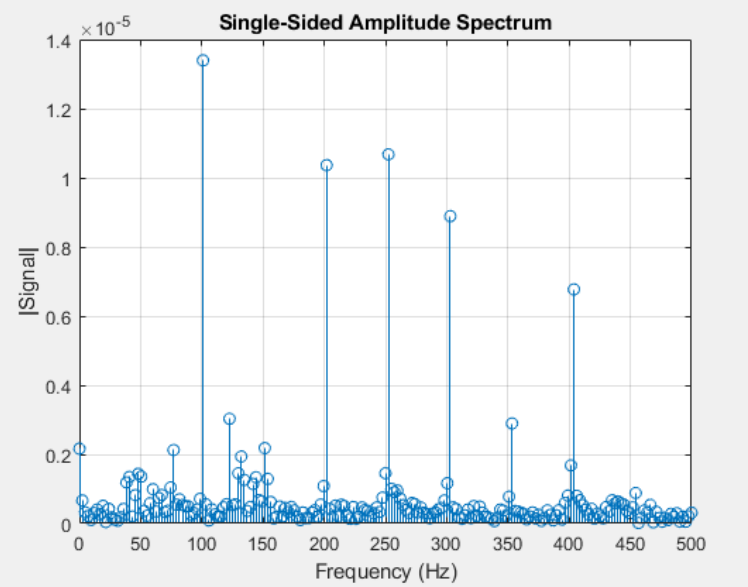

Figure 88: Micro-phone noise captured on the scope with fft analysis

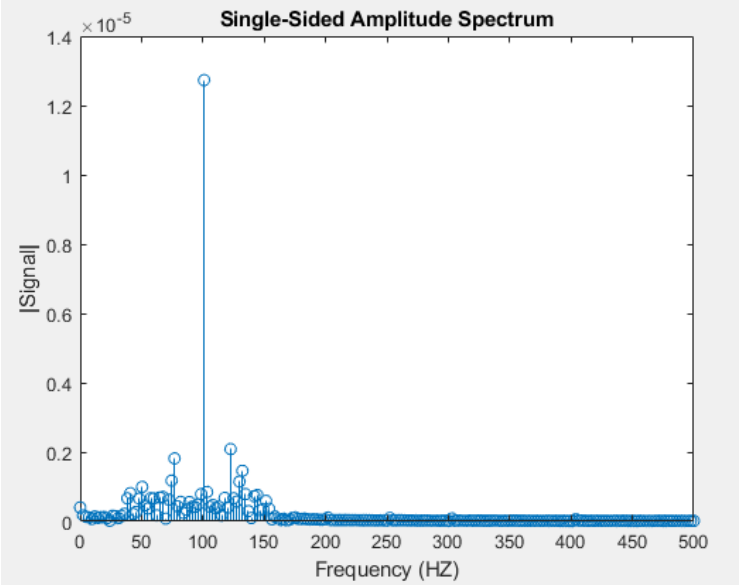

Figure 89: Micro-phone noise captured on the scope and passed through filtering and fft

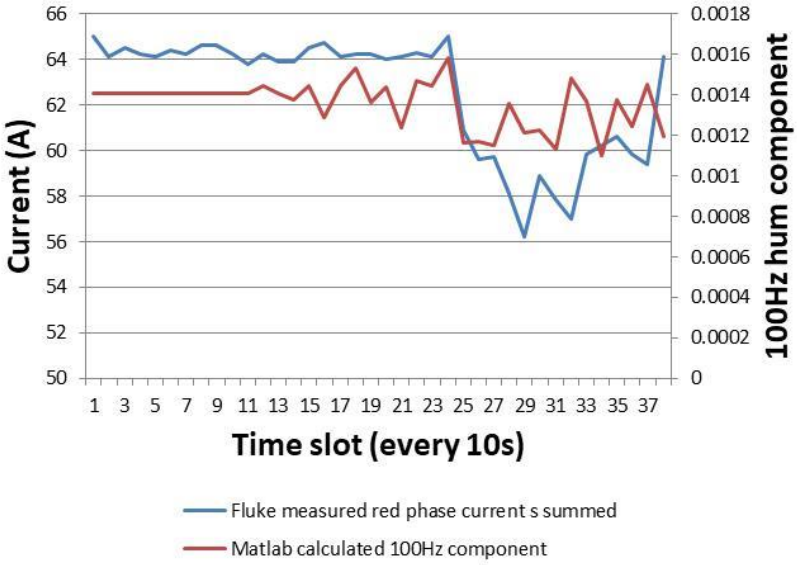

Figure 90: Micro-phone noise captured on the scope and passed through filtering and fft and time varying over a window (red) in volts plotted against time and current (dark blue)

The correlation between the 100Hz noise component and the load current is calculated as 0.48. This equates to a weak correlation.

LP 24	The testing undertaken indicated that it was not going to be possible to relate noise with loading.

LP 25	Even if further testing proved there to be a relationship between loading and noise under more highly loaded transformers it would require a significant amount of work to develop the maths and calibration process required for large scale roll out. It is unlikely that the calibration procedure could be achieved in a low enough time scale to keep the costs of installation below £50.

LP 26	There would also be challenges involved in capturing the data at a high enough sampling rate to enable a fast Fourier transform to be undertaken to pick up the 100Hz component. None of the low cost platforms had this capability and an FPGA board would probably be required. These are significantly more expensive at the moment but are dropping in price.

9.3 Summary

A microphone is not a promising candidate for long scale testing. There is some evidence of correlation between noise pick up and load but this is very weak. In addition there is a not insignificant amount of post-processing then required to extract the 100Hz component and the process this and determine a load current. This would be site specific and a calibration technique would be required on site to associate a load with a 100Hz component. It is unlikely that type calibrating in the laboratory would allow roll out over different sites because of the variation of transformer type and size on the Network. The signals would also be at risk from other noise sources.

	Comment
Functionality	Not clear
Failure mode	Fail dead
Stability/reliability	Difficult to gather meaningful data and post processing is very data intensive
Ease of deployment	Needs packaging and linking to hardware platform
Calibration	Would definitely need calibration as no direct link between load and 100Hz component of noise for all transformer types as there are too many independent variables

Test	Comments
Linearity	Unable to gather meaningful results
Effect of adjacent steel work	NA
Effect of adjacent conductors	NA
Effect of temperature	Unable to gather meaningful results
Accuracy	Unable to gather meaningful results
Correlation with load	0.48
Sensitivity	Unable to gather meaningful results
Repeatability	Unable to gather meaningful results
Power/excitation	Linked to hardware platform and powered through 3.3V serial link

10 Sensor F: Strain gauge

10.1 Hardware

The strain gauges were attached to the cable so that any thermal expansion under load is detected by the strain gauge.

Two types of strain gauge were assembled for testing.

1) A quarter bridge gauge, which has a long coil designed for use on problematic materials, this requires that 3 matched resistors are used to complete the Wheatstone bridge circuit as shown in Figure 91.
2) A full bridge gauge was also used as shown in Figure 92. This has the advantage that the 4 resistances in the bridge circuit have identical resistance and temperature coefficient of resistance

There are several key challenges in the use of strain gauges on cables. Most adhesives don't bond well onto polythene including cross linked polyethylene (XLPE). Two specific adhesives are available for use with polythene.

- 3M-High-Performance-Industrial-Plastic-Adhesive-4693 www.3m.com/3M/en_US/company-us/all-3m-products/~/3M-High-Performance-Industrial-Plastic-Adhesive-4693/?N=5002385+3293241344&rt=rud
- Loctite plastics bonding system www.loctiteproducts.com/p/sg_plstc/overview/Loctite-Plastics-Bonding-System.htm

The 3M product is a viscous resinous product whereas the Loctite product consists of a cyanoacrylate ('superglue') adhesive with a surface pre-treatment for plastics with hard to bond surfaces. The Loctite product was used and appeared to work well.

The output from the bridge circuit is a voltage signal in the μV range, therefore, an amplifier circuit is required. The university uses strain gauges within mechanical engineering and they have a bespoke amplifier circuit as a pre-packaged system which is kept under properly calibrated conditions. This was tried in the first instance. The bespoke box is expensive as it includes an analogue meter. It is should be noted that it is notoriously difficult to set up strain gauges.

Figure 91: 150 mm quarter bridge strain gauge

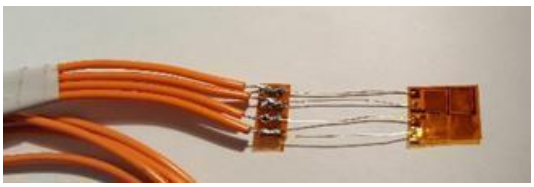

Figure 92: 4mm full bridge strain gauge

Table 10-1 : Cost of sensor F hardware

Vendor	Part	Qty	Unit cost	Line cost	System Total
Omega	4mm 1k Ohm full bridge	1	£17.50	£17.50	
Omega	terminal pad	1	£5.70	£5.70	
	University amplifier circuit (cost approx.)	1	£6.77	£6.77	
RS	240R resistor	1	£0.57	£0.57	
Amazon	Power supply	1	£4.99	£4.99	
Rapid	LinkitOne PCB (Arduino compatible)	1	£44.24	£44.24	
					£79.77

The cost of the hardware is shown in Table 10-1 while the wiring diagram is in Figure 93.

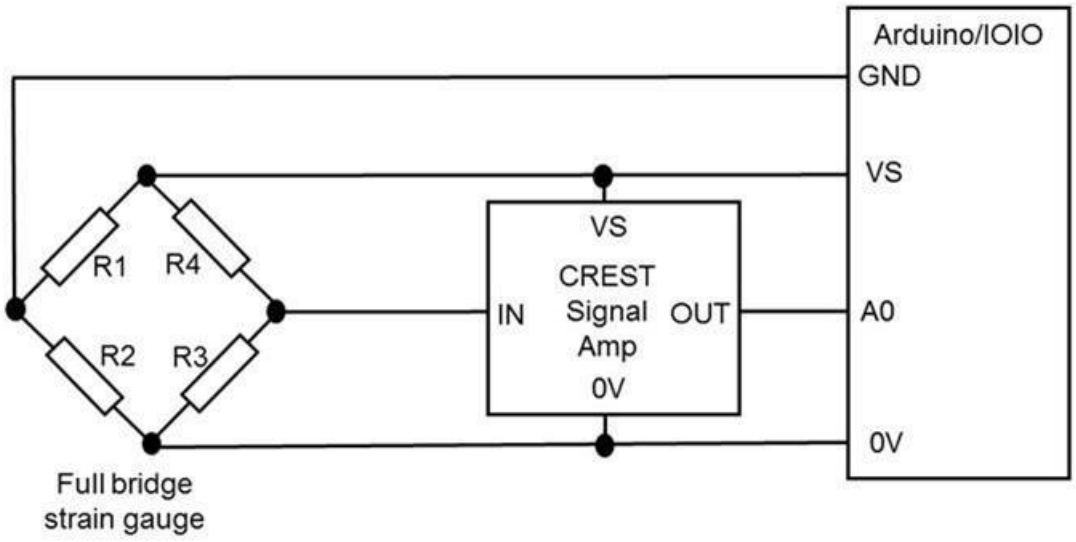

Figure 93: Wheatstone bridge circuit used for strain gauge measurement, where VS is the supply and OUT is the amplified voltage signal to be measured by analogue input A0.

LP 27	The long quarter bridge strain gauge was difficult to attach and came loose easily. Therefore, it is not recommended

10.2 Rig testing

Figure 94 shows the calibration unit from the mechanical engineering department at Loughborough. This unit is used to help the mechanical engineers get the strain gauges working and has detailed instructions. The output can also be sent to an oscilloscope.

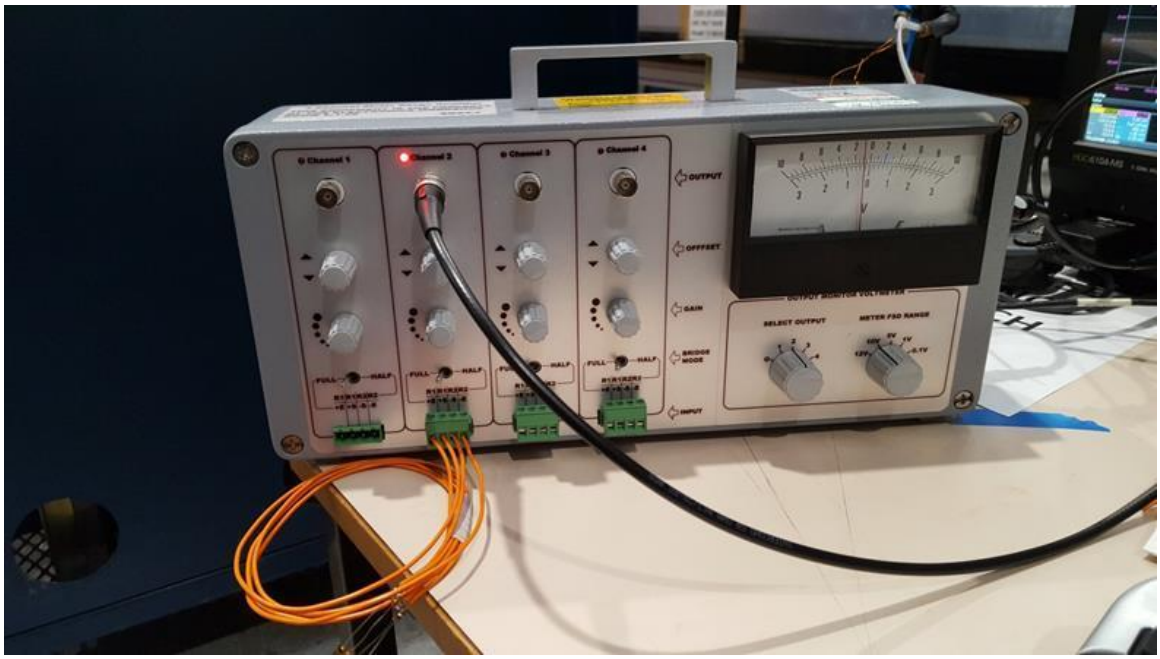

Figure 94: Photo of bridge and amplifier test unit from Loughborough

The full bridge and quarter bridge strain gauge were connected to the 3 phase and single phase cables respectively to try and determine if loading on the cable produced sufficient thermal expansion to be measurable. Figure 95 shows the full bridge strain gauge connected to the 3 core cable on the test rig.

Figure 96 shows how this is connected internally as the data sheet did not have a detailed wiring diagram and the cabling had to be traced under a magnifying lamp.

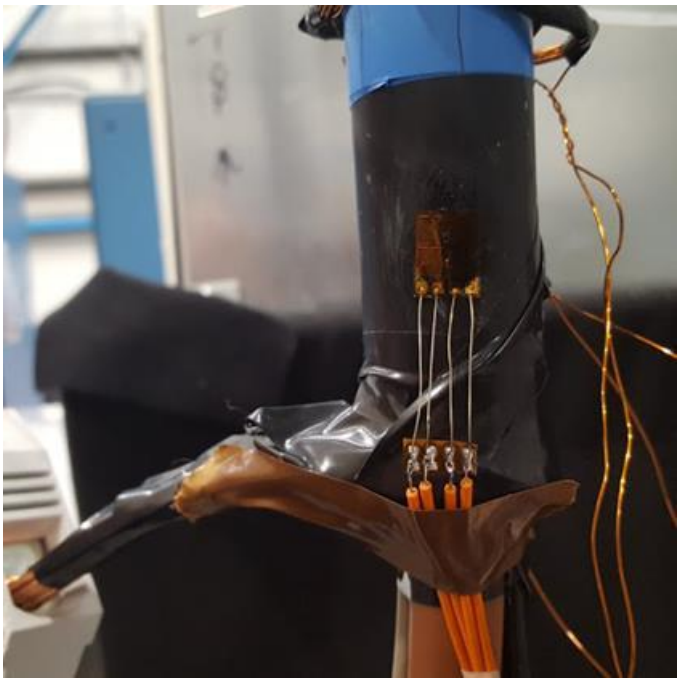

Figure 95: Photo of full bridge strain gauge. The enamel wires to the right are from sensor C, the wires into the white terminal block to the left are the copper screen of the cable.

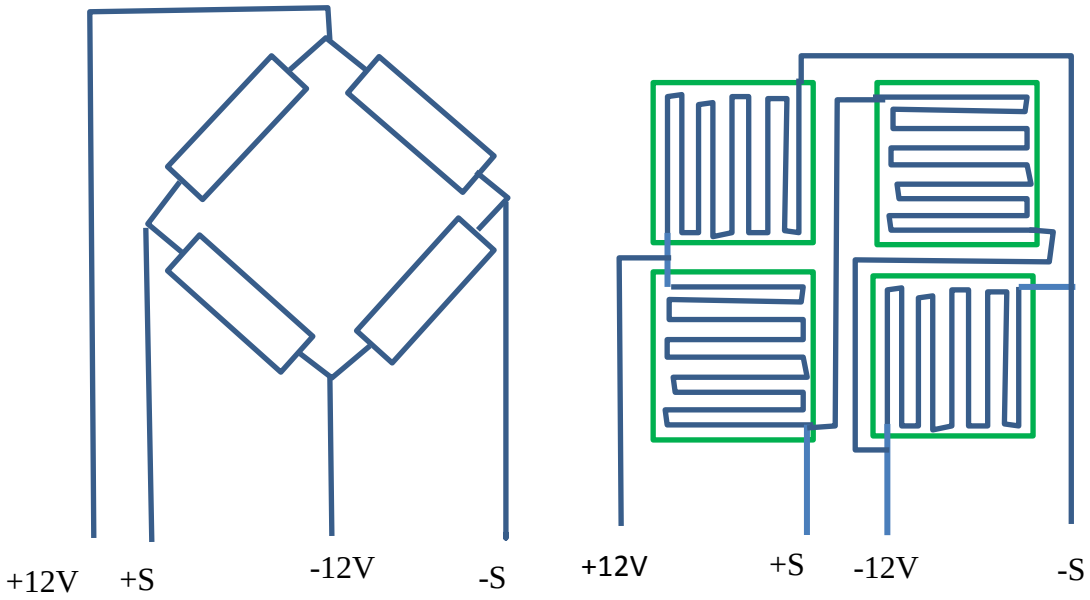

Figure 96: Connections of full bridge strain gauge.

The results of the full bridge strain gauge under different load currents are shown in Figure 97 and Figure 98. There is some evidence on the scope of a shift in Wheatstone bridge sensing element with load current. However, the signal has a clear noise pick up but the correlation between average output and load current is acceptable at -0.93.

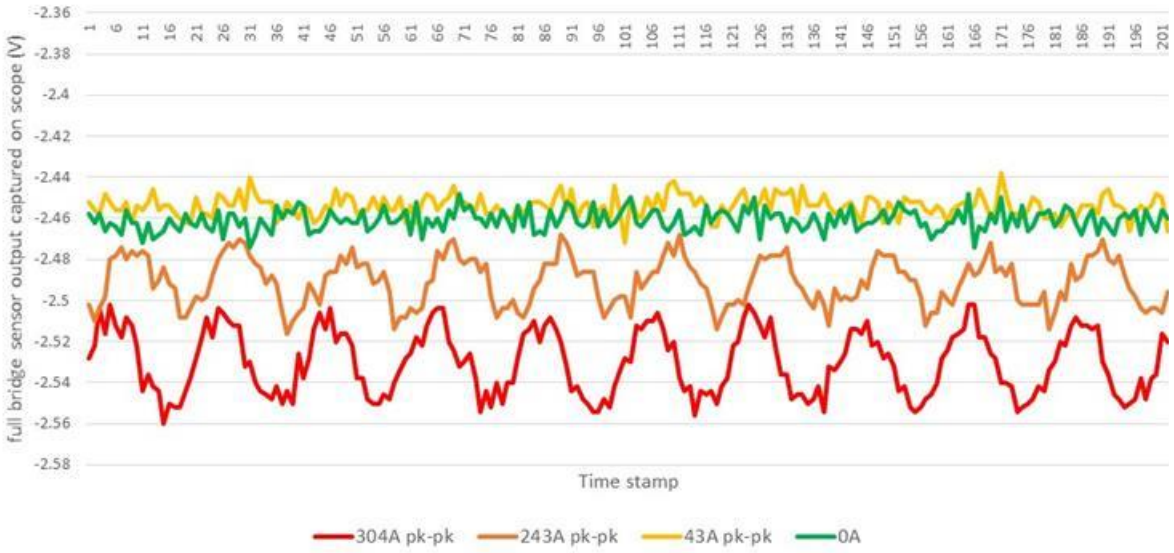

Figure 97: Sensor measure on full bridge strain gauge showing ac noise pick up as well as dc variation

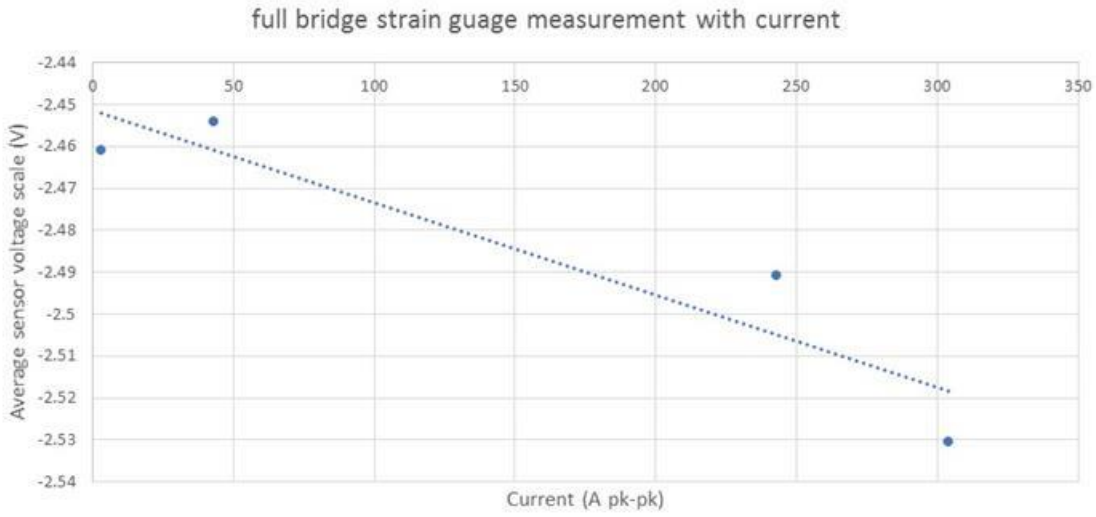

Figure 98: Sensor measure on full bridge strain gauge current against sensor reading

LP 28	The strain gauge did show some correlation between strain gauge measurement and load current. However, this was not very accurate.

The experiment was repeated with a quarter bridge strain gauge. This was done on the single core cable as there was more space on this one for the length of the sensor. The results are not as good and there is at least one spurious result as shown in Figure 99 and Figure 100). This results in a poorer correlation of -0.16 which indicates almost random correlation because of the spurious result.

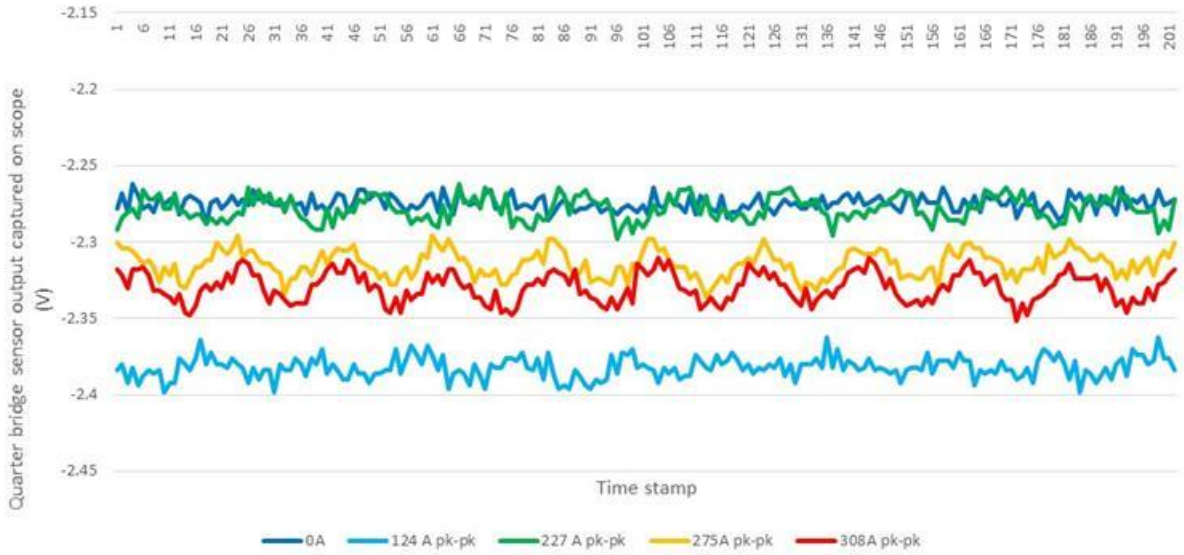

Figure 99: The quarter bridge strain gauge showing ac noise pick up as well as dc variation plus a spurious result at 124A. The different coloured plots represent different currents in the multicore cable under test.

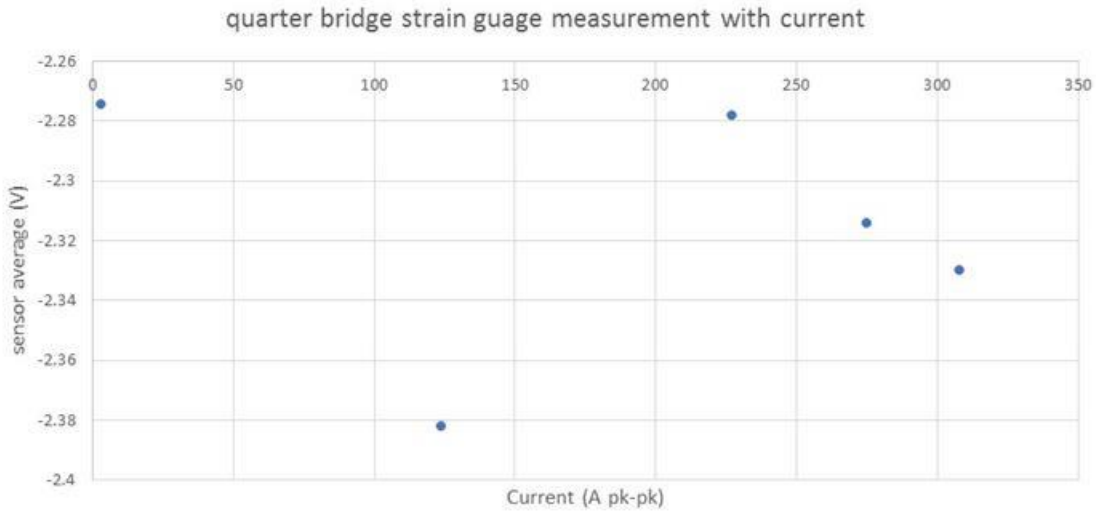

Figure 100: Sensor measure on quarter bridge strain gauge current against sensor reading

LP 29	The quarter bridge strain gauge measurements were less accurate and there was at least one ambiguous data point. This type of strain gauge is not recommended.

It isn't practical to use the wheatstone bridge from Mechanical engineering to undertake long term experiments as this unit is more costly than the target budget. Therefore, a PCB version was made up and provided by the technicians. The circuit for this is shown below. This was connected to the full bridge circuit as shown in Figure 102.

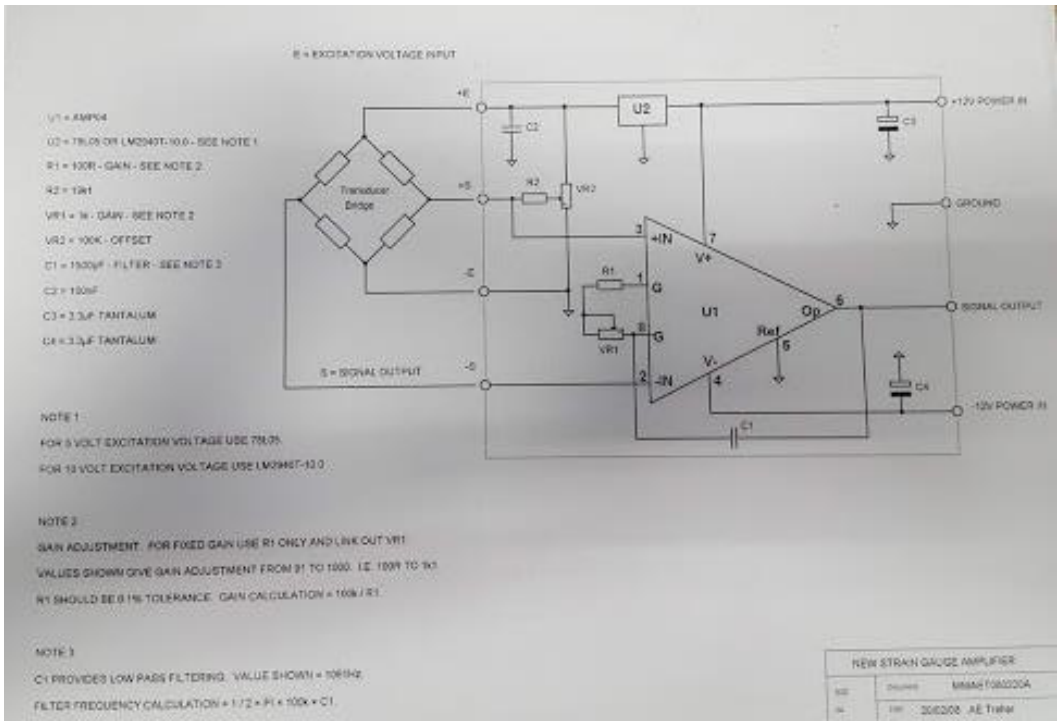

Figure 101: Strain gauge PCB circuit

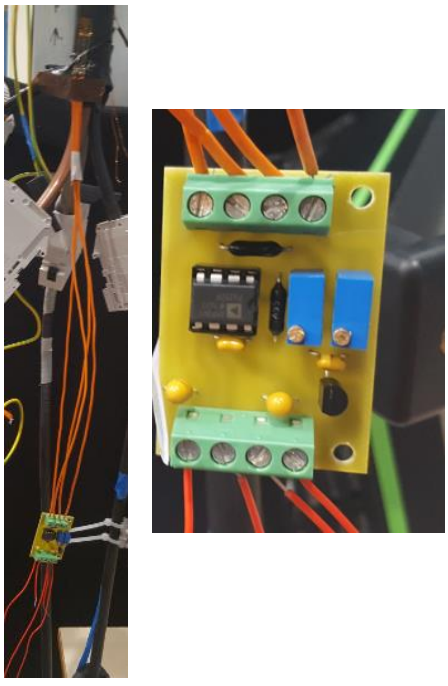

Figure 102: Sensor measure on full bridge with amplifier circuit

No meaningful results were obtained using the small amplifier circuit. This just highlights the difficult of these types of measurements.

10.3 Summary

A strain gauge is not a promising candidate for long scale testing.

	Comment
Functionality	Unlikely to be useful
Failure mode	Fail dead
Stability/reliability	Unstable values
Ease of deployment	Needs packaging and linking to hardware platform with Wheatstone bridge with variable resistors which would need setting up on site.
Calibration	Difficult to do on site

Test	Comments
Linearity	Some evidence of linearity on test rig
Effect of adjacent steel work	NA
Effect of adjacent conductors	NA
Effect of temperature	A full bridge circuit is not impacted by temperature as this is compensated for. A half bridge circuit is.
Accuracy	Estimated to be around 25% out at higher currents and worse at lower loading
Correlation with load current	-0.91
Sensitivity	Overly sensitive
Repeatability	Some repetition possible
Power/excitation	Linked to hardware platform and Wheatstone bridge. The higher the supply voltage (within limits) the easier it is to see a reading. The output is also linked to an Amplifier which may be susceptible to OpAmp drift. The power requirements +/-12V are incompatible with low voltage consumer electronics so additional power conditioning would be needed.

11 Sensor G: Temperature sensors

As current passes through a conductor it heats up due to I^2R losses. Two approaches are investigated to detect this rise in temperature to try to relate back to load. The first is the ultra-low-cost approach of using temperature labels, traditionally used to alert technicians to a temperature problem during routine inspections. The second approach investigates the cost to transmit an over-temperature signal by GPRS.

There are several issues that are important to consider when developing a measurement strategy. In many cases an indirect measurement leading to an inferred value may not be directly portable between different substation environments because of changes to hardware and other parameters that may be present in the system. An example of this is inferring transformer loading through transformer top oil temperature.
In the WPD run FALCON project several distribution transformers were monitored over a year and the parameters used to tune a model of each transformer which could then be used to infer the loading based on the measured transformer top oil temperature and ambient temperature
This process is complicated for several reasons;

- There is a large variety in transformer size, type, manufacturer, year of manufacture etc so very few transformers are the same
- There are three different models of a transformer that can be used. In FALCON the IEC60076 model provided a better correlation to the measured data and was deemed the most appropriate for use with the Distribution transformers under study.
- The models rely on information which if not given (almost certainly not available) needs to be estimated through a calibration tuning process. This information includes; R (ratio of load losses at rated current to no load losses), $\Delta\theta_{or}$ the top oil temperature at rated load, $\tau_o$the oil time constant.
- Fixing R to a typical value based on transformer size allows a real value of load to be used to tune the other two parameters using a weighted regression method
- The method needed to be applied over the period of a week to tune the parameters but was then sufficiently accurate across the seasons.
- The accuracy with which each top oil parameter could be calculated from loading data and ambient air temperature to check the tuned parameters was variable from <1% up to >5%

This then results in an onerous process of calibrating each transformer temperature measurement in situ. The data needs to be stored for a week and then analysed to allow the parameters to be tuned before being updated into a processor to allow for data values to be inferred. Any changes to the transformer (e.g. adding additional cooling) will result in the need for re-calibration. The measurement system is dependent on the ambient temperature, so this also needs to be recorded and used in the calculation. Wind and solar effects were indicated in work by EA Technology [29] to be negligible.
As direct physical models are complex to produce, and many rely on detailed layout information. It is not practical to develop the sensors based purely on a theoretical

approach as the time necessary, for example, to calculate the magnetic field at any point due to 3D current flows is complex and time consuming and not likely to be accurate Therefore, a practical empirical method of calibrating sensors will be used.

LP 30	Calibrating a temperature measurement in one location with or without Utility found equipment does not guarantee calibration in other locations or with other pieces of equipment.

LP 31	Temperature calibration may change due to external influences such as temperature or over time.

11.1 Sensor G1: Thermal stickers/transducers

Four main types of dynamic labels were procured for testing on live conductors:

1) Reversible temperature labels, which show the real-time temperature.
2) Irreversible temperature labels which show the maximum temperature which has been reached
3) 'Timestrip' Time duration labels, which shows the duration since the label was activated by pressing a button.
4) 'Timestrip Plus' Temperature duration labels which show the duration the label has been at a given temperature

The concept of this sensor type is that once the individual label types are proven, a combined label would be designed for use by DNOs or other electrical operation and maintenance (O&M) organisations which would include all 4 types in a single label, with temperatures optimised for electrical conductors and time durations optimised for DNO substation inspection regimes. At present this information is not automatically transmitted back to a central data store, but as the technology is very low cost – it is being investigated.

Table 11-1 : Cost of sensor G1 hardware

Vendor	Part	Qty	Unit cost	Line cost	System Total
RS	Temperature Label, 40°C to 71°C, 9 Level	1	£1.11	£1.11	
RS	Temperature Label 71°C to 110°C	1	£1.17	£1.17	
Sigma Merck	temperature duration label 2	1	£1.00	£1.00	
Sigma Merck	temperature duration label 3	1	£1.00	£1.00	
					£4.28

Leaving the stickers on the cable on the test rig yielded very little in the way of information. The tests being run were not at sufficiently high temperature to heat the cables and there was no changes to the label during the test runs. Eventually a hair dryer and a remote

thermometer were used to elicit a response. The reading on the 40°C to 71°C label went up to 48°C. However, the remote thermometer only read about 58°C as a maximum when pointed at the label through the test. This suggests that this is not a very accurate method of determining the temperature. It was impractical on the rig to elicit a response from the temperature duration labels as there is insufficient heating over long periods of time to trigger a response.

Figure 103: Thermal sticker change after hairdryer

LP 32	Thermal stickers are low cost devices that show temperature. However, it is not clear if there is a business case for their use as these would need to be manually observed.

11.2 Sensor G2: Temperature alarm

A thermistor was chosen for use as a temperature sensor as they are low cost and require minimal extra circuitry to produce a voltage signal related to temperature. Therefore, thermistors are commonly used in consumer electronics devices such as programmable thermostats and temperature displays.

This circuit uses a voltage-controlled switch based on a transistor. The output of the transistor is used to trigger the input of an alarm system auto-dialler module.
Auto-dialler modules can be used to call preprogramed numbers and give recorded spoken messages or to send text messages, typically for alarm systems. The auto-dialler was used as an expedient proof of concept but could be replaced with a cheaper low-end microcontroller and a GPRS chip.

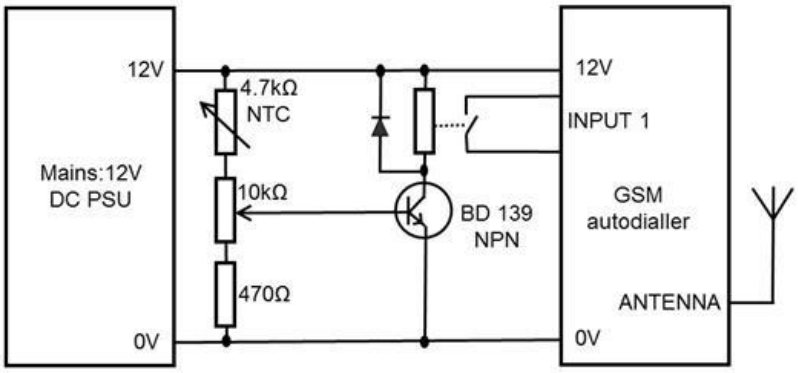

Figure 104: Circuit diagram of temperature switch circuit.

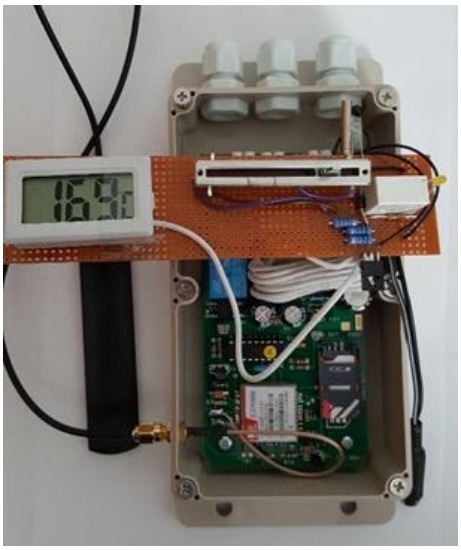

Figure 105: temperature alarm with GSM text message warnings. The LCD display is a self-contained unit used for testing.

LP 33	A temperature alarm works fine from detection through to received text message. It is an expensive option compared to some of the other sensors and platforms which could offer better data at higher fidelity for lower price.

LP 34	A temperature alarm sensor would not to be calibrated on site – as it is not directly looking for a load current – but would look instead at ensuring that the tank temperature (as a proxy for top oil temperature) did not exceed values set by standards (60^{o}C above 20^{o}C ambient BSEN600-76-2_2011).

Table 11-2 : Cost of sensor G2 hardware

Vendor	Part	Qty	Unit cost	Line cost	System Total
RS	BD 139 BP NPN transistor	1	£1.00	£1.00	
RS	stripboard	1	£4.24	£4.24	
RS	10k NTC thermistor 5% tolerance	1	£0.51	£0.51	
RS	100k Pot	1	£1.44	£1.44	
RS	1k resistor	1	£0.02	£0.02	
RS	12v relay	1	£0.48	£0.48	
RS	1n4007 diode	1	£0.48	£0.48	
RS	power supply	1	£9.78	£9.78	
RS	220Ω ±5% 1W	1	£0.09	£0.09	
RS	10k potentiometer	1	£0.24	£0.24	
RS	hook up wire	1	£2.70	£2.70	
gsm-activate	GSM auto-dialler	1	£78.33	£78.33	
					£99.31

11.3 Rig testing

The temperature alarm and auto-dialler sends an automatic text signal which was proven to work. However, it is also possible to look at directly obtaining a value from the thermistor to get a time varying signal. It should be noted that in the field there is a time delay between load current and cable/transformer heating up. So this would need to be considered. The thermistor circuit was attached to the cable and connected to the IOIO board which was hooked into a phone as shown below.

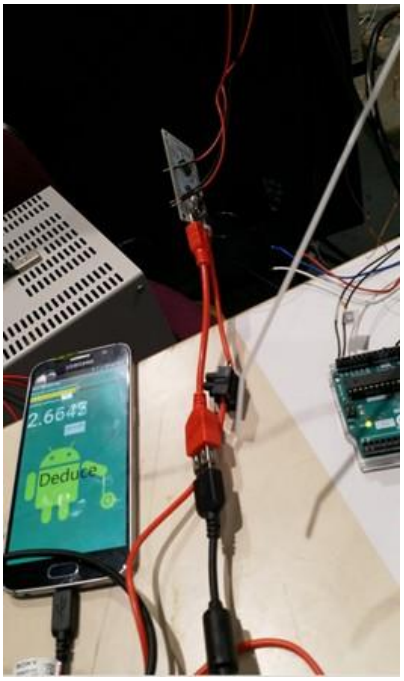

Figure 106: IOIO board recording reading on mobile App

As the load current was insufficient to heat the cable a hairdryer was used to check that a suitable response was obtained. It was difficult to get a fix on the temperature with the remote thermometer. However, Figure 107 shows the variation in temperature against the IOIO reading taken over several heating and cooling cycles. The difficulty of temperature measurement is impacting the reading and it is almost certain that if this were repeated in a proper thermal chamber that significantly better results would be obtained. However, as a first stage rough test it shows that temperature does give an appropriate reading into the platform.

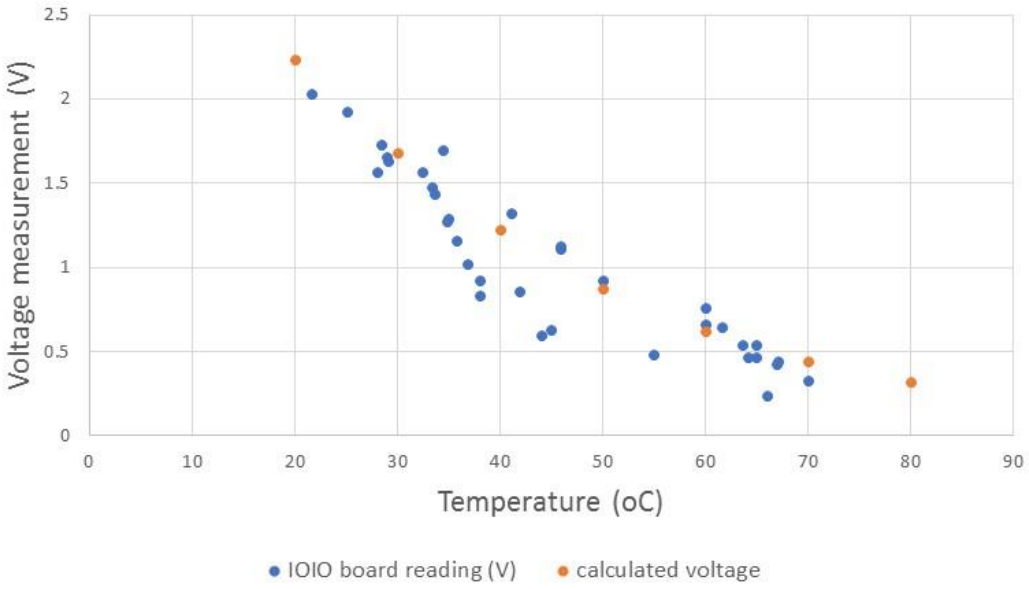

Figure 107: Thermistor reading against temperature measured with a thermal camera being heated by a hairdryer

As an aside it was easier to get the thermistor working this way round (voltage decreases with temperature) to stay within the 3.3V limits of the IOIO board- but as the temperature increases the measurement accuracy reduces giving lower accuracy at higher temperature. This would need to be swapped over if further testing were to be done such that a higher temperature gave higher voltage to improve accuracy.

11.4 Substation testing

An attempt was made to capture data on the substation – but with such low loading there was no possible way that this would result in anything meaningful.

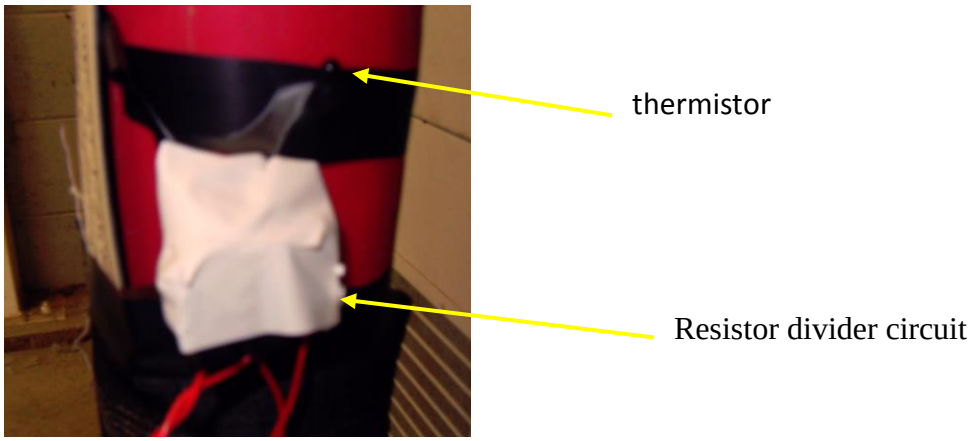

Figure 108: Thermistor connected to 11kV cable

LP 35	It should be possible to link a temperature measurement device such a thermistor to a transformer to give an indication of loading. However no representative hardware was available to test properly and calibration on site may be needed.

11.5 Summary

A temperature measurement device is not a promising candidate for long scale testing.

	Comment
Functionality	Not clear
Failure mode	Fail dead
Stability/reliability	Stable and reliable
Ease of deployment	Needs packaging and linking to hardware platform
Calibration	Would definitely need calibration as no direct link between load and transformer top oil temperature because of transformer variability

Test	Comments
Linearity	Linear – but within temperature limits
Effect of adjacent steel work	NA
Effect of adjacent conductors	NA
Effect of temperature	Difficult to do under the test conditions available
Accuracy	Unable to gather meaningful results
Correlation	Unable to gather meaningful results. Also there would be a time lag that would need to be considered
Sensitivity	Unable to gather meaningful results
Repeatability	Unable to gather meaningful results
Power/excitation	Linked to hardware platform and powered through I/O power connector at 5V or 3.3V

12 Sensor H: Thermal imaging

12.1 Hardware

An alternative to looking measuring temperature is to try thermal image detection. The principle was tried first using a normal SLR camera and had the concept worked the principle would have been be applied to a mobile phone camera. A digital SLR was modified at CREST by replacing the infra-red blocking filter inside the camera with a visible blocking filter, thereby converting the camera to an infra-red camera. A remote-control camera release was also fitted to prevent camera shake and enable long timed shutter release times.

Figure 109: Modified DSLR camera

The parts used were:

- Canon EOS 400D
- Nikkor 35mm AF prime lense
- YongNuo MC-36R wireless remote control
- Visible light blocking filter

Settings:

The following settings were used on the camera:

- Aperture: F5.6
- Exposure: 5 seconds
- Focus: 0.5m (manual)
- ISO: 500

The settings were informed by previous work at CREST using infra-red photography for electro-luminescence imaging of solar photovoltaic modules.

12.2 Rig testing

Focusing was done manually by measuring the distance to the object since the auto focus system doesn't work with the modified optical path.

As seen in Figure 110 there is no appreciable difference in colour or brightness in the cable with a 40°C temperature rise. The tape measure in the image is a focusing aid since the cameras manual and autofocus features are calibrated for visible wavelengths. The experiment was intended as a proof of concept if successful a repeat test would have been attempted with a modified smartphone, but it was decided not to progress this concept any further.

Figure 110: Infra-red image of Steel wire armoured cables (SWA) at 60°C (top) and 20°C (bottom).

LP 36	Thermal imaging using an android phone is not going to be suitable as measuring through a conventional camera by changing the filtering couldn't be made to work.

12.3 Summary

Thermal imaging is not a promising candidate for long scale testing.

	Comment
Functionality	Unable to get working properly
Failure mode	Fail dead
Stability/reliability	Unable to get working properly
Ease of deployment	Not clear as didn't proceed with development onto Phone platform
Calibration	Would definitely need calibration as no direct link between load and transformer top oil temperature because of transformer variability

Test	Comments
Linearity	Unable to get working properly
Effect of adjacent steel work	NA
Effect of adjacent conductors	NA
Effect of temperature	Unable to get working properly
Accuracy	Unable to gather meaningful results
Correlation with load current	Unable to gather meaningful results
Sensitivity	Unable to gather meaningful results
Repeatability	Unable to gather meaningful results
Power/excitation	Phone cable connector

13 Platform I: Android phone

13.1 Hardware

In addition to being a communication platform to get information from a sensor to the outside world, android phones have several in built sensors that can be used, including a magnetometer, accelerometer and micro-phone. In this report the magnetometer is the only feasible sensor that could give meaningful results.

In addition to the phone, of which there were 3 available as shown in Table 13-1. it is necessary to ensure there is a mounting available on the cable as distance impacts results. The figure below shows the mounting that was designed within the University for allowing the phone to be securely fastened to a cable to ensure distances are fixed and constant.

Figure 111: photos of hardware setup and connector

The costs below include an old mobile phone that was donated and a prototype attachment unit which was developed as part of the trial. Both costs would need to be added in for a commercial product. At present the App used within the Android phone uses Android version 6 (Marshmallow) and API 23 because the Sony Xperia phone used for testing was not upgradable to Android version 7.

Table 13-1 : Phones available for testing

	OS	API	Release date	Maximum OS	Notes
Samsung S4	4.2.2	17	2013		Not compatible with DEDUCE App.
Sony M4	5.0	23	2015	6.0	
Samsung S6	7.0	24	2015		

Table 13-2 : Cost of sensor I hardware

Vendor	Part	Qty	Unit cost	Line cost	System Total
Amazon	USB wall charger	1	£3.99	£3.99	
	Sony Xperia Android phone with built in magnetometer[1]	1	donated	donated	
Amazon	H&S 2 Smartphone Tripod Mount Clamp	1	£3.99	£3.99	
RS	cable tie	2	£0.05	£0.10	
University	3D printed base	1	£5	£5	
Charnwood fasteners	1/4 Whitworth/UNC screw	1	£0.10	£0.10	
					£13.18

[1]The cost of this phone is around £50 on ebay

The wiring of the system is very straightforward and all that is required is a power supply. However, the coding of an App which measures the magnetometer data and translates it into useful information before being uploaded automatically to a central server is very complex. This process and the settings associated with it are included in the Appendix.

13.2 Settings and software

To test the accuracy of the magnetometer to measure current it was necessary to find the exact location of the chip within the device. Disassembly of an S6 is a very involved process requiring the use of heat to melt layers of glue. Magnetometer location was therefore identified iteratively by moving the phone near a high current cable to identify the strongest signal. Figure 112 and Figure 113 show the estimated location.

Figure 112 : Photograph of Samsung S6 with the approximate position of the magnetometer marked with a red arrow.

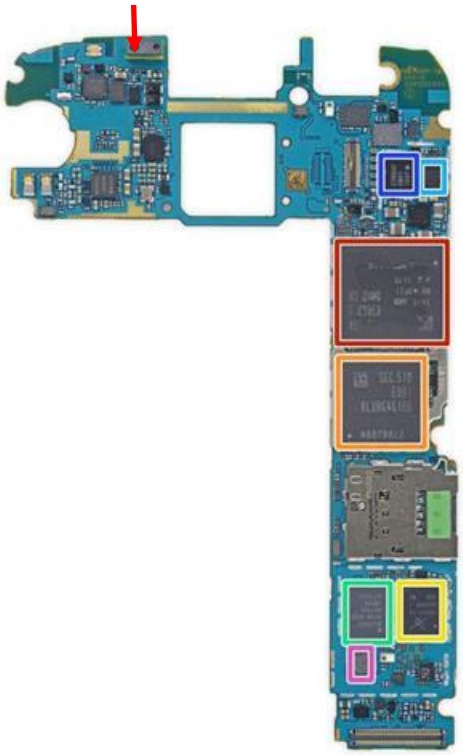

Figure 113 : Photograph showing Samsung S6 Main PCB with the approximate position of the magnetometer marked with a red arrow.

LP 37	Distance is a factor when turning magnetic field back to an estimate of load current. Therefore, the location of the sensor is important to estimate its distance from the centre of the cable.

The android API provides two sets of variables for app programmers can access

- 'Uncalibrated' which in fact is calibrated both for factory tolerances in the sensors sensitivity and transient changes in sensor sensitivity due to device temperature. This also includes a calibration factor for factors such as manufacturing tolerances and interference from metal components in the phone.

- 'Calibrated' which is compensated for so called hard-iron losses, which might change for example if the user puts the phone in a case with a magnetic latch. This calibration is done automatically by the device when sufficient device movement is detected.

User advice is to move the phone in a figure of eight motion when the phone requires calibration. Fundamentally the device needs to be rotated 360° in all three axes to recalibrate it.

13.2.1 Developing a bespoke App

One of the issues with using a mobile phone is the limitation of software available and the ability to capture data from that device. Using software from third-party developers also introduces issue of uncertainty over additional scaling factors and what sensor data is used (calibrated vs uncalibrated for example). The Apps available to date have monitoring ability and only one software solution allowed the data to be saved to the phone from which it could be extracted (although the time scale of the data capture was not available to vary).

To extract the data to a place where it could be useful it is necessary to not only write an App to extract the data from the sensor but also to send it to a server. Since the ultimate solution needs to contain information on loading as well as information on location and time stamping it is important to understand if this procedure is possible.

LP 38	It works well to use an Android phone as a control platform especially if the internal Magnetometer is being used. However bespoke App software is required to ensure methodology and Readings are transparent.

Appendix A contains some of the processes necessary to set up a phone and send the data onto the server. The lessons learnt from the process which would require future development are captured here:

- Future android phone coding needs to overcome limitations in the current code. For example, the App was setup with hardcoded sites. It will be important to have a process for adding new sites and ideally not hardcode site names.
- At present there is no requirement for access, accounts and passwords. This needs to be defined in advance of a field trial to avoid having to redo server code.
- There are limited local settings on the phone. However more settings need to be thought about and captured to give a complete picture of site where applicable (not just name)
- There is a button to delete data from the phone when it is full. However, this needs to be automated to automatically delete old records.
- The Android operating system is difficult to write code for compared with other languages. For example, it is not possible to just code task 1, then task 2 and then task3. This is because of the Android interface which behaves more like – Do task 1, Tell me when you've done task 1. This is to make the Android interface seamless to the user. This is asynchronous and away from the main thread. There are then lots of messages back and forth before task 2 can be asked for.
- At present there are lots of error and warning messages in the Android App code. These are related to user-based interfaces that are not necessarily applicable to this project. For example, if the Chinese keyboard has not been implemented. Therefore, there is a high risk of 'false-positive' error messages.

The code relating to measuring the magnetometer data and then translating this into meaningful results and uploading to a server is located on Github (an open source software depository under https://github.com/NeilStrickland/sensormonitor_client for the phone App and https://github.com/NeilStrickland/sensormonitor_server for the server App) so it has not been directly included as an Appendix. The key mechanism for undertaking the calculation uses the theory in section 5.1. A flow diagram of the process is shown in Figure 114.

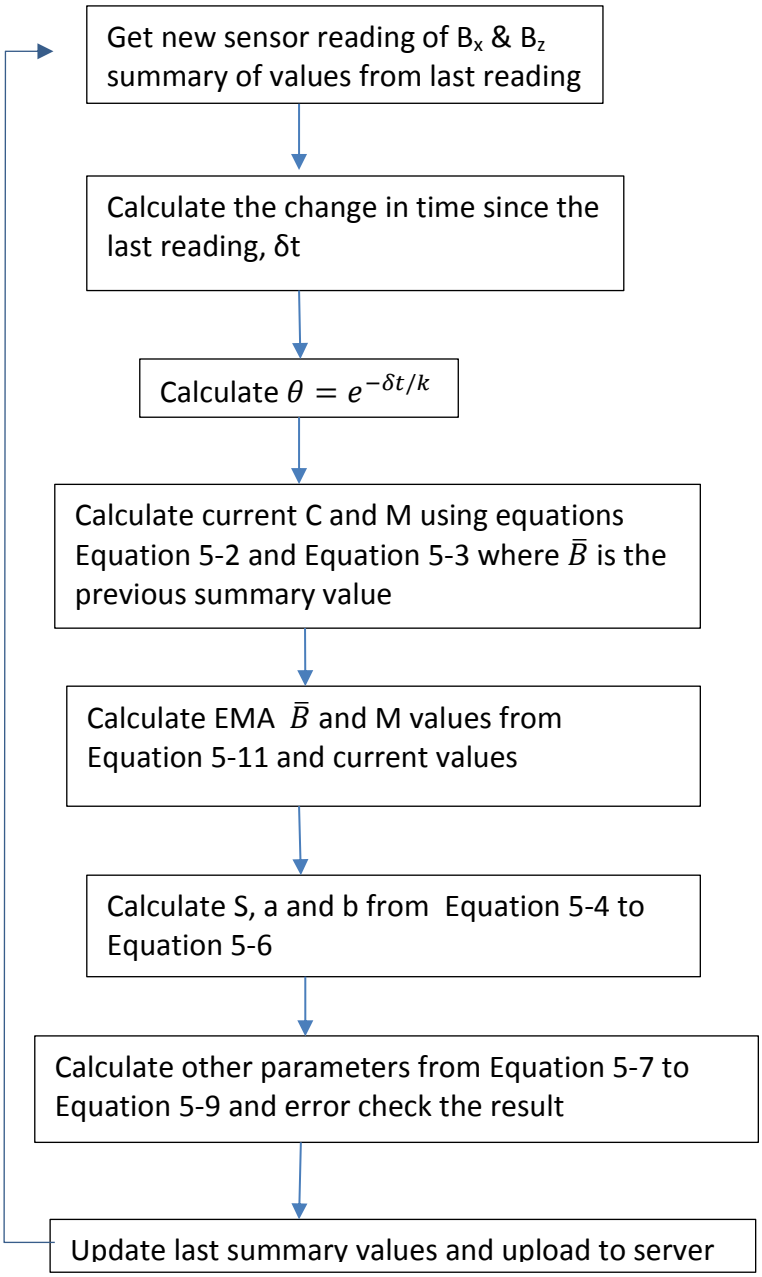

Figure 114 : Flow chart showing main calculation steps

13.3 Initial testing

Testing of a smartphone magnetometer was conducted using the following devices:

Table 13-3 : Summary of Android phones available

	Samsung S6 (SM G920F)	Samsung S4 mini GT-19195	Sony Xperia M4 Aqua E2303
Android version	7.0 'Nougat'	4.4.2 'KitKat'	6.0.1 'Marshmallow'
API version	24	19	23
Gyroscope/acceleration	InvenSense MPU6500	InvenSense MPU6k	Bosch 3060102
Magnetic	Yamaha YAS537	Yamaha YAS532	Bosch 3060102
Barometer	ST LPS25H	None	None
RGB/IR	AMS TMD49XX	Sharp GP2A	Capella CM36286

LP 39	Different phones have different sensors, and these may be in different locations within the phone. If a variety of android types are to be used in large scale testing, then any variance needs to be known so it can be accounted for.

Testing was conducted using two Apps:

- The Sensor Logger app coded by Savithru JayaSinghe of iRealitySoft, this app was chosen from several sensor datalogger apps for initial testing because it had the ability to both show data in real time and save data to phone memory in text or CSV format for ease of downloading to PC via USB cable.
- A bespoke Deduce App was coded by Prof Neil Strickland of Sheffield University, as the phone allows both "calibrated" and "uncalibrated" measurements of magnetic field and without access to the code it is not known which measurement is used in the software above. This also allowed data to be automatically downloaded to a server.

TT 7	An App which allows short term data to be logged and saved is a useful way of generating early stage results – even if it is not feasible for a long-term trial.

The current was increased from 0 to 120 Amps, each current step was held for 20 seconds. The current was then decreased back to zero. This is shown in Figure 115. To help logging of the data a large count-down timer was set to operate.

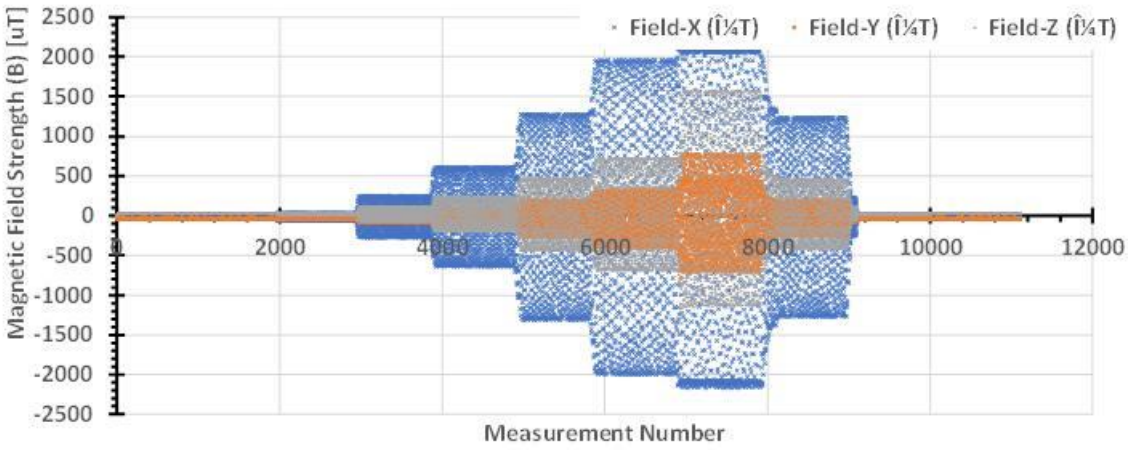

Figure 115 : Graph of Magnetic field measured against time / measurement ID using the sensor logger app on a single core cable.

LP 40	There is an obvious relationship between phone magnetometer measurement and current.

Magnetic field is reported by the android API in 3 axes X, Y and Z, where X is into the phone screen, Y is up the phone and Z through the sides of the phone. The orientation of the phone relative to the cable is shown in Figure 116.

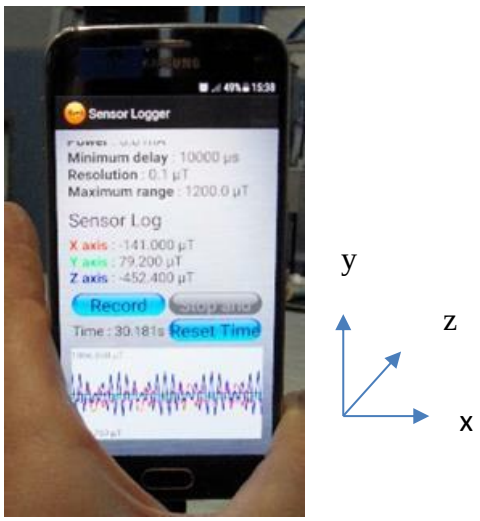

Figure 116 : Photograph showing sensor Logger.

Note that the centre of the magnetometer cannot be assumed to be exactly aligned with the centre of the cable in this test. However, one would expect to see little or no magnetic field in the Y axis, the greatest in the X axes and some in the Z axes. The current measurement is taken as the magnitude of X and Z.

LP 41	For early testing the quickest way to attach the phone to the cable was by tape. However, it means the phone is not necessarily the same distance from the centre of the cable and is not always at the same angle. This makes it difficult to test for consistency as distance is a factor. A method of fixing distance was developed to compensate for this.

The impact of the angle can be seen by plotting the X and Z components of magnetic field against each other over a fixed current value. The direct relationship between the x and y field increasing with current can also be observed as shown in Figure 117.

As the current increases – the impact of saturation of the magnetic field in the x direction can be observed as shown in Figure 118. There are several solutions that can be used to overcome this.

LP 42	At higher currents saturation may be an issue – However this can be mitigated.

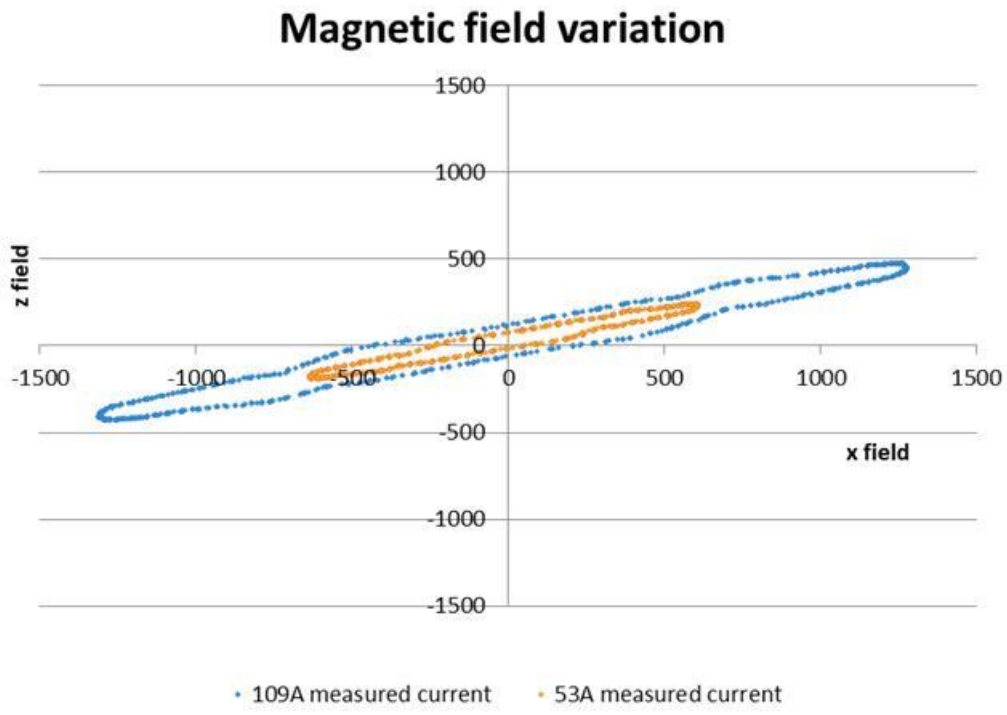

Figure 117 : Magnetic field (x vs z component) for 53A and 109A rms measured current using the sensor logger app.

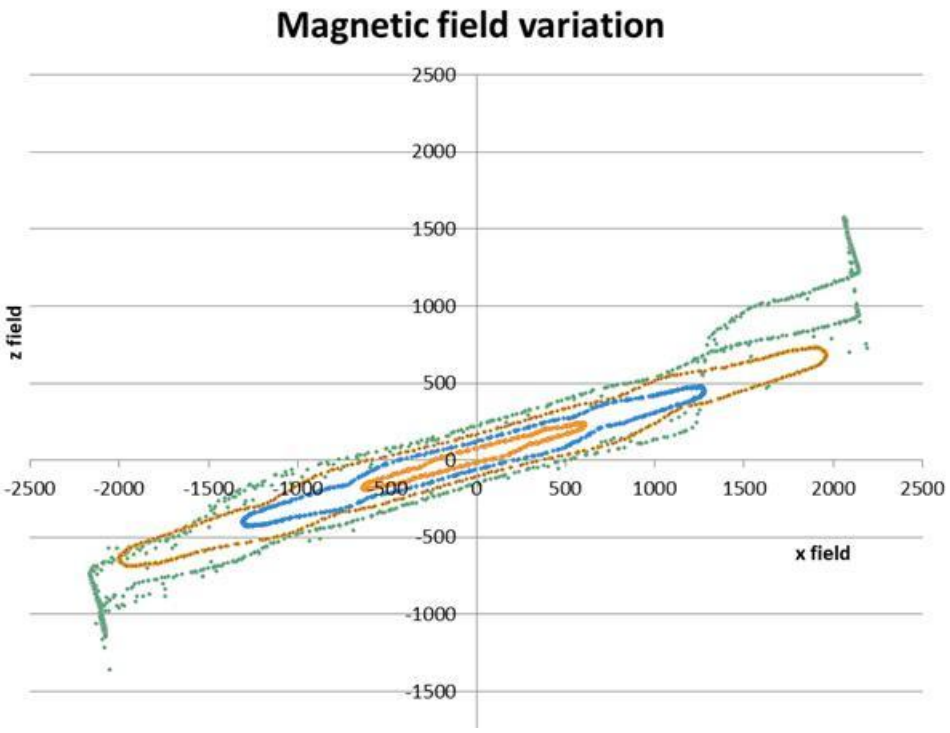

Figure 118 : Magnetic field (x vs z component) as current increase impacts of saturation on the x sensor can be seen for a current of 114A rms(using the sensor logger app).

Careful placing of the phone to utilise the z axis as well as the x axis (and even the y axis if needed) as shown below could be used. In addition, moving the sensors outwards to a larger radius will allow the same value of reading but at a higher current.

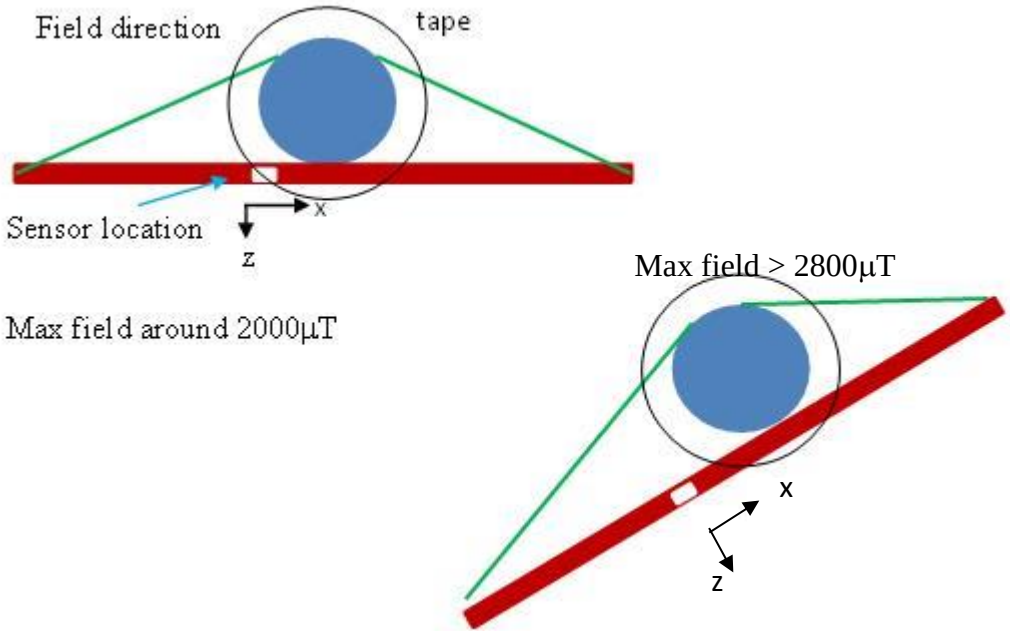

Figure 119 : Magnetic field (x vs z component) as current increase impacts of saturation on the x sensor can be seen for a current of 229A. Cross section viewed looking down the cable.

LP 43	Careful placement of the phone can be used to offset issues from saturation. As there are different ratings of substations and different cable types – it may be that a space holder is used for a range of types where angle and distance are carefully matched to rating.

13.3.1 Calibrated vs uncalibrated

As testing progressed in became apparent that there were issues around calibration. In the presence of a magnetic field and triggered by movement, the calibration factor can reset. The use of the Deduce App clearly shows when this is being applied – but it is equally visible on the sensor App.

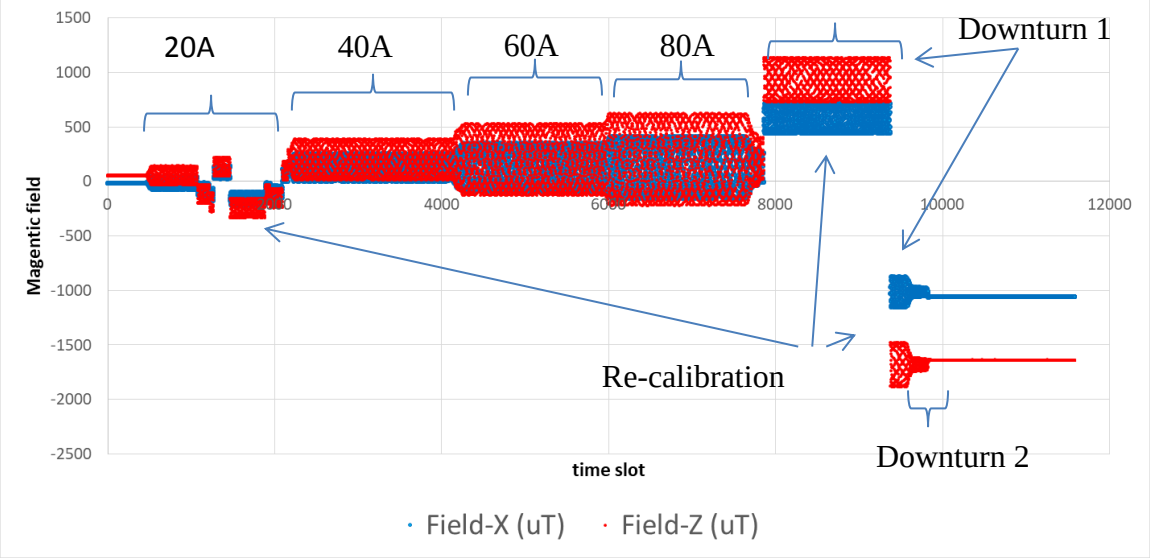

Figure 120 : Calibration factor being applied in the Sensor App on a 1 core cable by phone using Sensor App

LP 44	Using “calibrated” Android phone data can result in factors being arbitrary applied to the measurement at random points in the measurement. This is not so much of an issue for the un-calibrated data which is reported as uncalibrated plus a calibration factor.

It should be possible to remove this factor by careful analysis of the field as shown below. In this case, the sets of ellipses refer to different values of current.

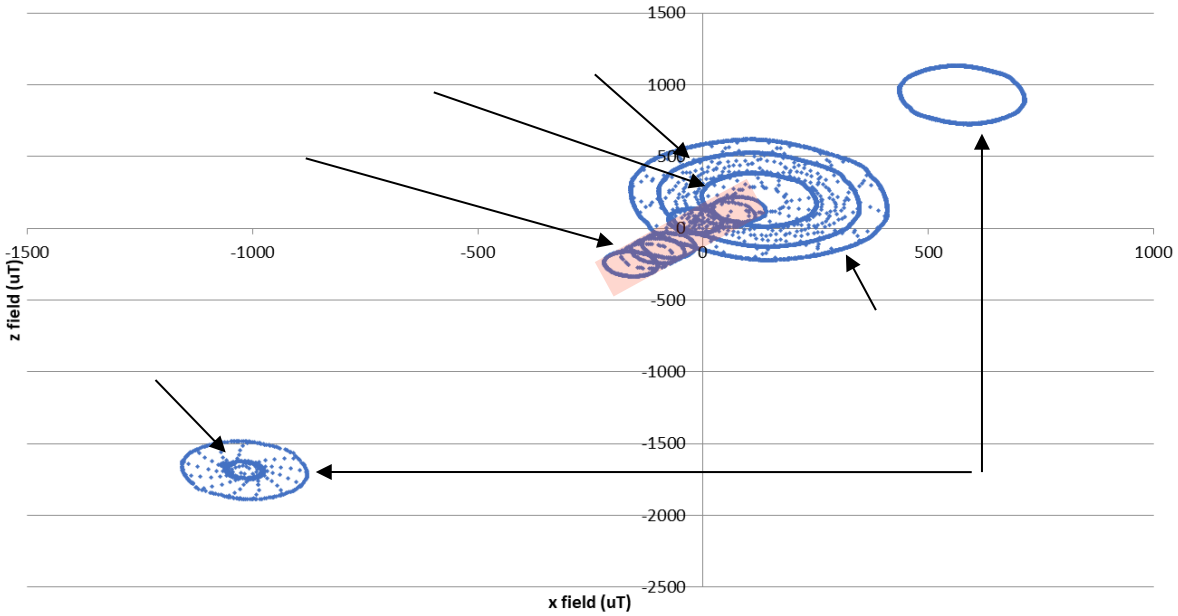

Figure 121 : Ellipses representing the different current set points

This measurement strategy of decoding the calibration factor is even more necessary on a 3-core cable measurement which appears to suffer from this type of re-calibration with regularity. The two figures below show the measured waveform and then the field as shown as a set of ellipses. The results for this cable are shown in the results section.

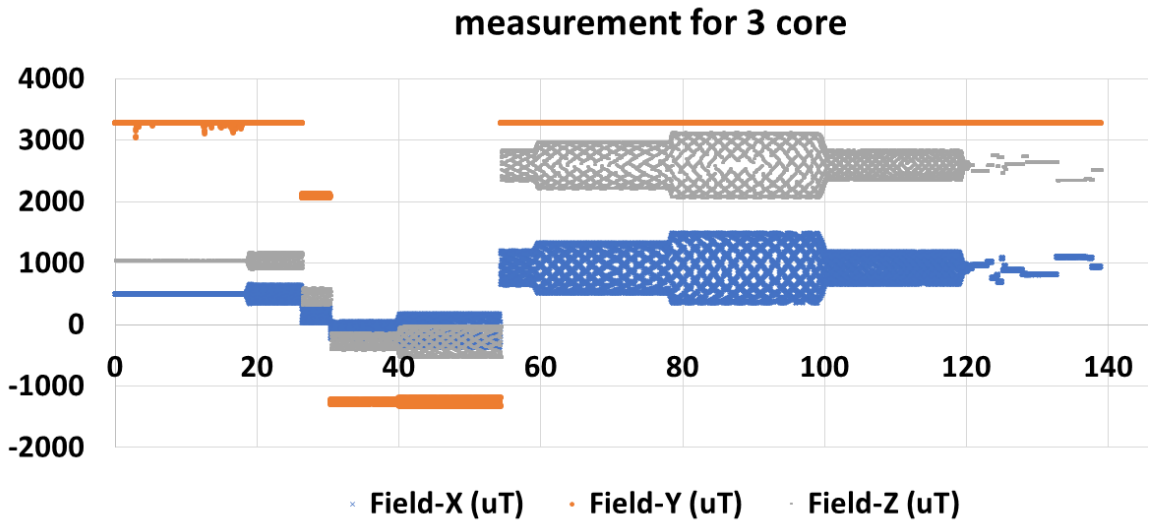

Figure 122 : Calibration factor being applied in the Sensor App on a 3-core cable by phone using Sensor App

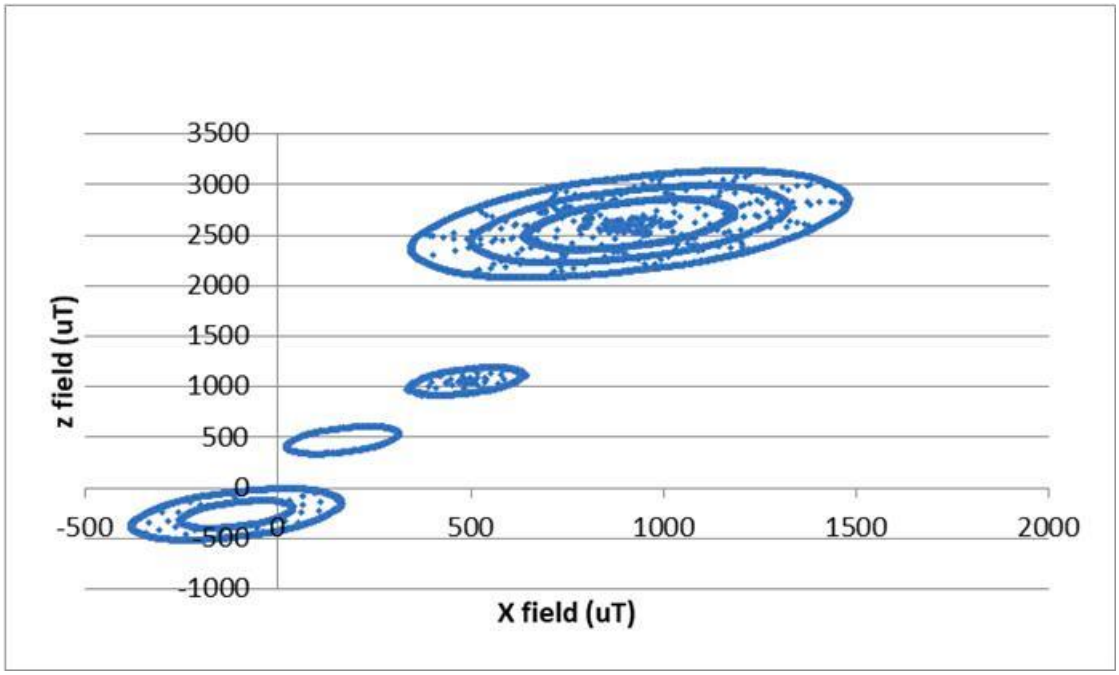

Figure 123 : Ellipses representing the different current set points on a 3-core cable

LP 45	It is possible to remove the impact of calibration, but this requires post processing or adaptive processing as results are being collected. It is much more straightforward to use the uncalibrated data. However, this can also be adjusted by the phone controller.

13.3.2 Measurement interval

The measurement interval in the app is set to 1ms (the minimum setting), in practise this means measurements are taken at 10ms intervals with the actual interval varying from 4 to 20ms depending on how much time the processor requires for other tasks as shown in Figure 125 and Figure 126. This is because taking sensor measurements is not a priority for the phone which concentrates on seamless user interface. The measurement interval must be carefully considered to avoid the phenomenon of aliasing, where a regular measurement might measure the same or adjacent point on the sine wave each time and give an unrepresentative impression of the overall magnitude. This can be seen in Figure 124.

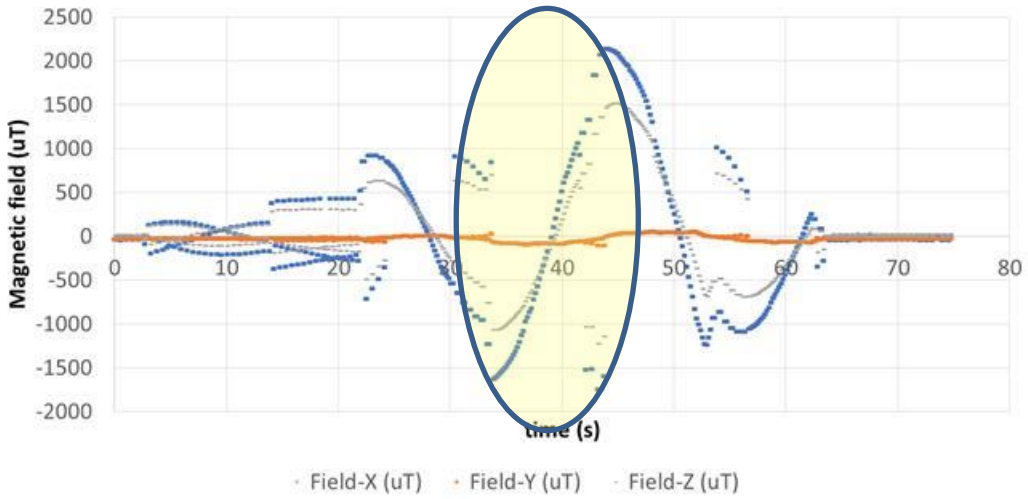

Figure 124 : Magnetic field (x, y, z component) showing impact of measurement when close to integer value of 1/frequency

The same App was operated on two identical phones, one with many other Apps running and a second with other Apps disabled. The phone with heavy processor use achieved an average 15ms measurement interval whereas the app economical phone achieved an average 10ms measurement interval. It may be possible to achieve shorter measurement intervals by using a higher specification phone or a phone dedicated to datalogging with no non-essential apps running.

Other issues with time sampling include whether the App is merely logging data or if it is uploading it to a server through the Wi-Fi system. So, while Figure 125 and Figure 126 are for the Sensor Logger App – where merely logs data. The same figure reproduced for the Deduce App which also uploads data is shown in Figure 127.

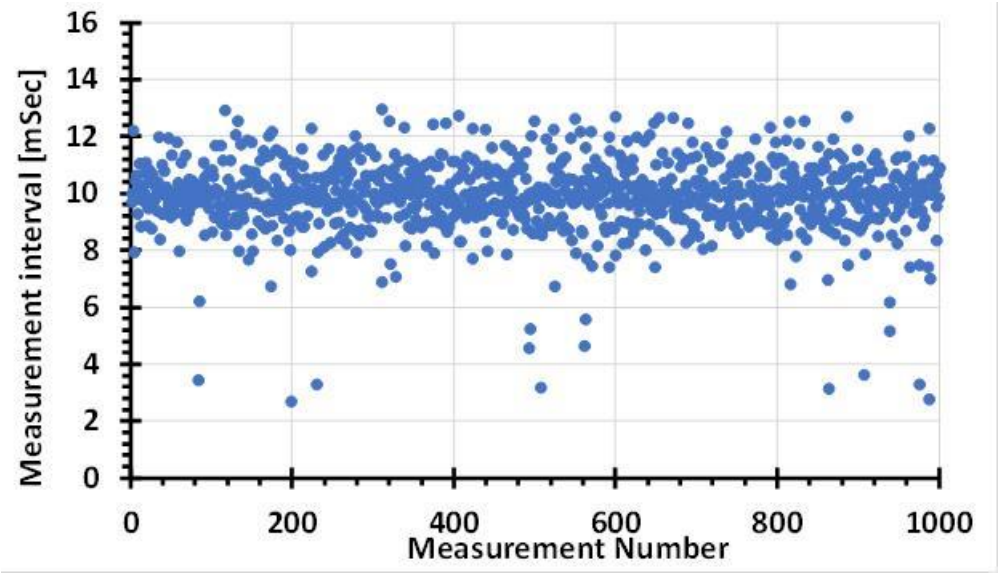

Figure 125 : Scatter plot showing the distribution of the measurement interval using the sensor logger App

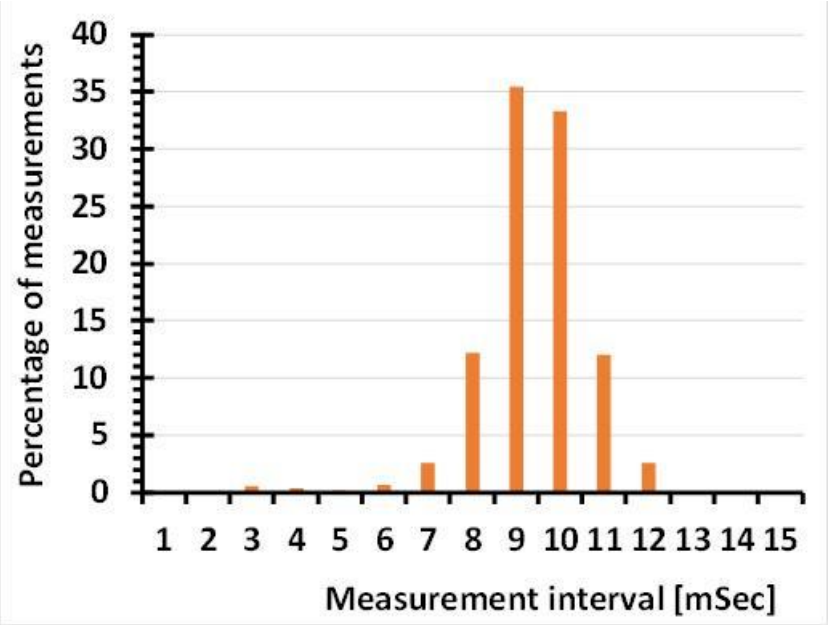

Figure 126 : Histogram of measurement interval.

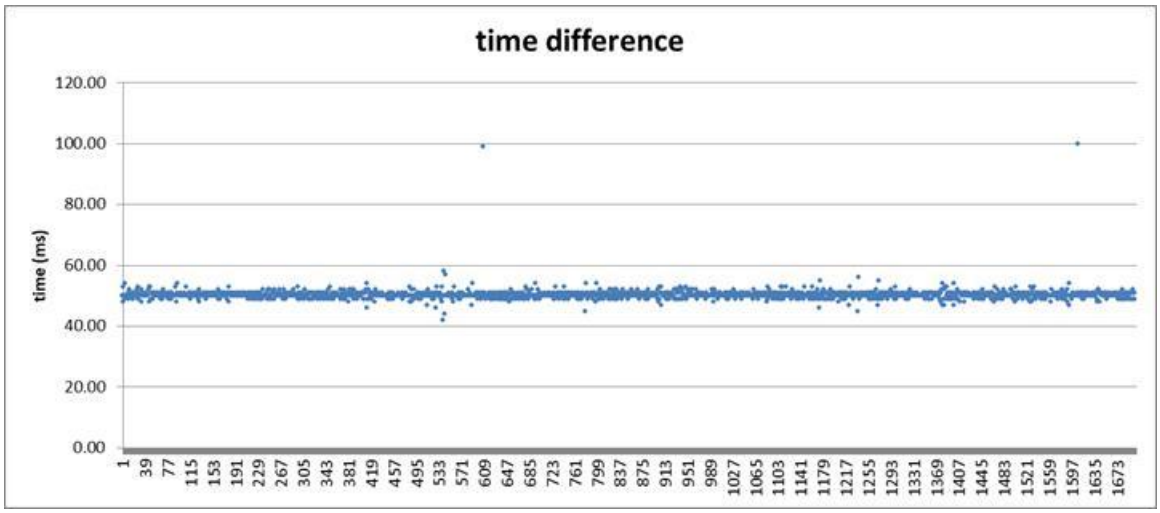

Figure 127 : Scatter plot showing the distribution of the measurement interval using the deduce App

LP 46	Android datalogger apps tend to measure with a randomised time interval, so the data must be carefully processed so aliasing effects don't introduce bias into values.

LP 47	The temporal resolution of measurements on a phone varies from any delay set in code dependent on the processor and other core phone specifications. It is also dependent on what other apps are running and their processor usage.

LP 48	Downloading the data to a server on a phone over Wi-Fi increases the measurement time further and sub 50ms measurement may not be possible.

13.3.3 Different Apps – Different Phones

This section aims to look at repeatability across different platforms. Figure 128 shows the sensor App and the Deduce App on two Samsung phones for a fixed current. The results indicate a similar level of magnetic field. However without understanding the calculation methodology and any averaging on the sensor App it is difficult to make more of a comment.

Figure 129 shows the same App on two phones. The Samsung 6 Deduce App appeared to only report a maximum number of points and therefore the last set of data has been lost (this is due to a fast logging time and a memory limit on the phone). The Samsung phone is both narrower and thinner than the Sony phone and the reading on the Sony phone is therefore proportionally lower for each set of currents.

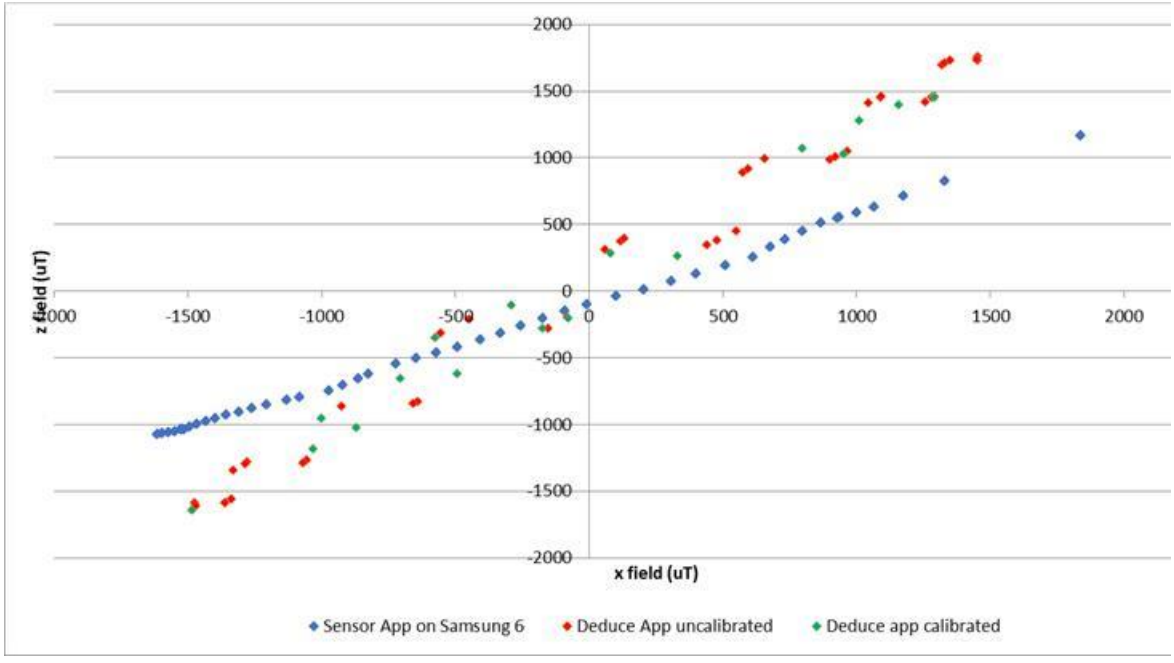

Figure 128 : Different Apps – same phone type (note one App uses calibrated data and uncalibrated while the other has uncalibrated only)

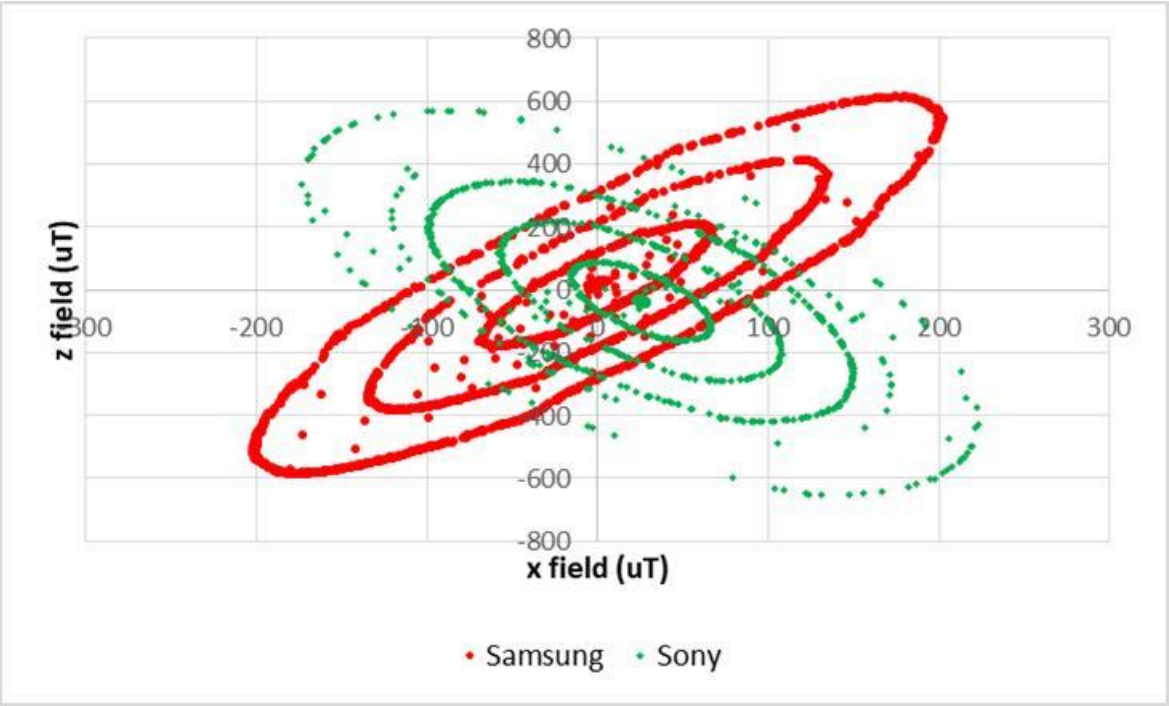

Figure 129 : Different phones – same App

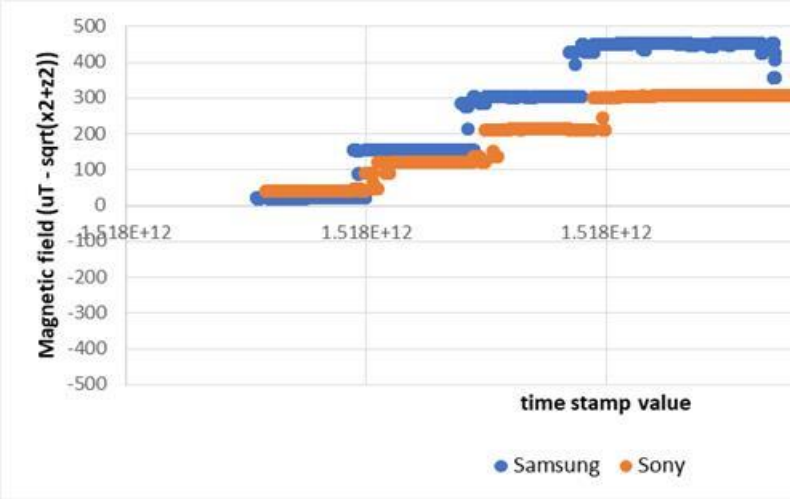

Figure 130 : Different phones – same App – time data

Note:
Samsung 6 phone 7.1mmx70mm with sensor 25mm from edge
Sony phone 7.6mmx72.5mm, sensor location not known

13.3.4 Effect of temperature

The cable was loaded to its maximum temperature and a heat gun used to heat the phone to 60°C. The phone was then allowed to cool naturally over several seconds. The high-level process can be seen in Figure 131 while the field plot is shown in Figure 132.

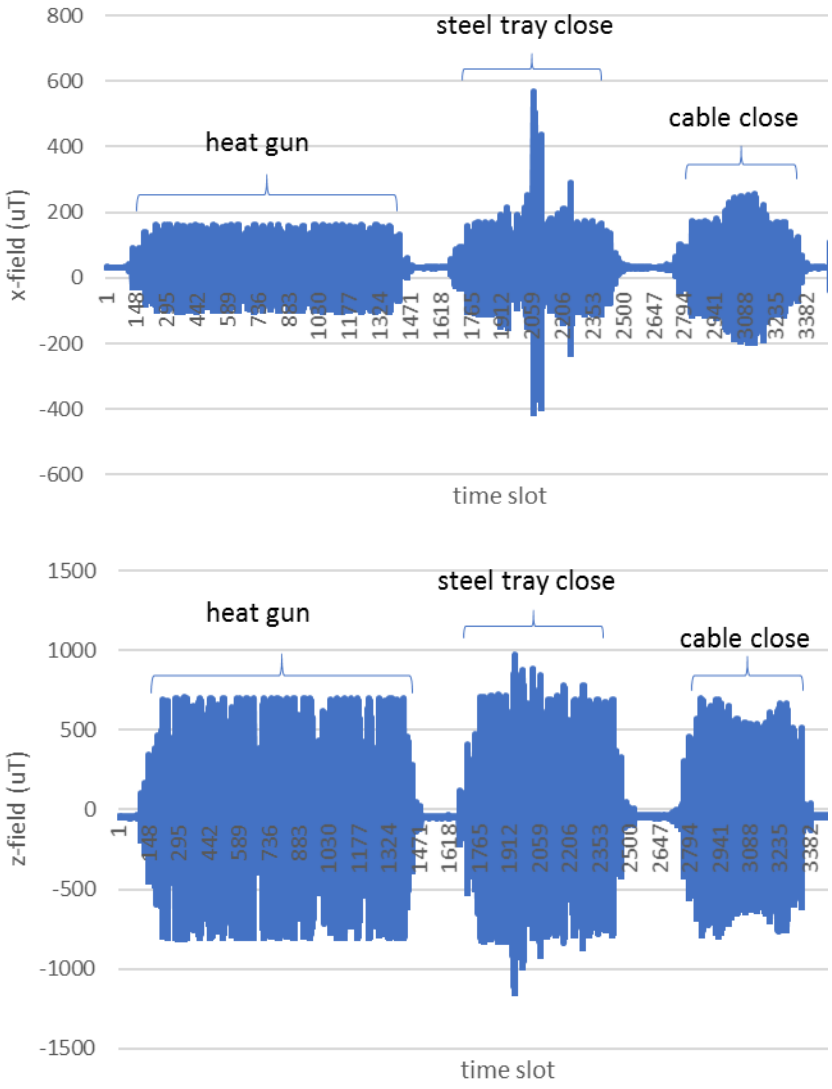

Figure 131 : Temperature run (Sony phone with deduce app)

LP 49	Temperature does not seem to impact the magnetometer reading as the phone is designed to internally compensate for this.

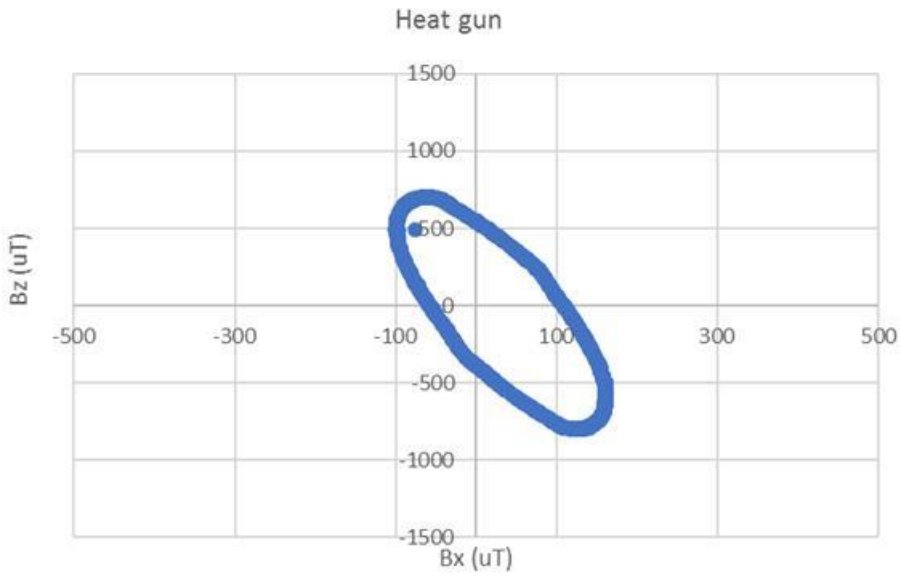

Figure 132 : Temperature run (Sony phone with deduce app)

The phone automatically adjusts for temperature and therefore no additional accounting for this needs to be considered.

13.3.5 Effect of adjacent metal work

The current was set to maximum and then a piece of steel cable tray was moved close to and around the single core cable. This clearly had the biggest impact as shown in Figure 133.

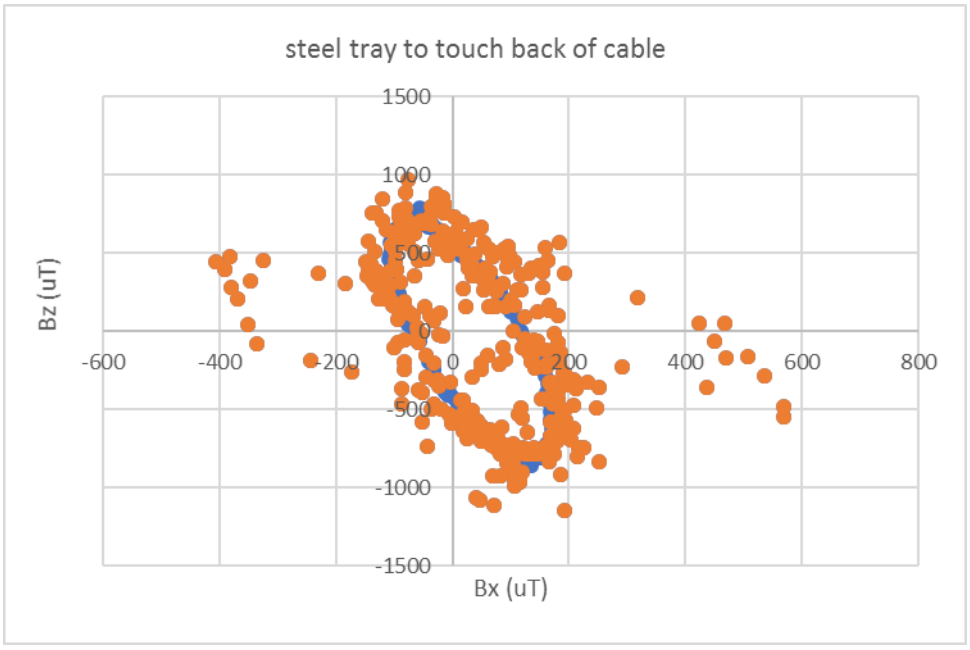

Figure 133 : Impact of nearby metal work (Sony phone with deduce app)

The cable tray was very close (touching the outside of the cable in places). It also acted to both increase and reduce the field depending on direction and the eddy currents induced. However, although this looks like a substantial impact, the largest measured field is around 707µT after the steel cable work is added compared to 700µT before the metal work is brought close. This is thought to be due to ampere's law

$$I = \int Hdl$$

So, unless the steel work is directly between the cable and the phone – there is always a path which enclose the phone and the cable but not the steel work (and its induced current).

13.3.6 Effect of adjacent conductor

The effect of moving another phase close to the conductor is that it impacts the field. This can clearly be seen below. The direction changes and the magnitude reduces. The magnitude reduction can be seen more clearly when x and z scales are the same.

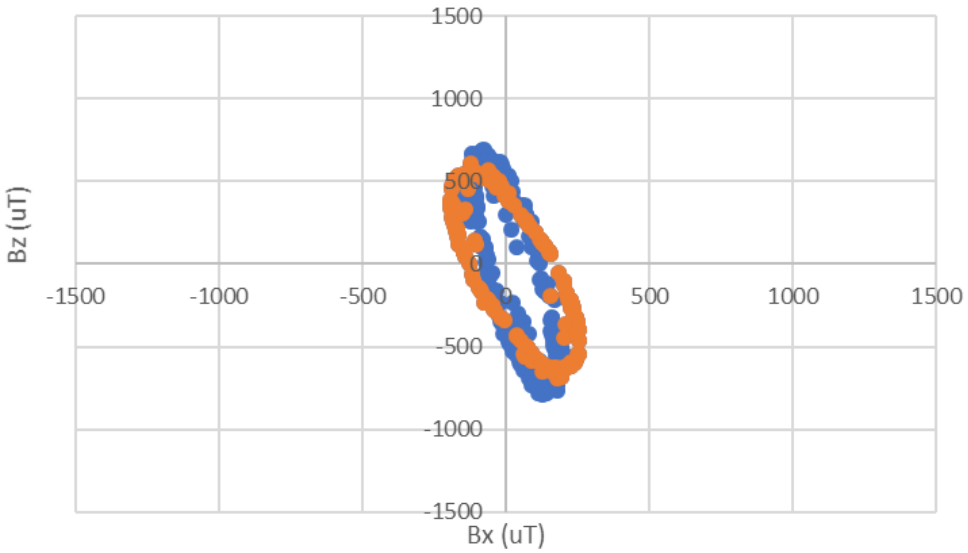

Figure 134 : Impact of touching cable (Sony phone with deduce app) – blue (not touching), orange (touching)

13.3.7 Effect of distance

Prior to the development of the clamping device the mobile phone was taped to the cable. This provided a quick method of installation but the results showed how sensitive the phone measurement is to distance with results taken on different days.

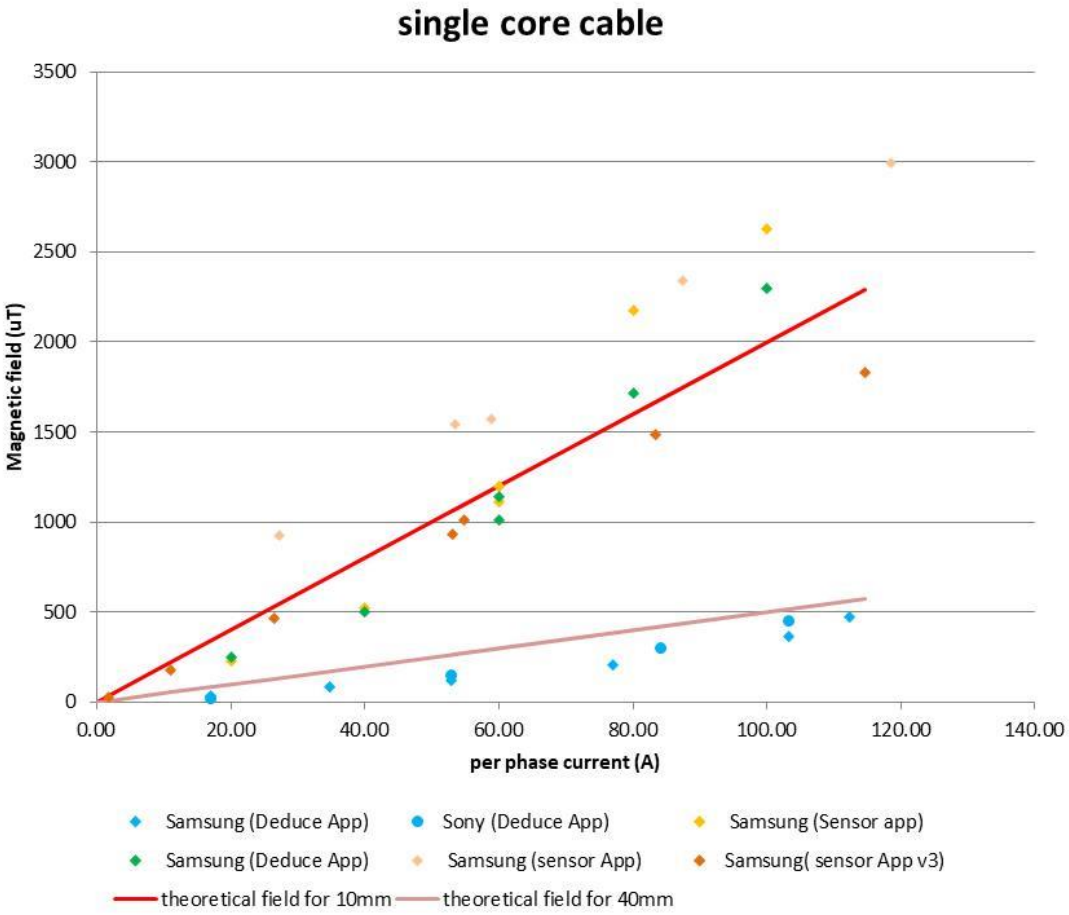

Figure 135 : Early testing showing results variability under different installation conditions

13.4 Rig testing

For proper testing the current clamp device was designed and all the following results use this as a means of fixing the distance from the phone to cable. The phone was tested on the single core cable, 3 core cable and trefoil cable in the rig and then tested at the substation.

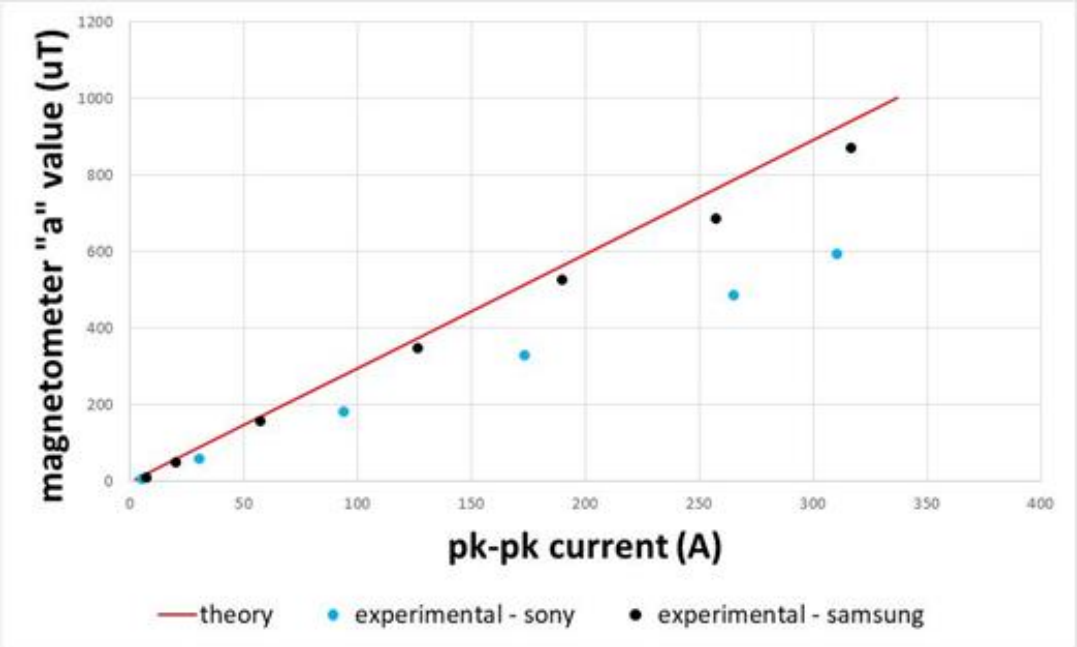

Figure 136 : Measured magnetic field against measured current for a single core cable

LP 50	Using a phone to calculated load current is possible. There is a good degree of linearity and correlation. The accuracy of the direct back calculation of current from the phone (Equation 5-18) is less than would be liked. However, a lower magnetometer reading shows a higher value of current than would be obtained in the field and therefore there is an inherent safety margin. To get more accurate results a “phone factor” is suggested which could be used to multiply to the calculated current.

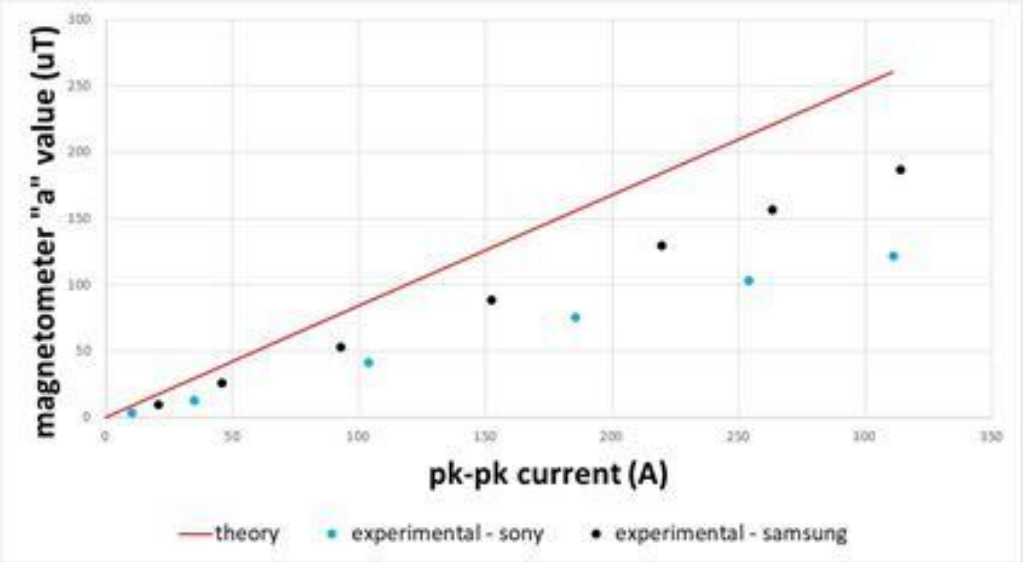

Figure 137 : Measured magnetic field against measured current for a three core cable

LP 51	Calculation on three core and single core cables show different levels of accuracy. This means a phone factor would be required which would depend on cable type.

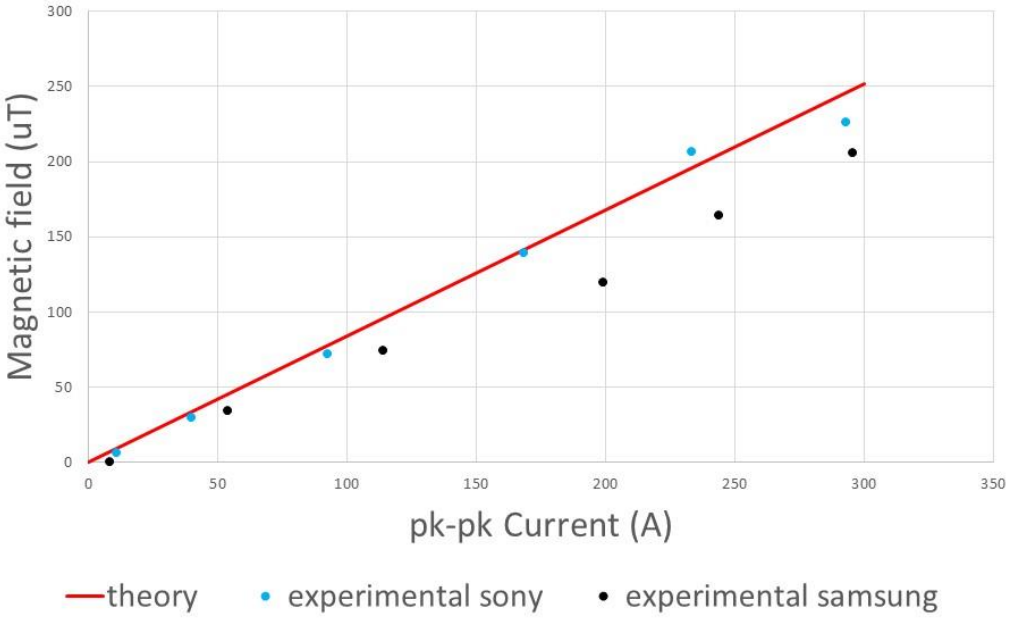

Figure 138 : Measured magnetic field against measured current for a trefoil cable

LP 52	There is some inconsistency between phone types depending on cable type. It could mean that certain phones are more suitable for certain types of cable. This could be related to location and direction of sensor. It is recommended that phones be pre-calibrated to cables int eh laboratory prior to deployment.

The graphs show a good correlation between measured field and current (both better than 0.999). Also shown on the graph is the calculated current for values of r= 33.7 mm (single phase cable) and d_3 = 30 mm with r_4 = 40mm (three phase cable). Unfortunately the experimental values show poor accuracy compared to theory. There is a factor of 1.5 out on the single phase cable and 2.1 out on the 3 phase cable for a Sony Xperia phone. However the results for the trefoil cable appear to be reversed with the Sony looking close and the Samsung out by a factor of 1.7. This appears to be a function of phone type and would need resolving by more repeated testing on different cable types.

Table 13-4 : correlation of sensor measurement with current

Coil	Correlation co-efficient
Single phase	0.999
3 phase	0.999

Prior to testing on the substation the phone was installed at a domestic property over a two day period to check reliability. The results are shown below captured over a 10s interval and show the true spikey nature of a domestic supply. There are recent developments in the USA regarding using mobile phones to test loading on cables. One of the Utilities offers this option as part of an electricity management package.

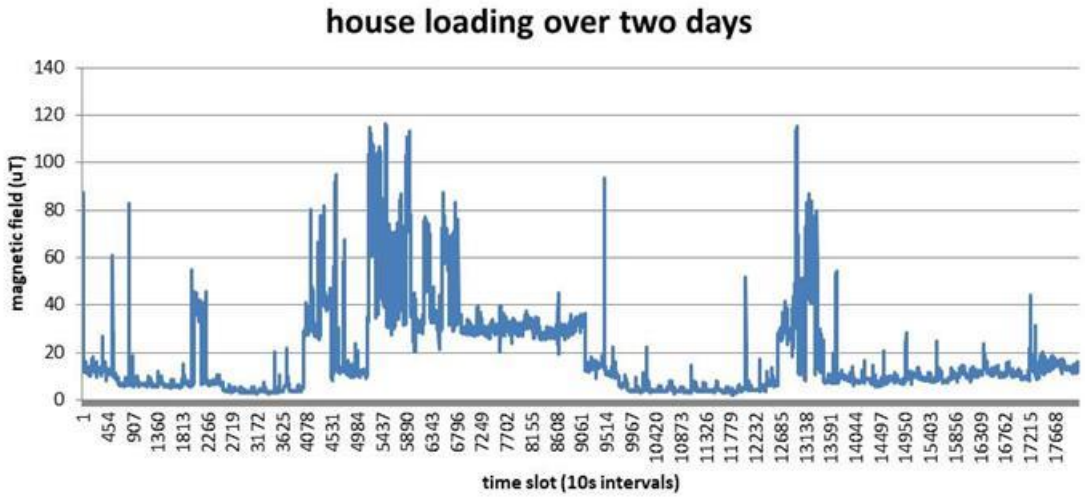

Figure 139 :domestic property single phase field measurement over two days.

13.5 Substation testing

The Sony phone was tested on both the single core LV feeder and the 3 core 11kV cable between the RMU and the transformer as shown in Figure 140.
The results were captured on a server and compared to those generated using the Fluke power quality analyser with a 10s logging time stamp. The results are shown in Figure 141 and Figure 142 for each cable type.
The results look very close and the variation of the load over time has been clearly captured even on the HV cable where the current in small.

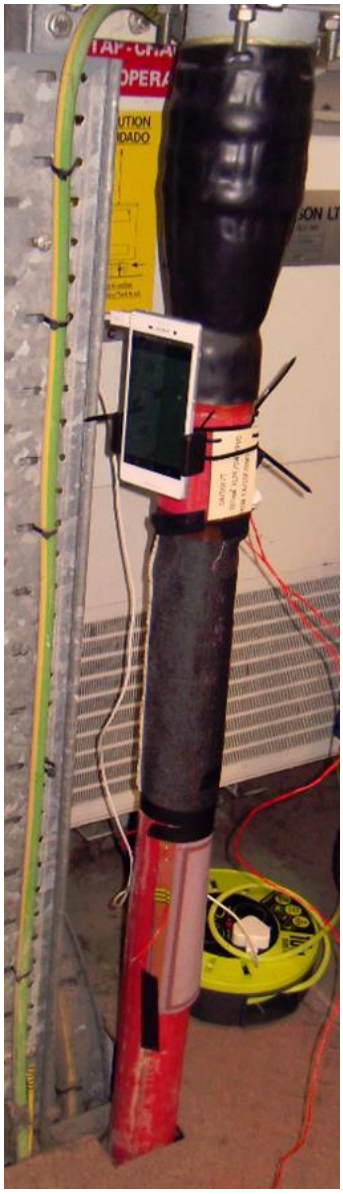

Figure 140 :substation installation of android phone

LP 53	Installing the phone was the easiest of the sensor installation options. The phone was cable tied to the cable and the phone clipped into place and then App started. A USB power supply was connected to the phone to ensure it didn't run out of charge.

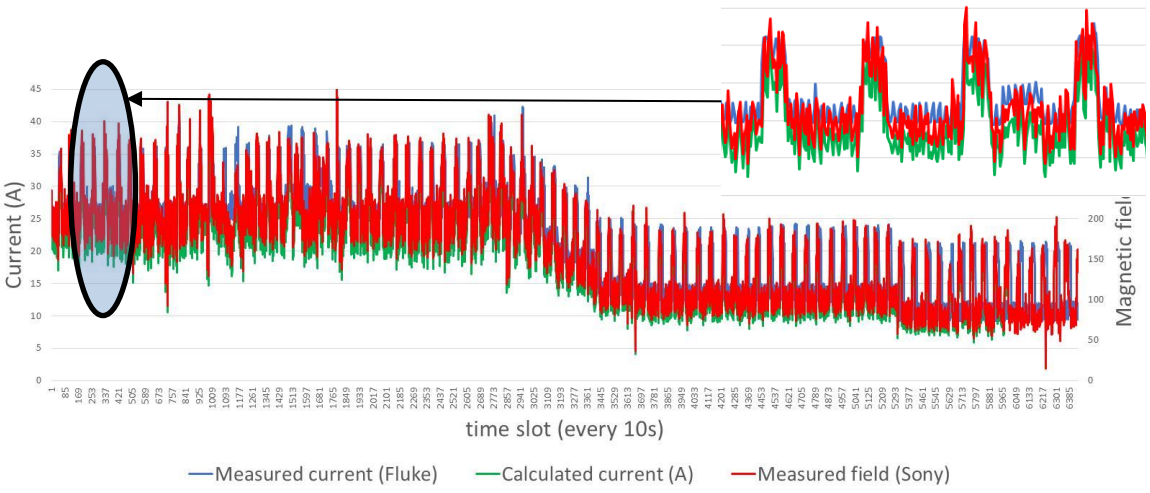

Figure 141 : Fluke measured substation current, measured magnetic field and calculated current on a single core cable between transformer and distribution board

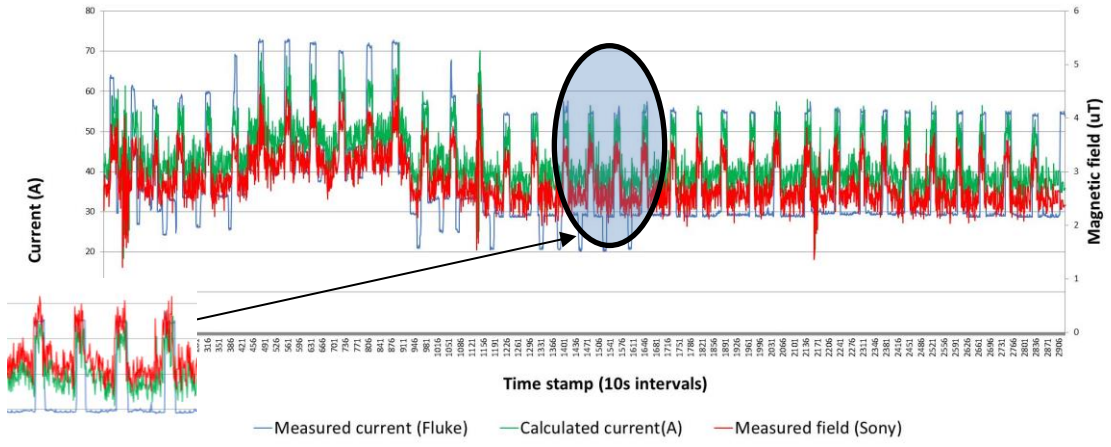

Figure 142 : Fluke measured substation current, measured magnetic field and calculated current on a three core cable 11kV cable to the transformer

LP 54	A mobile phone magnetometer was successfully used to log data at a substation on both the LV and HV cable and the data was sent via WI-Fi to a server.

13.6 Summary

A magnetometer is a promising candidate for long scale testing. However, the issue of distance of sensor from cable along with subsequent comparison to theory will enable knowledge of pre-calibration pre-deployment vs deployment calibration to be considered.

	Comment
Application	Can be used • to provide data from close to real time for DNR (several seconds) helping with fault restoration although not directional • exception reporting • load profiling • MDI The magnetometer part of the phone can provide a single phase or three phase estimate of current
Data Location	Can be sent • Locally but only in small quantities as limited by phone memory • Server – to be accessed by anyone in the company
Data fidelity	Time spans can be set to • Near real time (<15s) • 10min intervals and above The data can be time stamped but isn't synchronous
Data backup	• Very small local backup with link to server
Data form	The data can be in the following form • Time stamped in any relevant format eg Peak/RMS over different time intervals where RMS is peak/root (2)
Failure mode	• Fail dead

Test	Comments
Linearity	Linear up to saturation but mathematical post-processing can be used to derive not saturated values
Effect of adjacent steel work	Substantial impact on field direction (both positive and negative). However, indication is that net field remains similar to that measured without steel. Therefore, this may not be an issue – further investigation is needed.
Effect of adjacent conductors	<10cm away some impact. Very close nearby cables (touching) in this instance reduces the field and therefore the measurement by approx. 20%

Effect of temperature	No obvious impact
Stability/reliability	Appears stable
Ease of deployment	Very straightforward, two cable ties onto a fixture to clip phone in place and addition of a power lead
Calibration	Pre-lab based calibration appears to be an option rather than on-site calibration. It may be that some phone types don't require this.
Time constants	Delay of around >10ms for raw data and suggested 10s for average data to help remove issues with anti-aliasing
Accuracy	7.5% - However very sensitive to distance of sensor – so proper fixture required
Correlation to loading	0.999
Sensitivity	Mostly to distance and adjacent conductors.
Repeatability	Repeatable over different phones and with different Apps
Data Storage	Data can be stored (for small time periods) at 10ms intervals or uploaded to a server in 50ms intervals. Post processing of data will add to this.

Other factors	Comments
Primary sensing element	Magnetometer
Power/excitation	Phone charging cable connected to 230V needed
Amplification	Not needed and in fact distance increases may be used to desensitise
Analogue filtering	Not required
Data conversion	Maybe done on phone
Digital information processing	Elliptical curve fitting process required to capture data
Digital communication processing	Method proven at simple level with time stamp and auto-download to a server based on location. Additional setup procedures need to be sorted.
Communication	Mobile network

14 Platform J: IOIO interface unit

The IOIO is an I/O board that can plug into an android phone and can be used to input/output analogue and digital control signals. The board can then be accessed via an App. As with the Android phone, the coding and setup are complex, but the hardware connection is straightforward as shown below. This board in conjunction with the phone offers an alternative to the Arduino. Also shown is the circuit diagram for connecting an analogue input (in this case a thermistor).

The IOIO board has 60 IO pins including 16 10 Bit A/D converters and compatibility with I^2C.

Table 14-1 : Cost of sensor J hardware

Vendor	Part	Qty	Unit cost	Line cost	System Total
	Android Phone	1	donated	donated	
proto-pic.co.uk	SparkFun IOIO OTG	1	£39.73	£39.73	
Amazon	USB wall charger	1	3.99	£3.99	
pimoroni.com	SparkFun Hydra Power Cable	1	£4.58	£4.58	
					£43.80

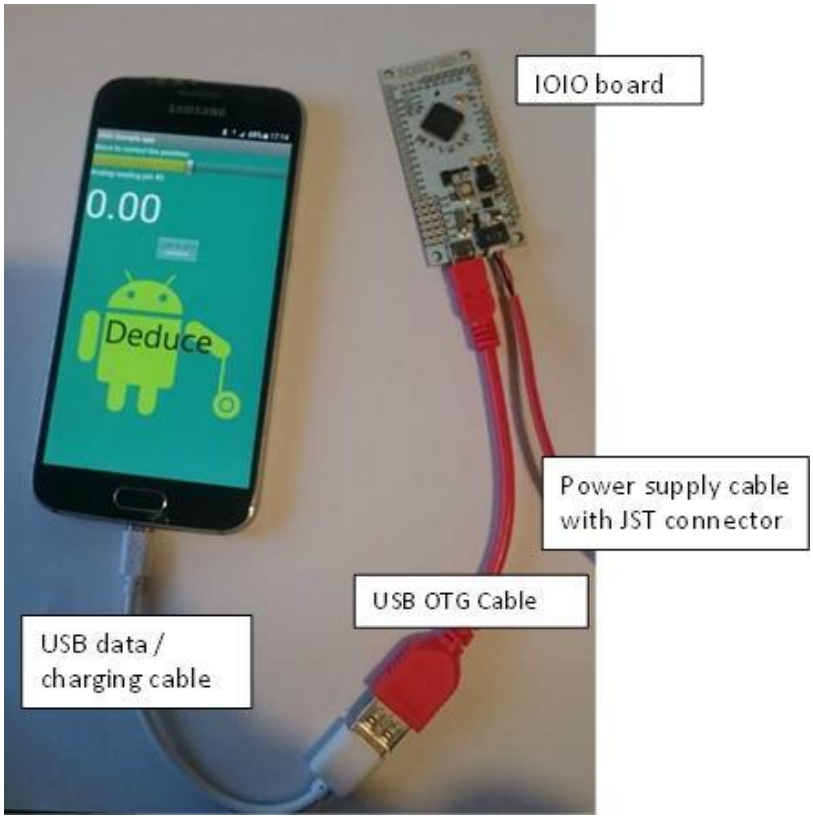

Figure 143: photos of phone connected to IOIO board configured for 1 AI

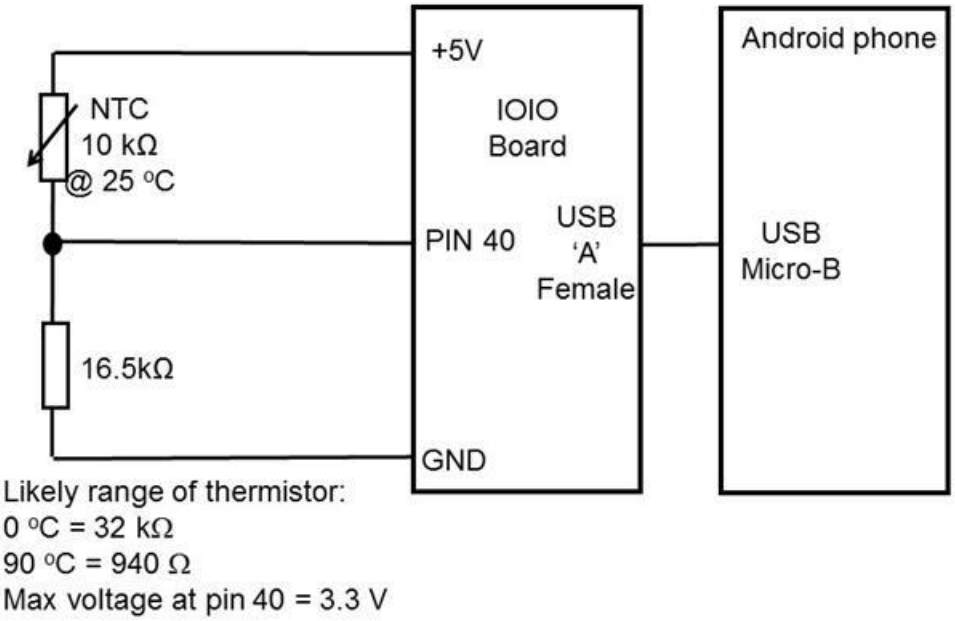

Figure 144: wiring diagram for thermistor connected to IOIO board

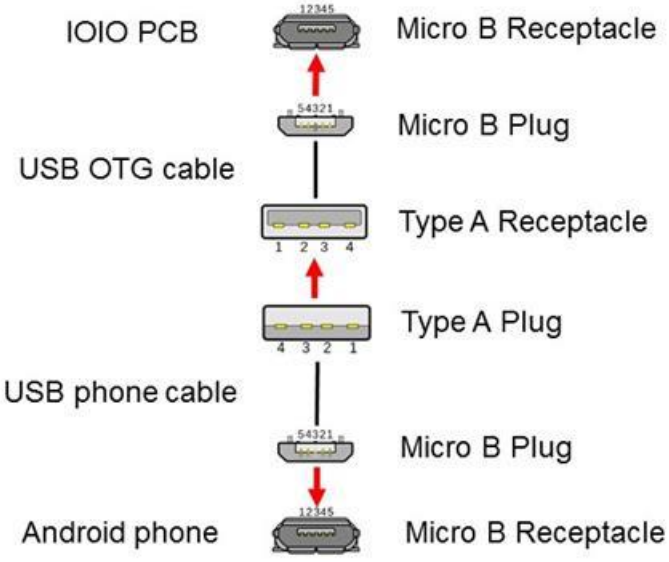

Figure 145: IOIO to Phone USB configuration

The wiring configuration is shown in Table 14-2. The IOIO board data is read in through a phone App. The setup for this is listed in the appendix. The data capture rates are therefore similar to the Android phone and dependent on the applications running.

Table 14-2: USB wiring configuration

Name	Description	Insulation colour	Type A/B pin	Mini / micro A/B pin
V_{BUS}	+5 V	Red	1	1
D–	Data–	White	2	2
D+	Data+	Green	3	3
ID	OTG end identifier: GND=host, Floating=device	no wire	N/A	4
GND	Signal ground	Black	4	5

TT 8	Not all phone charging cables have a data line connected. Therefore, the cable used needs to be specifically tested in advance otherwise the system won't work. The quickest test is to plug the phone into a PC and check if basic handshaking has occurred (device appears in windows explorer or device manager).

TT 9	The jst cable supplied by the company selling the IOIO boards had the +/- polarity reversed. This not only stopped the IOIO board from working but also tripped an electronic fuse in the PCs USB port which required resetting by rebooting the PC.

TT 10	Some of the libraries and documentation around the IOIO board specify the use of old versions of operating systems. It is recommended that these are ignored as the IOIO board will operate on the more modern operating systems. However, this did take a while to sort.

LP 55	An IOIO board offers a neat solution to turn a mobile phone into a controller with up to 60 I/O. It would allow the phone to be connected to any of the sensors under investigation.

14.1 Rig testing

The results for this are shown in section 12.2. However the hardware setup is shown below.

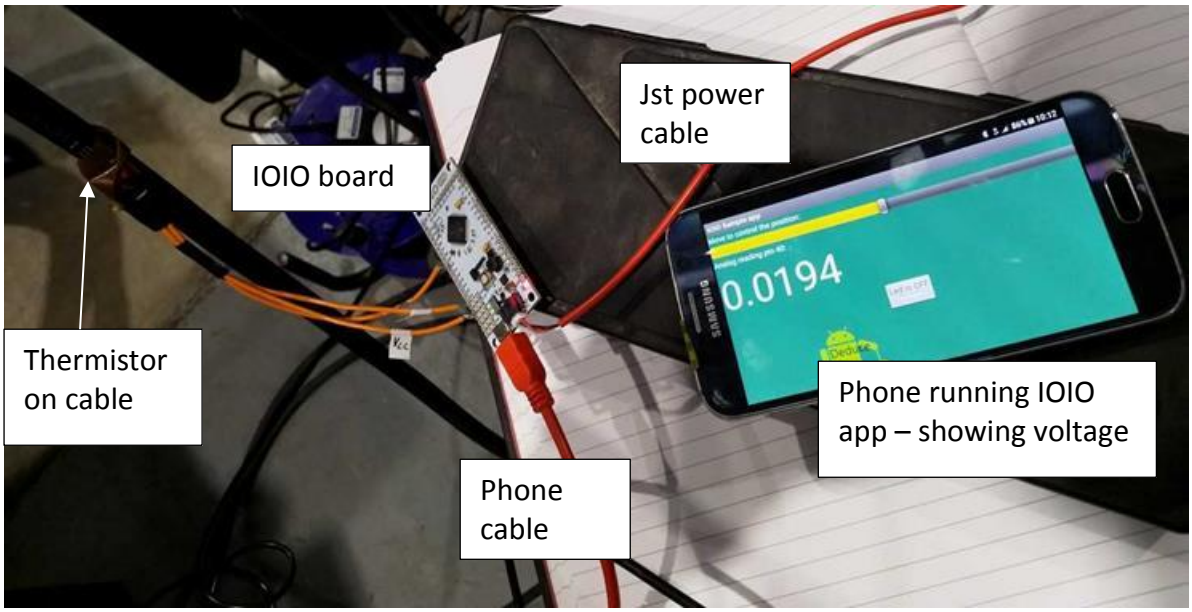

Figure 146: wiring diagram for thermistor connected to IOIO board

14.2 Summary

Summary	Comment
Application	Can be used • to provide data from close to real time for DNR (several seconds) helping with fault restoration although not directional • exception reporting • load profiling • MDI The IOIO board provides a direct IO platform link into a mobile phone
Data Location	Can be sent • Locally but only in small quantities as limited by phone memory • Server – to be accessed by anyone in the company
Data fidelity	Time spans can be set to • Near real time (<15s) • 10min intervals and above The data can be time stamped but isn't synchronous
Data backup	• Very small local backup with link to server
Data form	The data can be in the following form • Time stamped in any relevant format eg Peak/RMS over different time intervals where RMS is peak/root (2)
Failure mode	• Fail dead

Test	Comments
Linearity	Depends on sensor type
Stability/reliability	Appears stable
Ease of deployment	Needs connecting to mobile phone and to sensor – needs packaging
Calibration	Depends on sensor type
Time constants	Additional delay to phone - Delay of around >12ms for raw data
Accuracy	Depends on sensor type
Sensitivity	Depends on sensor type – but can only deal with voltage signals between 0 and 3.3V
Repeatability	Repeatable
Data Storage	Data can be stored as per mobile phone and post processing needed to turn raw data into load current

Other factors	Comments
Primary sensing element	Depends on sensor type
Power/excitation	Phone charging cable connected to IOIO board which then provides power to phone. Needs to be done this way due to complexity of power/data transfer over USB.
Amplification	Depends on sensor type
Analogue filtering	Depends on sensor type
Data conversion	Maybe done on phone
Digital information processing	Depends on sensor type
Digital communication processing	Maybe done on phone
Communication	Mobile network

15 Platform K: Arduino

The Arduino is a micro-controller device which can be used to read input signals and communicate with devices. The Arduino development system can be (and has been) used to read signals from both analogue and digital sensors, via voltage and I^2C serial signals respectively. Initial Arduino development used the low-cost Arduino Uno board which is adequate to read signals and transmit them to PC as ASCII text via USB. Sending data via GPRS requires considerably more memory, so the LinkitOne PCB was used which also has on-board WIFI, GPRS, GPS capability and a real time clock which is important for accurate data timestamping.

Table 15-1 : Cost of sensor k hardware

Vendor	Part	Qty	Unit cost	Line cost
RS	Arduino Uno	1	£14.99	£14.99
	- or -			
Rapid	LinkitOne PCB (Arduino compatible)	1	£44.24	£44.24

The Arduino PCBS can be linked to built-in libraries are available for commonly used add-on boards such as MEMS sensors. For example, a program to read data and I^2C MEMS sensor, calculate running averages and exponential averages and send data as ASCII text to USB port with a timestamp required only 120 lines of code including comments, variable definitions and spacing.

It is important to note the limitations of what 'Arduino compatible' does mean

- Rows of pins along outside edge of PCB standard pitch and physical pinouts
- Common voltages used
- Ability to upload code via built-in bootloader via USB avoiding the need for a separate programmer PCB as with off the shelf micro-controller chips
- Use of a common C++ library called 'Wiring' for core functions which can be coded, compiled and uploaded from the Arduino IDE.
- USB debug port sharing the same physical USB port used for code upload.

However there are also many differences even within the Genuine Arduino/Genuino range of PCBs in addition to third party PCBS including:

- Arduino libraries for third party devices such as sensor and communications boards may be compatible only with certain microcontrollers for example the Sparkfun MPU9250 library is compatible with the Arduino Uno and Mega but not the SEEED Studio LinkitOne.
- Digital pins used for the same serial protocol may vary between different PCBs
- Taking the Arduino Uno as the base case, other PCBs may have more analogue/digital channels and other serial and communication ports, for example the Mega has lots of extra analogue/digital pins. The LinkitOne has additional Grove ports and built in GSM/GPRS/Wifi/Bluetooth/GPS circuits.

- Some devices for example the LinkitOne, whilst using the same physical port for code upload and debug, these may appear as separate virtual COM ports on the host PC/Device.

Both I2C sensor PCBs which were tested had Arduino libraries available on GitHub so required minimal coding, they were easy to setup and worked as documented straight away.

Table 15-2 : Comparison of different Arduino type platforms

PCB	Controller Manuf	Controller part	CPU family	Bits	MHz	MB	Wiring		
							Data	**Clock**	**V**
Arduino Uno	Atmega	328P	AVR	8	20	1	A4	A5	3.3
Arduino Mega	Atmega	2560	AVR	8	256	4	A20	A21	5
LinkitOne	Mediatek	MT2502	ARM7EJ-S	32	260	4	A4	A5	3.3

The wiring layout is highly dependent on the sensor being connected. The photographs below show the Arduino Uno and LinkitOne PCBs used in the project.

Figure 147: Arduino Uno front side

Figure 148: Arduino bottom side

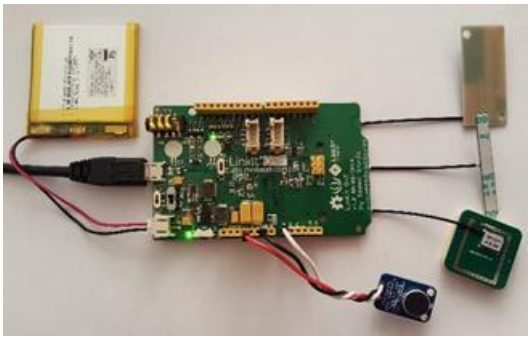

Figure 149: LinkitOne PCB front side with Battery, Wi-Fi, GPRS, GSM antennae and microphone.

Figure 150: Remote Logger by www.re-innovation.co.uk based around LinkitOne PCB modified for use on this project (the LinkitOne PCB is fitted to the rear of the Remote Logger PCB).

15.1 Settings and software

The Arduino settings and source code used are shown in Appendix 20

15.2 GSM/GPRS PCBs

Both GSM/GPRS communications PCBs come in shield format so were easy to connect and had Arduino libraries available. However the DFRobot setup was convoluted requiring multiple user interventions to reboot/upload/switch to debug operation. The manual was vague and it was not possible to even prove the fundamental communication between the Arduino and the Comms board let alone send an SMS. Sending an SMS is the simplest test for a GSM/GPRS comms board as SMS sending requires only an in-credit SIM card without the APN setup required for GPRS data communications.

Table 15-3 : Comparison of different Arduino GPRS platforms

			Compatibility	
Manufacturer	Model	Band	GiffGaff PP	Vodafone PP data only
Seeedstudio / Mediatek	LinkitOne	2G	✓	✓
Adafruit	Fona SIM808 Shield	2G		✖

Table 15-4 : GPRS setup for Adafruit Fona SIM808 shield

Adafruit Fona SIM808 Function	Default Arduino PIN
Rx	2
Tx	3
RST	4
RTS	5
RI	NC
Net	NC
Pwr	NC
Key	GND
DTR	NC

15.3 Rig testing

Two types of ‘9 axis’ movement PCBs were tested the Adafruit LSM9DS0 and the SparkFun MPU-9250. Two types of PCB were tested the Arduino Uno and the LinkitOne. The sensors and controllers were compared for measurement timing. No delays were set in the program, so data would be saved as fast as the sensor and controller allowed. No averaging or calculations were conducted on the raw data it was simply read from the sensor and written to the USB serial port. The MPU-9250 sample rate was set to the highest possible

which was 100Hz. The shortest measurement interval was with the MPU_9250 connected to the LinkitOne with 3 channels measured which averaged 31 seconds per measurement. The slowest was with the LSM9DS0 connected to the Arduino Uno with 9 channels measured which averaged 78s per measurement.

Table 15-5 : Sensor data capture rates using the serial link

Controller	Sensor	Data channels recorded				Measurement interval [sec]			
		Mag	Accel	Analogue	Total	Min	Mean	Max	Range
Arduino Uno	MPU_9250	3	0	0	3	22	43	46	24
Arduino Uno	MPU_9250	3	3	3	9	42	56	59	17
Arduino Uno	LSM9DS0	3	0	0	3	25	37	38	13
Arduino Uno	LSM9DS0	3	3	3	9	62	78	81	19
Linkit One	MPU_9250	3	0	0	3	9	31	50	41
Linkit One	MPU_9250	3	3	3	9	14	40	61	47
Linkit One	LSM9DS0	Library not compatible							
Linkit One	LSM9DS0	Library not compatible							

15.3.1 Calibration of A-D

It was noted that the analogue inputs float by up to 0.5V if nothing is connected to any of the terminals. If some terminals are left unconnected they tend to show the value from adjacent terminals. This is common even in high quality analogue dataloggers where adjacent channels are often time domain multiplexed into a single high precision analogue-digital circuit.

TT 11	It is wise to connect jumpers from unused analogue input terminals to ground to prevent misunderstandings in the measurements.

The scaling factor for DC voltage to reported reading was confirmed to be 205 +/-0.5%.

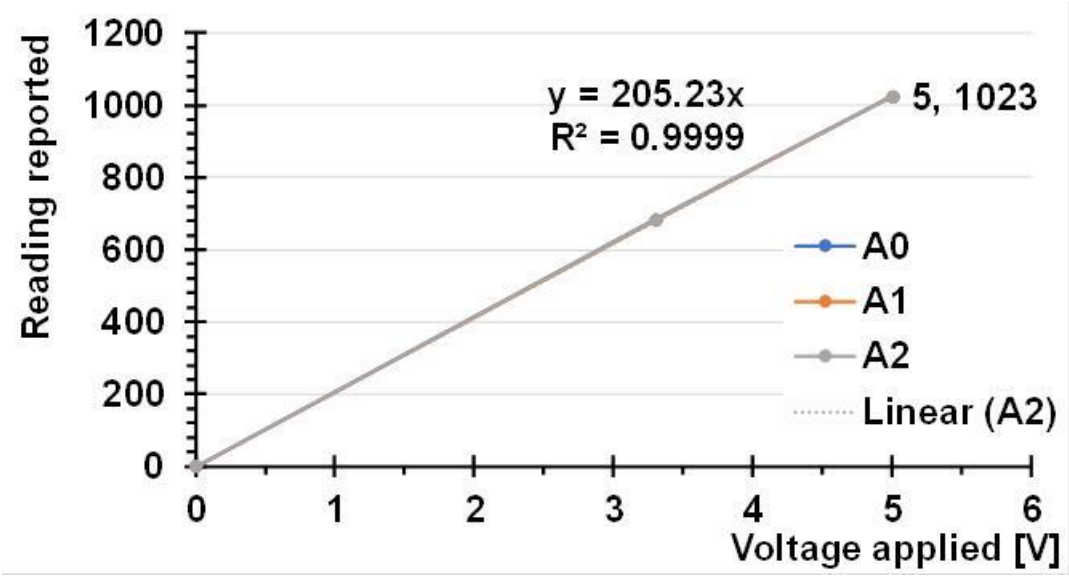

Figure 151: Linearity check of the Analogue input port on the Arduino Uno, between a voltage applied and the reading reported in the software using the analogRead method

LP 56	An Arduino offers an option as a control platform. Shields can be used to provide GPRS interfacing and local data storage. However, the processor size may be a limiting factor.

15.4 Summary

Summary	Comment
Application	Can be used • to provide data from close to real time for DNR (several seconds) helping with fault restoration although not directional • exception reporting • load profiling • MDI The Arduino is most useful in interfacing to the I2C sensors for which there are existing libraries
Data Location	Can be sent • Locally as limited by a shield which has a memory card inserted • Server – to be accessed by anyone in the company – however difficult to do as limited memory to deal with security issues
Data fidelity	Time spans can be set to • Near real time (<15s) • 10min intervals and above

	The data can be time stamped but isn't synchronous
Data backup	Only through addition of external shield
Data form	The data can be in the following form • Time stamped in any relevant format eg Peak/RMS over different time intervals where RMS is peak/root (2)
Failure mode	• Fail dead

Test	Comments
Linearity	Depends on sensor type
Stability/reliability	Appears stable
Ease of deployment	Needs connecting to mobile phone and to sensor – needs packaging
Calibration	Depends on sensor type
Time constants	Additional delay to phone - Delay of around >12ms for raw data
Accuracy	Depends on sensor type
Sensitivity	Depends on sensor type – but can only deal with voltage signals between 0 and 3.3V and up to 16 bits which needs careful planning as it doesn't deal nicely with floating point numbers
Repeatability	Repeatable
Data Storage	Only through addition of external shield and post processing needed to turn raw data into load current

Other factors	Comments
Primary sensing element	Depends on sensor type
Power/excitation	Phone charging usb cable connected to arduino board which then provides power to I2C devices
Amplification	Depends on sensor type
Analogue filtering	Depends on sensor type
Data conversion	Maybe done on arduino
Digital information processing	Depends on sensor type
Digital communication processing	Maybe done on Arduino but limited by memory
Communication	Mobile network through additional shield board

16 Platform L – Raspberry Pi

The data logging on the Arduino is fairly slow and the memory issues may make it unsuitable for secure communication over the internet. To help with this a Raspberry Pi was also investigated. While this is significantly faster and has more memory it only has digital IO. There is an AtoD chip that can be used with this system – an MCP 3008 chip (around £1.50) and libraries to help with setting this up.

The raspberry pi was set up as a server with a MySQL database to store data readings. The program was coded in python and this accessed the chip readings and downloaded these to the MySQL database. For testing purposes these were linked to the output of the coils that were connected firstly to the three phase cables and then to the trefoil arrangement. The data was logged internally and then extracted. All the code is included in the Appendix. The setup of the raspberry pi from scratch for this purpose has also been captured and is listed in the Appendix. The most straightforward method of sending data over the mobile network is to use a dongle – which can just be plugged straight into a USB port on the board. The Huawei dongle was chosen as this seemed a popular choice on the internet. A pay as you go SIM card was inserted and data passed over the network via this method.

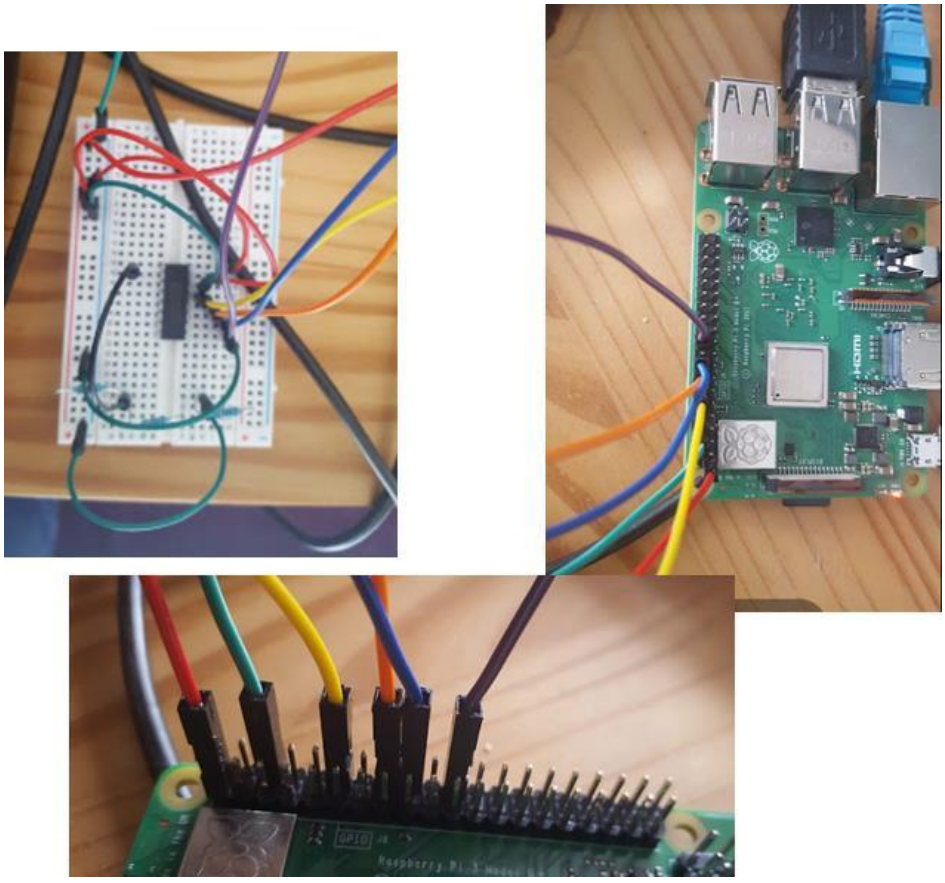

Figure 152: photo of wiring for raspberry pi with AI chip

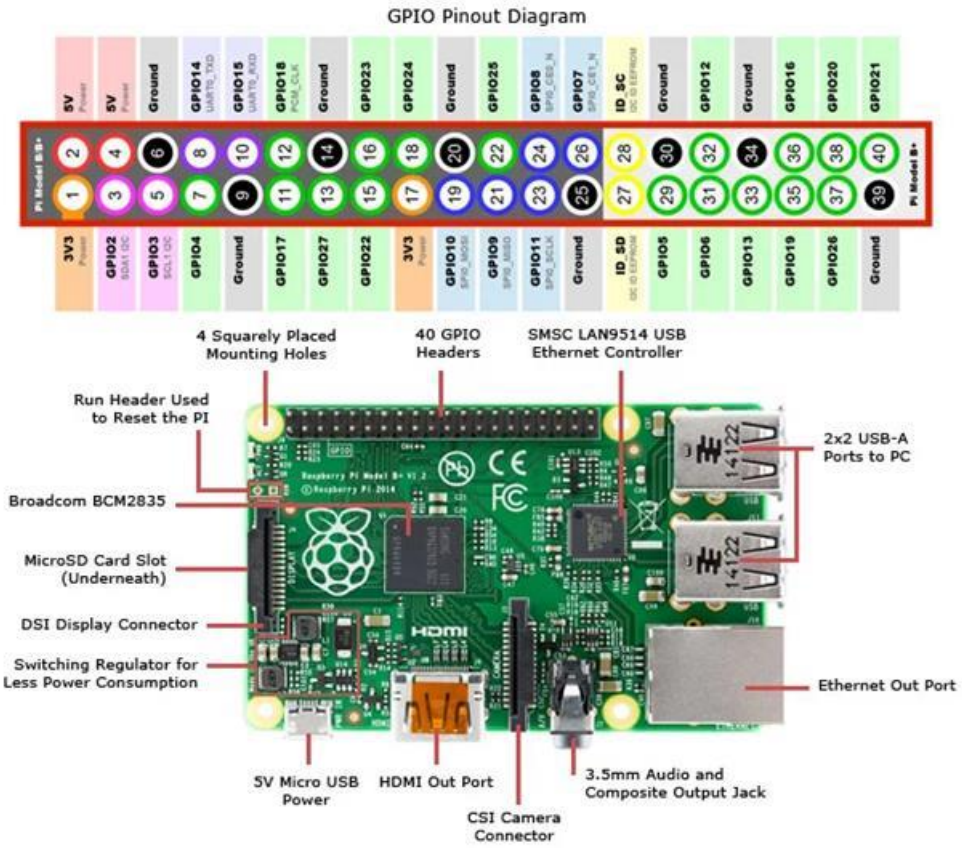

Figure 153: Raspberry pi IO ports

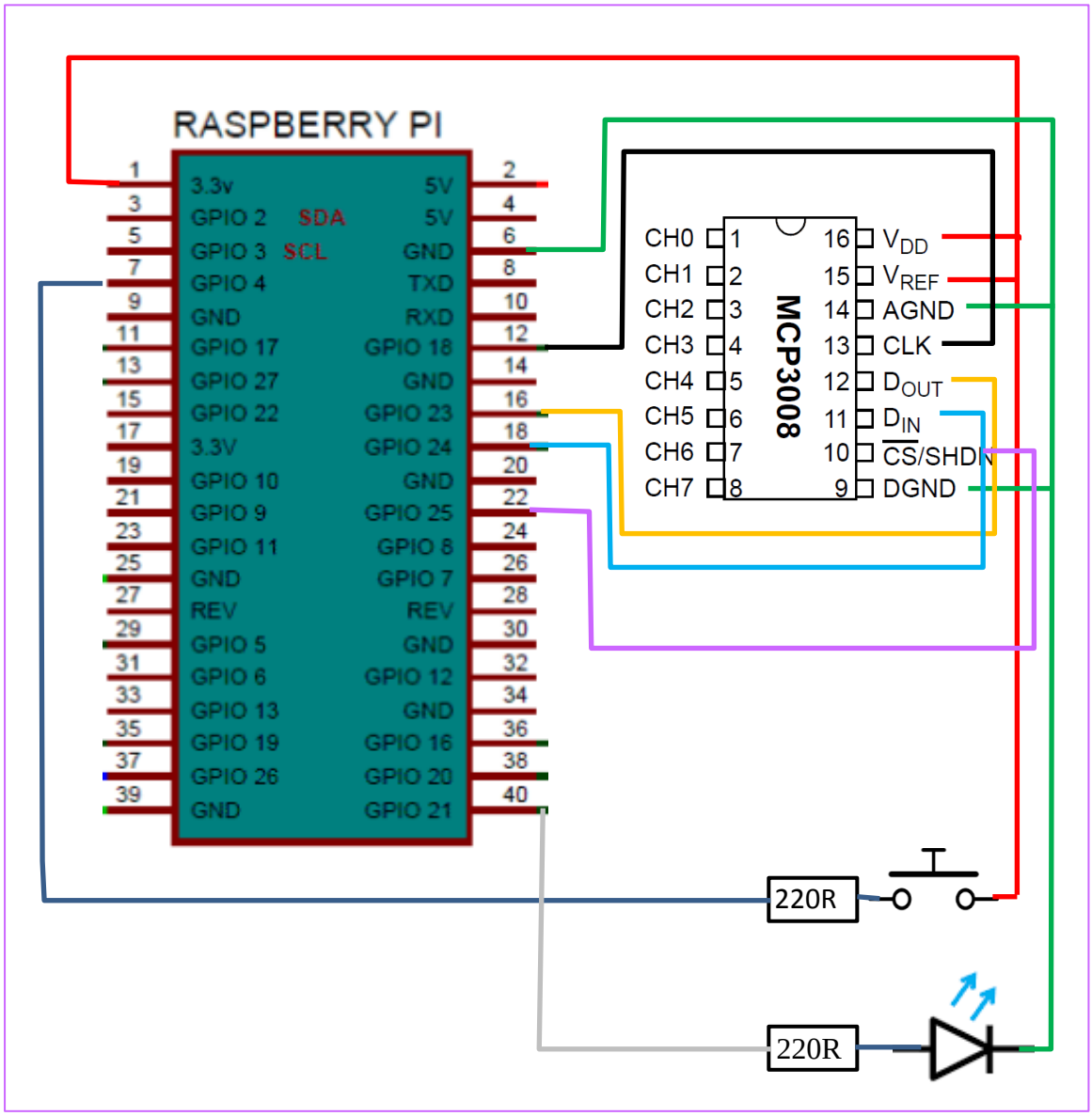

Figure 154: Raspberry pi wiring diagram for testing

Each measurement was time stamped and the timing resolution is shown in Figure 155.

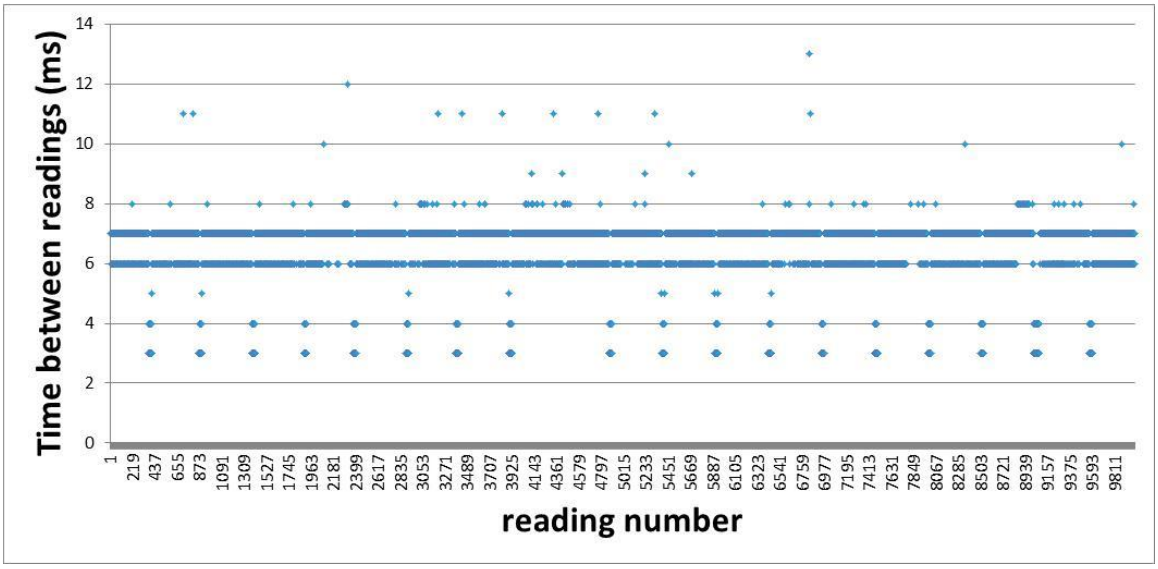

Figure 155: timing of data capture on raspberry pi

Using the raspberry pi with two coils at 90^{o} apart and using the code developed for the magnetometer to avoid any spurious spikes gives the readings in section 7.3.4. The raw data for this is shown in Figure 157 while the setup is shown in Figure 156

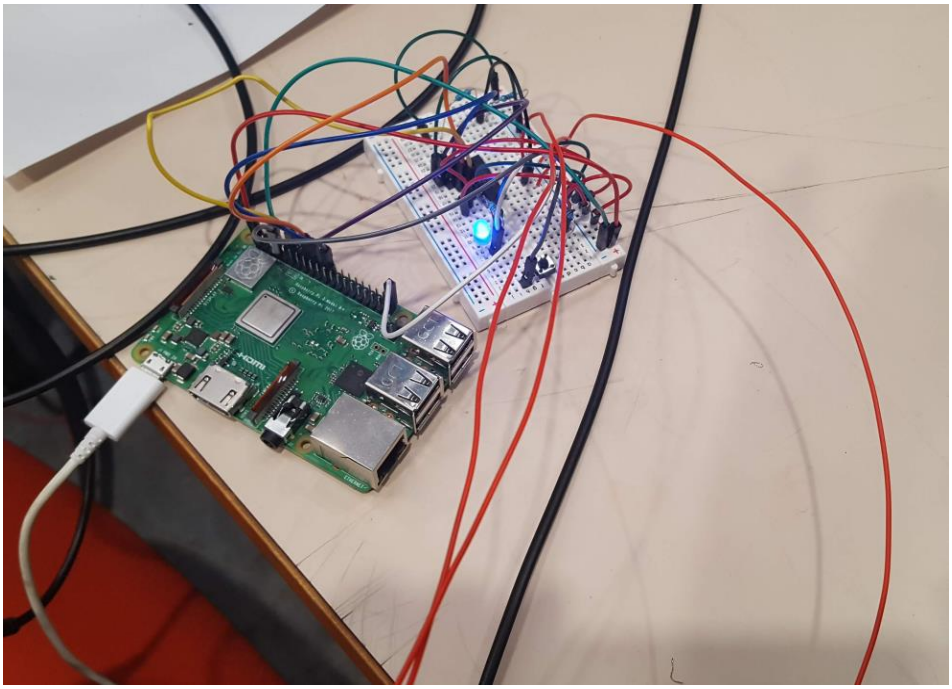

Figure 156: Raspberry pi wired to log the data on the coils. The blue LED shows when data logging occurs and a push button starts and stops the logging

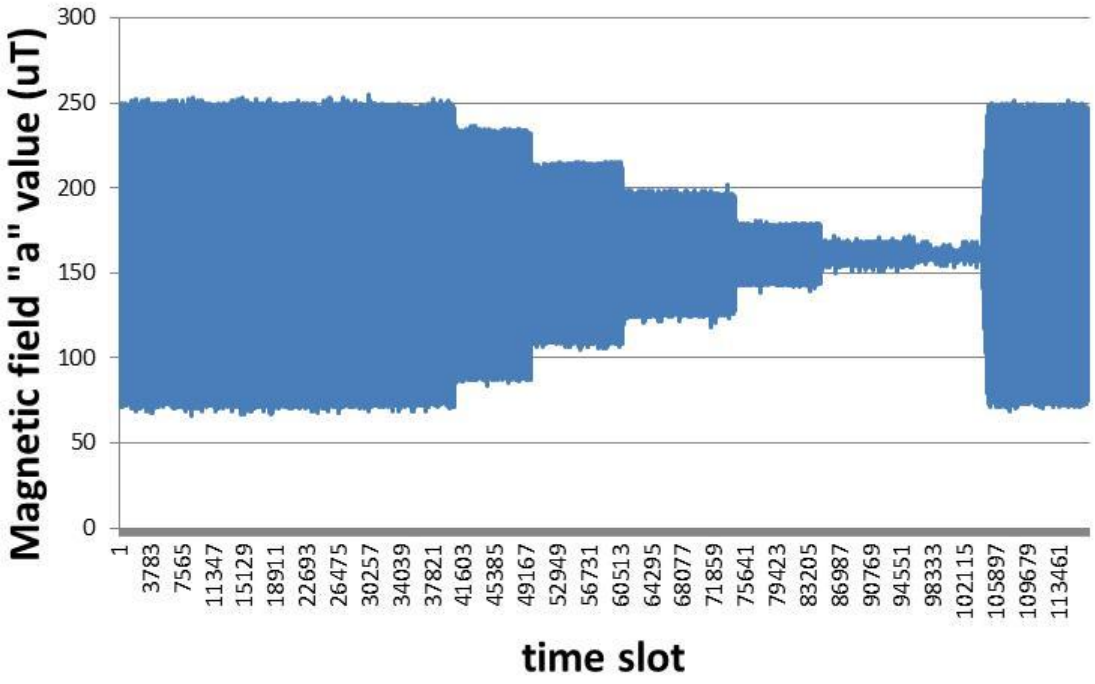

Figure 157: Raspberry pi data logged on 3 core cable

LP 57	A Raspberry pi is a useful platform for gathering, processing and sending on data. There is sufficient memory to enable an on board database to be set up and the processing of the signals is not as limited by other applications as the mobile phone. The interface to analogue inputs is provided by a low cost chip for which library functions are available.

16.1 Summary

Summary	Comment
Application	Can be used • to provide data from close to real time for DNR (several seconds) helping with fault restoration although not directional • exception reporting • load profiling • MDI The Raspberry Pi has the quickest data logging and this could help capture more accurate readings
Data Location	Can be sent • Locally and stored on raspberry pi acting as a server • Server – to be accessed by anyone in the company
Data fidelity	Time spans can be set to • Near real time (<15s) • 10min intervals and above The data can be time stamped but isn't synchronous
Data backup	• Locally and stored on raspberry pi acting as a server
Data form	The data can be in the following form • Time stamped in any relevant format eg Peak/RMS over different time intervals where RMS is peak/root (2)
Failure mode	• Fail dead

Test	Comments
Linearity	Additional AtoD chip needed to get AI. Linearity depends on sensor type and AtoD converter has 12 bit accuracy
Stability/reliability	Appears stable
Ease of deployment	Needs connecting to AtoD chip
Calibration	Depends on sensor type
Time constants	Around 7ms but some quicker data capture
Accuracy	Depends on sensor type
Sensitivity	Depends on sensor type – but can only deal with voltage signals between 0 and 3.3V and up to 12 bits
Repeatability	Repeatable
Data Storage	Locally and stored on raspberry pi acting as a server

Other factors	Comments
Primary sensing element	Depends on sensor type
Power/excitation	Phone charging usb cable connected to raspberry pi board which then provides power to chip. However, suggested usb supply to

	separate board to prevent drop in voltage if dongle used
Amplification	Depends on sensor type
Analogue filtering	Depends on sensor type
Data conversion	Maybe done on raspberry pi
Digital information processing	Depends on sensor type
Digital communication processing	Maybe done on raspberry pi
Communication	Mobile network through dongle or shield

17 Conclusions and recommendations

A summary of the sensors tested are as follows:

Table 17-1 : Summary table

Sensor	Advantages	Disadvantages	Deploy for further testing
Magnetometer	Already exists on a mobile phone platform	May need to calculate a "phone factor" prior to installation on site	Yes
Hall effect Chip		Unable to get working	No
I2m coil	Quick to install	Theory around back calculation of current still needs work	Yes
Accelerometer		No obvious relationship has been developed. Would require on-site calibration	No
Microphone		Significant amount of processing and its not clear if the control platforms would be able to log data to sufficient fidelity. Correlation poor and on-site calibration would be needed	No
Strain gauge		Difficult to get working Fragile to install and Likely to have some drift	No
Temperature sensors		Previous work suggests that installation on transformers is possible but calibration on site and model tuning would be needed. Results not sufficiently detailed within this work.	No
Thermal Imaging		Unable to get working	No
Platform	**Advantages**	**Disadvantages**	**Deploy for further testing**
Mobile phone	Can connect directly to the Network to upload and download information	No immediate analogue inputs available. Internal magnetometer sensor may be used	Yes
IOIO board	Provides the IO ports for the phone	Adds additional cost to the mobile phone platform	Maybe
Arduino	Easy to use and code	Needs a shield to connect to the mobile network and the lack of memory may be an issue for processing and uploading data securely	No
Raspberry Pi	Powerful with good onboard storage	Needs an additional IO chip to give analogue inputs. This is not as expensive as that required by the phone. This has the fastest of all the data logging solutions that were tried	Yes

A high level summary of all the testing is provided in the table over

	Sensor Type									Platform			
	Magnetometer	Hall Effect chip	I2m coil sensor	Accelerometer	Audio Microphone	Strain gauge	Thermal stickers	Thermal transducer	Low cost thermal imaging	Android Phone	Sensor with IOIO board and phone	Arduino	Raspberry Pi
Cost	£14	£2	£13	£19	£9	£31	£4	£99	£350	£13 + phone	£35 + phone	£49	£37 dongle
Application													
Monitoring load close to real time < 10s	✓	×	✓	×	×	×	×	×	×	✓	✓	✓	✓
Load profiling (30min peak)	✓	×	✓	×	×	×	×	×	×	✓	✓	✓	✓
Exception reporting (> max value)	✓	×	✓	×	×	×	×	✓	×	✓	✓	✓	✓
MDI	✓	×	✓	×	×	×	?	✓	×	✓	✓	✓	✓
Data storage													
Uploaded to a server										✓	✓	?	✓
Stored locally										✓	✓	✓	✓
Data form													
Current peak	✓	×	✓	×	×	×	×	×	×	✓			
Current RMS	✓	×	✓	×	×	?	×	×	×	✓			
1 phase	✓	×	×	×	×	×	×	×	×	✓			
3 phase (cable)	✓	×	✓	×	×	×	×	×	×	✓			
Load from transformer	×	×	×	?	?	×	?	?	×	×			
Data Quality													
Linearity	✓	×	✓	?	?	✓	?	✓	×	✓	✓	✓	✓
Correlation with load	> 0.999	×	> 0.996	×	0.48	-0.91	?	?	×	> 0.999			
Accuracy	> 7.5%	×	> 10%[1]	×	?	< 25%	?	?	×	> 7.5%			
Recommend for Field Trial	✓	×	✓	×	×	×	×	×	×	✓	×	×	✓

✓ Tested, satisfactory > better than

× Tested, unsuitable < worse than

? Test not conclusive

[1]There is still significant theory needed to back calculate current for distributed windings and this value could be easily improved.

It is recommended that the magnetometer and i2m coil be taken forward for further testing.

18 Appendix A - Summary of learning points

LP 1	Sensors to measure current in multicore/trefoil cables are not commercially available and there is no available published literature on measurement solutions. These are the most popular type of cable on the distribution Network. Therefore, measuring these types of cable without separating the cores with a single sensor may be valuable.
LP 2	Low cost control platforms for logging data operate at a time span that is comparable to the frequency of the supply. Care is therefore needed to deal with aliasing and post data processing. In particular, it is recommended that traditional calculation of RMS is not used on fast changing signals such as magnetic field.
LP 3	Good RMS values can be obtained from looking for the peak values over a fixed time span (eg 1 second) and dividing by the square root of 2 if the data isn't corrupted. However this isn't guaranteed.
LP 4	Using an exponential moving average method with principle component analysis (calculating the "a" dimension of the magnetic field when plotted as an elliptical curve) is the most suitable method for removing the impact of aliasing and also ensuring that spurious data points do not disrupt the information while getting clean boundary changes when the current changes.
LP 5	Pre-fabricated MEMs sensor development boards help reduced time scales to development and are set up to easily interface through common platforms. These may also come with libraries which speed development on the coding.
LP 6	A magnetometer detects magnetic field on three axes. Saturation on one sensor vector doesn't impact any of the other sensor axes and it's still possible to obtain meaningful relationships between load current and magnetic field – even if not all the chip's sensor axes are used.
LP 7	However, Saturation of sensor output even on one axis of a magnetometer compromises the ability to accurately check measurements against theory using principle component analysis.
LP 8	Not all magnetometers are equally useful for measuring field. Careful selection is needed to get a magnetometer fit for purpose.
LP 9	The magnetometer field appeared to increase slightly with temperature. This is in keeping with previously published work. In this application the impact is minimal.
LP 10	MEMs magnetometers are able to measure fields which can track the loading on a cable.
LP 11	Installing the MEMs magnetometers at a substation took less than 5 minutes – attach the device to the cable and provide power to the platform unit. Further work is needed on packaging this solution to give it an appropriate IP rating and allow the connectors to be better developed.
LP 12	The cost of the MEM's magnetometer is such that more than one may be applied to different cables (limited by the IO of the platform) and these may be daisy chained on the I^2C bus. The theoretical limit is 127 but this is lower in practice.
LP 13	It could be possible to pick up some harmonic content within the system, but the maths needs to be further developed. This is also limited by the processor of the platform device.

LP 14	A hall effect measurement device did not provide a suitable measurement reading to allow output to be correlated to load current.
LP 15	There are many different methods to produce turns or wire onto something suitable to go round a cable. Material with conductive thread could be best for large scale implementation as the coils may be made to tighter specifications in a manufacturing environment (eg straight sides) and these can be easily overlapped for multi-coil designs and stacked to increase the number of turns. In addition waterproofing and adding suitable fastenings eg Velcro could ensure fast installation.
LP 16	The new coil designs were all easily installed either by tape or cable ties. These were then plugged into an amplifier and level shift circuit before connection to a raspberry pi.
LP 17	The new coil designs showed good correlation between measurement and load current in a balanced system.
LP 18	At this stage the maths behind the i2m coil needs further development to take into account factors such as the distributed nature of the windings or the lumping together of the windings and also to look at imbalance.
LP 19	There was no impact on the readings in the presence of a thermal source (heat gun) and only a very small change in value with close by metal work.
LP 20	The coils have to fit 180^{o} around the cable these mean the coils sides have to be a set distance apart. The sewn coil offers the best opportunity for a single design as it can be folded to give the straight edges 180^{o} apart. The PCB and wired coil would need to be made in different sizes for large scale roll out.
LP 21	Although the coil itself can pick up the harmonics. The platform it is connected to may limit the use of this information through the data logging resolution and also timing.
LP 22	The testing undertaken indicated that it was not going to be possible to relate vibration with loading.
LP 23	Even if further testing proved there to be a relationship between loading and vibration under more highly loaded transformers it would require a significant amount of work to develop the maths and calibration process required for large scale roll out. It is unlikely that the calibration procedure could be achieved in a low enough time scale to keep the costs of installation below £50.
LP 24	The testing undertaken indicated that it was not going to be possible to relate noise with loading.
LP 25	Even if further testing proved there to be a relationship between loading and noise under more highly loaded transformers it would require a significant amount of work to develop the maths and calibration process required for large scale roll out. It is unlikely that the calibration procedure could be achieved in a low enough time scale to keep the costs of installation below £50.
LP 26	There would also be challenges involved in capturing the data at a high enough sampling rate to enable a fast Fourier transform to be undertaken to pick up the 100Hz component. None of the low cost platforms had this capability and an FPGA board would probably be required. These are significantly more expensive at the moment but are dropping in price.
LP 27	The long quarter bridge strain gauge was difficult to attach and came loose easily. Therefore, it is not recommended

LP 28	The strain gauge did show some correlation between strain gauge measurement and load current. However, this was not very accurate.
LP 29	The quarter bridge strain gauge measurements were less accurate and there was at least one ambiguous data point. This type of strain gauge is not recommended.
LP 30	Calibrating a temperature measurement in one location with or without Utility found equipment does not guarantee calibration in other locations or with other pieces of equipment.
LP 31	Temperature calibration may change due to external influences such as temperature or over time.
LP 32	Thermal stickers are low cost devices that show temperature. However, it is not clear if there is a business case for their use as these would need to be manually observed.
LP 33	A temperature alarm works fine from detection through to received text message. It is an expensive option compared to some of the other sensors and platforms which could offer better data at higher fidelity for lower price.
LP 34	A temperature alarm sensor would not to be calibrated on site – as it is not directly looking for a load current – but would look instead at ensuring that the tank temperature (as a proxy for top oil temperature) did not exceed values set by standards (60^{o}C above 20^{o}C ambient BSEN600-76-2_2011).
LP 35	It should be possible to link a temperature measurement device such a thermistor to a transformer to give an indication of loading. However no representative hardware was available to test properly and calibration on site may be needed.
LP 36	Thermal imaging using an android phone is not going to be suitable as measuring through a conventional camera by changing the filtering couldn't be made to work.
LP 37	Distance is a factor when turning magnetic field back to an estimate of load current. Therefore, the location of the sensor is important to estimate its distance from the centre of the cable.
LP 38	It works well to use an Android phone as a control platform especially if the internal Magnetometer is being used. However bespoke App software is required to ensure methodology and Readings are transparent.
LP 39	Different phones have different sensors, and these may be in different locations within the phone. If a variety of android types are to be used in large scale testing, then any variance needs to be known so it can be accounted for.
LP 40	There is an obvious relationship between phone magnetometer measurement and current.
LP 41	For early testing the quickest way to attach the phone to the cable was by tape. However, it means the phone is not necessarily the same distance from the centre of the cable and is not always at the same angle. This makes it difficult to test for consistency as distance is a factor. A method of fixing distance was developed to compensate for this.
LP 42	At higher currents saturation may be an issue – However this can be mitigated.
LP 43	Careful placement of the phone can be used to offset issues from saturation. As there are different ratings of substations and different cable types – it may be that a space holder is used for a range of types where angle and distance are carefully matched to rating.

LP 44	Using “calibrated” Android phone data can result in factors being arbitrary applied to the measurement at random points in the measurement. This is not so much of an issue for the un-calibrated data which is reported as uncalibrated plus a calibration factor.
LP 45	It is possible to remove the impact of calibration, but this requires post processing or adaptive processing as results are being collected. It is much more straightforward to use the uncalibrated data. However, this can also be adjusted by the phone controller.
LP 46	Android datalogger apps tend to measure with a randomised time interval, so the data must be carefully processed so aliasing effects don’t introduce bias into values.
LP 47	The temporal resolution of measurements on a phone varies from any delay set in code dependent on the processor and other core phone specifications. It is also dependent on what other apps are running and their processor usage.
LP 48	Downloading the data to a server from a mobile phone over Wi-Fi increases the measurement time further and sub 50ms measurement may not be possible.
LP 49	Temperature does not seem to impact the magnetometer reading as the phone is designed to internally compensate for this.
LP 50	Using a phone to calculated load current is possible. There is a good degree of linearity and correlation. The accuracy of the direct back calculation of current from the phone is less than would be liked. However, a lower magnetometer reading shows a higher value of current than would be obtained in the field and therefore there is an inherent safety margin. To get more accurate results a “phone factor” is suggested which could be used to multiply to the calculated current.
LP 51	Calculation on three core and single core cables show different levels of accuracy. This means a phone factor would be required which would depend on cable type.
LP 52	There is some inconsistency between phone types depending on cable type. It could mean that certain phones are more suitable for certain types of cable. This could be related to location and direction of sensor.
LP 53	Installing the phone was the easiest of the sensor installation options. The phone was cable tied to the cable and the phone clipped into place and then App started. A USB power supply was connected to the phone to ensure it didn’t run out of charge.
LP 54	A mobile phone magnetometer was successfully used to log data at a substation on both the LV and HV cable and the data was sent via WI-Fi to a server.
LP 55	An IOIO board offers a neat solution to turn a mobile phone into a controller with up to 60 I/O. It would allow the phone to be connected to any of the sensors under investigation.
LP 56	An Arduino offers an option as a control platform. Shields can be used to provide GPRS interfacing and local data storage. However, the processor size may be a limiting factor.
LP 57	A Raspberry pi is a useful platform for gathering, processing and sending on data. There is sufficient memory to enable an on board database to be set up and the processing of the signals is not as limited by other applications as the mobile phone. The interface to analogue inputs is provided by a low cost chip for which library functions are available.

19 Appendix B – Android Phone setup

19.1 Service Codes

Various technician screens are available in android which are not normally seen by the user, these are accessed by typing the following codes into the phones keypad:

#0# Hardware diagnostics
* #1234# to check software version of phone.
*#12580*369# to check software and hardware information.
*#0228# Battery status (ADC, RSSI reading)
*#0011# Service Menu

The diagnostics code *#0*# can be used to check the SENSOR_STATUS_ACCURACY variable as shown.

Figure 158 : Photograph showing Android sensor diagnostic summary screen.

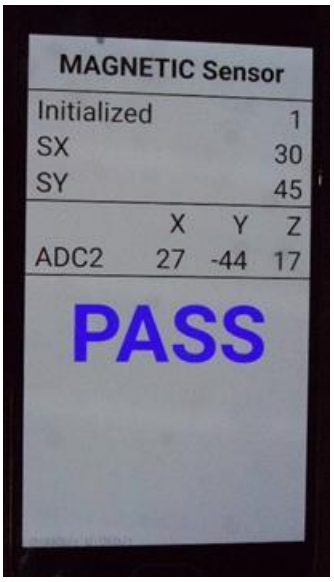

Figure 159 : Photograph showing Android magnetic sensor self-test screen.

https://stackoverflow.com/questions/28265596/uncalibrated-magnetometer-issues
https://developer.android.com/guide/topics/sensors/sensors_position.html#sensors-pos-magunc

19.2 Enable developer settings on the phone

Procedure

- Search "*android phone enable developer mode*"
- Select *settings*
- Select *about device*
- Select *software info*

- Select *build no* and *tap this 7 times*
-

This gives developer options at the bottom of the settings menu

- Go back to *settings*
- Select *developer options*
- Select *USB debugging*
- Turn this on

19.3 Upload the App to the Phone

The software is written in a package called *Android Studio*
To load the software from Android studio to the phone

- Plug the USB cable from the computer into the phone
- On the menu bar of Android studio there is a picture of a green triangle and a green triangle next to traffic lights. Either will do but the traffic light option allows extra debugging. Click on this
- Select *deployment target*
- Select *real devices* (as opposed to a simulated or emulated device)
- Choose the phone from the list and click *ok*

At this point it is probable that extra libraries will be needed (either to deal with the device or Android version or randomly!). The software will tell you it needs to install these. Click ok and the software will download libraries and download software to phone. The phone will launch automatically.

19.4 Using the Deduce App on the phone

- Go to settings
- Select the site (e.g. Castle Black) ultimately this will be a list of substations
- Choose the server – for this report that is *bim*
- Use the slider to move between pause and data capture. A counter increments when data is captured but is difficult to see if this is at too high a rate.
- There is a button to delete the readings off the phone (but not the server)

19.5 Viewing the data

The server is located at

Bim.shef.ac.uk/sensormonitor/view_data.php

Select the site and the click refresh

Data can be copied and pasted in html or as csv.

Information on the sensors can be found at
Developer.android.com/reference/android/hardware/sensorevent.html

19.6 Checking the server

To ensure the server is ok
Go to bim/shef.ac.uk/sensormonitor/sync_test.php

Send false readings to the data base to test

- *Randomise* to set a random field
- *Record* to pretend to record this
- *Upload* to upload to the server

Select nothing under server id and when upload is clicked the server selects an ID number and sends it back to appear on the screen.

19.7 Changing the smartphone app Java code

The software is version controlled through Github.com

There are two versions of code – 1 to set up the server and the other to deal with the phone App.

To access the code a login is needed with Github. The login ID needs to be emailed to the software owner so that access to edit may be granted.

In Android studio's

- In the menu bar select VCS (version control software)
- Select check out from version control under Github
- Link to https://github.com/NeilStrickland/sensormonitor_client.git
- Select either the sensor monitor server or sensor monitor client and select *clone*
- This downloads into the Android studios and should launch automatically
- After changes have been made these can be committed back to Github (little up arrow and in the menu bar)
- This is currently under a public repository. A private repository costs $84 pa.

Note: when this is being setup for the first time it will take a while with lots of additional file downloads.

20 Appendix C – Android Source code for ellipse calculations

From github.com/NeilStrickland/sensormonitor_client

```
package com.example.neil.sensormonitor;

import android.hardware.Sensor;
import android.hardware.SensorEvent;
import android.os.AsyncTask;
import android.util.Log;

public class BCUMonitor {
    boolean saveReadings = true;
    boolean saveSummaries = true;
    int fadeTime = 1000; // milliseconds
    int saveReadingsInterval = 10000; // milliseconds
    int saveSummariesInterval = 10000; // milliseconds

    BCUReading latestReading = new BCUReading();
    BCUSummary latestSummary = new BCUSummary();
    long lastSavedReadingTimestamp = 0;
    long lastSavedSummaryTimestamp = 0;

    void addReading(BCUReading r) {
        latestReading = r;
        BCUSummary s = latestSummary;
        double delta_t = r.timestamp - s.timestamp;
        double fadeFactor = Math.exp(-delta_t/fadeTime);
        double Bx0 = r.BUx - s.Bx_bar;
        double By0 = r.BUy - s.By_bar;
        double Bz0 = r.BUz - s.Bz_bar;
        double Mxx = Bx0*Bx0;
        double Mxy = Bx0*Bz0;
        double Myy = Bz0*Bz0;
        s.Bx_bar  = fadeFactor * s.Bx_bar  + (1 - fadeFactor)*r.BUx;
        s.By_bar  = fadeFactor * s.By_bar  + (1 - fadeFactor)*r.BUy;
        s.Bz_bar  = fadeFactor * s.Bz_bar  + (1 - fadeFactor)*r.BUz;
        s.Mxx_bar = fadeFactor * s.Mxx_bar + (1 - fadeFactor)*Mxx;
        s.Mxz_bar = fadeFactor * s.Mxz_bar + (1 - fadeFactor)*Mxy;
        s.Mzz_bar = fadeFactor * s.Mzz_bar + (1 - fadeFactor)*Myy;
        double S = Math.hypot(s.Mxx_bar - s.Mzz_bar,2*s.Mxz_bar);
        s.a = Math.sqrt(s.Mxx_bar+s.Mzz_bar+S);
        s.b = Math.sqrt(s.Mxx_bar+s.Mzz_bar-S);
        if (Double.isNaN(s.a)) {s.a = 0;}
        if (Double.isNaN(s.b)) {s.b = 0;}
        s.Ux = 2*s.Mxz_bar;
        s.Uz = s.Mzz_bar - s.Mxx_bar + S;
        double nU = Math.hypot(s.Ux,s.Uz);
        if (nU > 0) {
            s.Ux = s.Ux / nU;
            s.Uz = s.Uz / nU;
        } else {
            s.Ux = 0;
            s.Uz = 0;
        }
        s.Vx = -s.Uz;
        s.Vz = s.Ux;
        double cU1 = 0;
        double cV1 = 0;
```

```
        if (s.a > 0) {cU1 = (Bx0 * s.Ux + By0 * s.Uz) / s.a;}
        if (s.b > 0) {cV1 = (Bx0 * s.Vx + By0 * s.Vz) / s.b;}
        double nC = Math.hypot(cU1,cV1);
        if (nC > 0) {
            cU1 = cU1/nC;
            cV1 = cV1/nC;
        }
        double delta_theta = Math.atan2(s.cU*cV1-
s.cV*cU1,s.cU*cU1+s.cV*cV1);
        if (delta_t > 0) {
            s.frequency = delta_theta / (2 * Math.PI * delta_t * 0.001);
        } else {
            s.frequency = 0;
        }
        s.cU = cU1;
        s.cV = cV1;
        s.timestamp = r.timestamp;

        if (saveReadings && (r.timestamp - lastSavedReadingTimestamp >
saveReadingsInterval)) {
            new SaveReadingTask().execute(latestReading);
            lastSavedReadingTimestamp = r.timestamp;
        }

        if (saveSummaries && (r.timestamp - lastSavedSummaryTimestamp >
saveSummariesInterval)) {
            new SaveSummaryTask().execute(latestSummary);
            lastSavedSummaryTimestamp = r.timestamp;
        }
    }

    void addReading(SensorEvent event) {
        Log.i("sensormonitor","addReading: T0");
        if (event.sensor.getType() ==
Sensor.TYPE_MAGNETIC_FIELD_UNCALIBRATED) {
            BCUReading r = new BCUReading(event);
            addReading(r);
        }
    }

    private class SaveReadingTask extends AsyncTask<BCUReading, Void,
Void> {
        @Override
        protected Void doInBackground(BCUReading... xs) {
            AppDatabase db = App.get().getDb();
            for (BCUReading x : xs) {
                db.bcuReadingDao().insert(x);
            }
            return null;
        }
    }

    private class SaveSummaryTask extends AsyncTask<BCUSummary, Void,
Void> {
        @Override
        protected Void doInBackground(BCUSummary... xs) {
            AppDatabase db = App.get().getDb();
            for (BCUSummary x : xs) {
                db.bcuSummaryDao().insert(x);
            }
```

```
                return null;
            }
        }
    }
```

21 Appendix D – Arduino Source code used for testing

Code for the Arduino Uno and LinkitOne boards was written in a form of C++ using the Arduino IDE on a PC and uploaded to the boards via USB cable. The various digital sensors and other add-on boards (Wi-Fi, LCD display) were selected because open source Arduino libraries are available for them. This meant that they can be setup and controlled with a few lines of code, avoiding the need to send and receive numerous serial data commands.
The following libraries were added in the Arduino IDE.

- Adafruit_LSM9DS0
- Adafruit_Sensor
- SparkFunMPU9250-DMP

```
#include <Wire.h>
#include <SPI.h>
#include <Adafruit_LSM9DS0.h>
#include <Adafruit_Sensor.h>
#include <SparkFunMPU9250-DMP.h>

boolean LSM9DS0_found = false;
boolean MPU9250_found = false;

unsigned long timeNow = 0;
unsigned long mSecInHour = 3600000;
unsigned long TimeNow =0;
int millisecs =0;
int seconds = 0;
byte minutes = 0;
byte hours = 0;

int raw_x;
int raw_y;
int raw_z;
int accel_raw_x;
int accel_raw_y;
int accel_raw_z;
int raw_x_9250;
int raw_y_9250;
int raw_z_9250;
int raw_accel_x_9250;
int raw_accel_y_9250;
int raw_accel_z_9250;


int raw_a0;
int raw_a1;
int raw_a2;

// i2c
Adafruit_LSM9DS0 lsm = Adafruit_LSM9DS0();
// You can also use software SPI
//Adafruit_LSM9DS0 lsm = Adafruit_LSM9DS0(13, 12, 11, 10, 9);
// Or hardware SPI! In this case, only CS pins are passed in
//Adafruit_LSM9DS0 lsm = Adafruit_LSM9DS0(10, 9);
```

```
MPU9250_DMP imu;

void setupSensor()
{
  // 1.) Set the accelerometer range (2G,4G,6G,8G,16G )
  lsm.setupAccel(lsm.LSM9DS0_ACCELRANGE_2G);
  // 2.) Set the magnetometer sensitivity (2GAUSS,4GAUSS,8GAUSS,12GAUSS)
  lsm.setupMag(lsm.LSM9DS0_MAGGAIN_12GAUSS);
  // 3.) Setup the gyroscope (245DPS,500DPS,2000DPS)
  //  lsm.setupGyro(lsm.LSM9DS0_GYROSCALE_245DPS);
}

void setup()
{
  pinMode(A0, INPUT);
  pinMode(A1, INPUT);
  pinMode(A2, INPUT);

#ifndef ESP8266
  while (!Serial);     // will pause Zero, Leonardo, etc until serial
console opens
#endif
  Serial.begin(9600);

// Try to initialise and warn if we couldn't detect the chip
  if (!lsm.begin())
  {
    Serial.println(F("Oops ... unable to initialize the LSM9DS0. Check
your wiring!"));
    while (1); { Serial.println(F("Found LSM9DS0 9DOF, measurements in
Gauss"));}
  }
  else
  {
    LSM9DSO_found = true;
  }

//  if (imu.begin() != INV_SUCCESS)
//  { while (1) { Serial.println("No MPU-9250 found, Check
connections"); }
//  imu.setSensors(INV_XYZ_ACCEL | INV_XYZ_COMPASS); // Enable chosen
sensors:
//  imu.setAccelFSR(2); // Set accel = +/-2g (2, 4, 8, 16g allowed) FSR is
+/- 4912 uT
//  imu.setLPF(188); // Set accel & gyro LPF corner freq 188, 98, 42, 20,
10, 5 Hz allowed
//  imu.setSampleRate(4); // Set accel/gyro sample rate 4Hz to 1kHz
allowed
//  imu.setCompassSampleRate(1); // Set mag sample rate (1-100Hz allowed)
//  MPU9250_found = true;
// }

  Serial.println(F("MilliSecsApprox,TimeElapsed, mag_x, mag_y, mag_z, "));
  Serial.println(F("accel_x, accel_y, accel_z, a0, a1, a2 "));
  Serial.println(F(""));
 }

void loop()
{
```

```
  TimeNow = millis();
  hours = TimeNow/mSecInHour;
  minutes = (TimeNow-(hours*mSecInHour))/(mSecInHour/60);
  seconds = (TimeNow-(hours*mSecInHour)-(minutes*(mSecInHour/60)))/1000;
  millisecs = TimeNow-(hours*mSecInHour)-(minutes*(mSecInHour/60))-
(seconds*1000);

//  lsm.read();
//  if ( imu.dataReady() )
//  { imu.update(UPDATE_ACCEL | UPDATE_COMPASS);}

//  raw_x = lsm.magData.x;
//  raw_y = lsm.magData.y;
//  raw_z = lsm.magData.z;
//  accel_raw_x = lsm.accelData.x;
//  accel_raw_y = lsm.accelData.y;
//  accel_raw_z = lsm.accelData.z;

  if (MPU9250_found)
  {
  raw_x_9250 = 1000 * imu.calcMag(imu.mx);
  raw_y_9250 = 1000 * imu.calcMag(imu.my);
  raw_z_9250 = 1000 * imu.calcMag(imu.mz);
  raw_accel_x_9250 = 1000 * imu.calcAccel(imu.ax);
  raw_accel_y_9250 = 1000 * imu.calcAccel(imu.ay);
  raw_accel_z_9250 = 1000 * imu.calcAccel(imu.az);
  }

  raw_a0 =  analogRead(A0);
  raw_a1 =  analogRead(A1);
  raw_a2 =  analogRead(A2);

  Serial.print(TimeNow);
  Serial.print(", ");
  Serial.print(hours);
  Serial.print(":");
  Serial.print(minutes);
  Serial.print(":");
  Serial.print(seconds);
  Serial.print(".");
if (millisecs<100)     // need to add leading zeros for fractional
millisecs
{ Serial.print("0"); }
if (millisecs<10)
{ Serial.print("0"); }
  Serial.print(millisecs);
  Serial.print(", ");

if (LSM9DSO_found)
  {
  Serial.print((int) (raw_x) );          Serial.print(F(", "));
  Serial.print((int) (raw_y) );          Serial.print(F(", "));
  Serial.print((int) (raw_z) );          Serial.print(F(", "));
  Serial.print((int) (accel_raw_x) );    Serial.print(F(", "));
  Serial.print((int) (accel_raw_y) );    Serial.print(F(", "));
  Serial.print((int) (accel_raw_z) );    Serial.print(F(", "));
}
  else { Serial.print("-9999,-9999,-9999,-9999,-9999,-9999,");}
```

```
  if (MPU9250_found)
  {
  Serial.print((int) (raw_x_9250) );          Serial.print(F(", "));
  Serial.print((int) (raw_y_9250) );          Serial.print(F(", "));
  Serial.print((int) (raw_z_9250) );          Serial.print(F(", "));
  Serial.print((int) (raw_accel_x_9250) );    Serial.print(F(", "));
  Serial.print((int) (raw_accel_y_9250) );    Serial.print(F(", "));
  Serial.print((int) (raw_accel_z_9250) );    Serial.print(F(", "));
}
  else { Serial.print("-9999,-9999,-9999,-9999,-9999,-9999,");}

  Serial.print((int) (raw_a0) );          Serial.print(F(", "));
  Serial.print((int) (raw_a1) );          Serial.print(F(", "));
  Serial.print((int) (raw_a2) );          Serial.print(F(" "));
  Serial.println(F(""));
}
```

22 Appendix E – Raspberry Pi code

```
import math
import time
import datetime
import threading
import mysql.connector
import RPi.GPIO as GPIO
import Adafruit_GPIO.SPI as SPI
import Adafruit_MCP3008

def current_timestamp():
    epoch = datetime.datetime.utcfromtimestamp(0)
    current_datetime = datetime.datetime.now()
    return round((current_datetime - epoch).total_seconds() *
1000.0)

class SensorMonitor:
    def __init__(self):
        self.site_id = 1
        self.BCU_reading_site_id = 0
        self.watcher = None
        self.connection = None
        self.cursor = None
        self.mcp = None
        self.current_BCU_summary = BCU_summary()
        self.current_BCU_summary.site_id = self.site_id

    def GPIO_setup(self):
        # Software SPI configuration:
        # note this software sets the GPIO mode to be GPIO pin
related
        CLK  = 18
        MISO = 23
        MOSI = 24
        CS   = 25
        self.mcp = Adafruit_MCP3008.MCP3008(clk=CLK, cs=CS,
miso=MISO, mosi=MOSI)

        #set GPIO pin 4 - physical pin 7 to be a push button input
        GPIO.setup(4, GPIO.IN, pull_up_down=GPIO.PUD_DOWN)
        #set GPIO 21- physical pin 40 as an LED output - to go high
when recording
        GPIO.setup(21,GPIO.OUT)

    def GPIO_start(self):
        #detect when this has been pushed and if so call logging
routine

GPIO.add_event_detect(4,GPIO.RISING,callback=self.handle_button)

    def database_setup(self):
```

```
        self.connection =
mysql.connector.connect(user='sensormonitor',
                                    password='qvZ5nINAfHJvYlaq',
                                    host='localhost',
                                    database='sensormonitor')
        self.cursor = self.connection.cursor()

    def next_BCU_reading_site_id(self):
        i = self.BCU_reading_site_id
        self.BCU_reading_site_id = i+1
        return i+1

    def take_BCU_reading(self):
        r = BCU_reading()
        r.read(self.mcp)
        r.site_id = self.site_id
        r.site_record_id = self.next_BCU_reading_site_id()
        return r

    def handle_button(self,channel):
        print("Button was pushed!")
        if self.watcher is None:
            print("Starting")
            self.watcher = Watcher(self)
            self.watcher.start()
        else:
            print("Stopping")
            self.watcher.stop()
            self.watcher.join()
            self.watcher = None

class BCU_reading:
    add_query = ("INSERT INTO tbl_BCU_readings"
         "(site_id,site_record_id,timestamp,BUx,BUy,BUz)"
         "VALUES (%s, %s, %s, %s, %s,%s)")

    fmt = '| {0:>6} | {1:>6} | {2:>6} | {3:>9} | {4:>4} | {5:>4} |
{6:>4} |'

    def __init__(self):
        self.id = 0
        self.site_id = 0
        self.site_record_id = 0
        self.timestamp = 0
        self.BUx = 0
        self.BUy = 0
        self.BUz = 0

    def read(self,mcp):
        self.timestamp = current_timestamp()
        self.BUx = mcp.read_adc(0)
        self.BUy = mcp.read_adc(1)
        self.BUz = mcp.read_adc(2)

    def save(self,cursor):
```

```
        values=(self.site_id,self.site_record_id,self.timestamp,
                self.BUx,self.BUy,self.BUz)
        cursor.execute(self.add_query,values)
        self.id = cursor.lastrowid

    def show(self):

print(self.fmt.format(self.id,self.site_id,self.site_record_id,self.
timestamp,
                              self.BUx,self.BUy,self.BUz))

class BCU_summary:
    add_query = ("INSERT INTO tbl_BCU_summaries"

"(site_id,site_record_id,timestamp,Bx_bar,By_bar,Bz_bar,Mxx_bar,Mxz_
bar,Mzz_bar,a,b,Ux,Uz,Vx,Vz,cU,cV,frequency)"
         "VALUES (%s, %s, %s, %s, %s, %s, %s, %s, %s, %s, %s, %s,
%s, %s, %s, %s, %s, %s)")

    fmt = '| {0:>6} | {1:>6} | {2:>6} | {3:>9} | {4:>4} | {5:>4} |
{6:>4} |{7:>4} |{8:>4} | {9:>4} |{10:>4} |{11:>4} |{12:>4} |{13:>4}
|{14:>4} |{15:>4} |{16:>4} |{17:>4} |{18:>4} |'

    def __init__(self):
        self.fadeTime = 1000.0 # milliseconds
        self.id = 0
        self.site_id = 0
        self.site_record_id = 0
        self.timestamp = 0
        self.Bx_bar = 0
        self.By_bar = 0
        self.Bz_bar = 0
        self.Mxx_bar = 0
        self.Mxz_bar = 0
        self.Mzz_bar = 0
        self.a = 0
        self.b = 0
        self.Ux = 0
        self.Uz = 0
        self.Vx = 0
        self.Vz = 0
        self.cU = 0
        self.cV = 0
        self.frequency = 0
        self.BUx=0
        self.BUy=0
        self.BUz=0
        self.last_save_time = current_timestamp()
        self.save_interval = 10000 # milliseconds
        self.latest_reading = None

    def add_reading(self,r):
        self.latest_reading = r
        delta_t = r.timestamp - self.timestamp
        fadeFactor = math.exp(-delta_t/self.fadeTime)
```

```
        Bx0 = r.BUx - self.Bx_bar
        By0 = r.BUy - self.By_bar
        Bz0 = r.BUz - self.Bz_bar
        Mxx = Bx0*Bx0
        Mxy = Bx0*Bz0
        Myy = Bz0*Bz0
        self.Bx_bar  = fadeFactor * self.Bx_bar  + (1 -
fadeFactor)*r.BUx
        self.By_bar  = fadeFactor * self.By_bar  + (1 -
fadeFactor)*r.BUy
        self.Bz_bar  = fadeFactor * self.Bz_bar  + (1 -
fadeFactor)*r.BUz
        self.Mxx_bar = fadeFactor * self.Mxx_bar + (1 -
fadeFactor)*Mxx
        self.Mxz_bar = fadeFactor * self.Mxz_bar + (1 -
fadeFactor)*Mxy
        self.Mzz_bar = fadeFactor * self.Mzz_bar + (1 -
fadeFactor)*Myy
        S = math.hypot(self.Mxx_bar - self.Mzz_bar,2*self.Mxz_bar)
        self.a = math.sqrt(self.Mxx_bar+self.Mzz_bar+S)
        self.b = math.sqrt(self.Mxx_bar+self.Mzz_bar-S)
        if (math.isnan(self.a)):
            self.a = 0
        if (math.isnan(self.b)):
            self.b = 0
        self.Ux = 2*self.Mxz_bar
        self.Uz = self.Mzz_bar - self.Mxx_bar + S
        nU = math.hypot(self.Ux,self.Uz)
        if (nU > 0):
            self.Ux = self.Ux / nU
            self.Uz = self.Uz / nU
        else:
            self.Ux = 0
            self.Uz = 0
        self.Vx = -self.Uz
        self.Vz = self.Ux
        cU1 = 0
        cV1 = 0
        if (self.a > 0):
            U1 = (Bx0 * self.Ux + By0 * self.Uz) / self.a
        if (self.b > 0):
            cV1 = (Bx0 * self.Vx + By0 * self.Vz) / self.b
        nC = math.hypot(cU1,cV1)
        if (nC > 0):
            cU1 = cU1/nC
            cV1 = cV1/nC
        delta_theta = math.atan2(self.cU*cV1-
self.cV*cU1,self.cU*cU1+self.cV*cV1)
        if (delta_t > 0):
            self.frequency = delta_theta / (2 * math.pi * delta_t *
0.001)
        else:
            self.frequency = 0
        self.cU = cU1
        self.cV = cV1
```

```
        self.timestamp = r.timestamp

    def should_save(self):
        return ((self.timestamp - self.last_save_time) >
self.save_interval)

    def save(self,cursor):
        self.site_record_id = self.site_record_id + 1
        values=(self.site_id,self.site_record_id,self.timestamp,
                self.Bx_bar,self.By_bar,self.Bz_bar,self.Mxx_bar,
                self.Mxz_bar,self.Mzz_bar,self.a,self.b,self.Ux,

self.Uz,self.Vx,self.Vz,self.cU,self.cV,self.frequency)
        cursor.execute(self.add_query,values)
        self.id = cursor.lastrowid
        self.last_save_time = current_timestamp()

    def show(self):

print(self.fmt.format(self.id,self.site_id,self.site_record_id,self.
timestamp,

self.Bx_bar,self.By_bar,self.Bz_bar,self.Mxx_bar,

self.Mxz_bar,self.Mzz_bar,self.a,self.b,self.Ux,

self.Uz,self.Vx,self.Vz,self.cU,self.cV,self.frequency))

class Watcher(threading.Thread):
    def __init__(self,monitor):
        super(Watcher, self).__init__()
        self.monitor = monitor
        self._stop_event = threading.Event()

    def stop(self):
        self._stop_event.set()

    def stopped(self):
        return self._stop_event.is_set()

    def run(self):
        while (not self._stop_event.is_set()):
            GPIO.output(21,1)
            m = self.monitor
            r = m.take_BCU_reading()
            r.save(m.cursor)
            r.show()
            s = m.current_BCU_summary
            s.add_reading(r)
            if s.should_save():
                s.save(m.cursor)
                s.show()
        GPIO.output(21,0)

def handle_button(channel):
```

```
    global watcher
    print("Button was pushed!")
    if watcher is None:
        print("Starting")
        watcher = Watcher()
        watcher.start()
    else:
        print("Stopping")
        watcher.stop()
        watcher.join()
        watcher = None

sm = SensorMonitor()
sm.database_setup()
sm.GPIO_setup()

print('Reading MCP3008 values, press Ctrl-C to quit...')
print('-' * 57)
current_datetime = datetime.datetime.now()
print ("Current time %s"  % current_datetime)

sm.GPIO_start()

while True:
    time.sleep(10)
```

23 Appendix F – IOIO board code

```
package ioio.examples.simple;

import ioio.lib.api.AnalogInput;
import ioio.lib.api.DigitalOutput;
import ioio.lib.api.IOIO;
import ioio.lib.api.PwmOutput;
import ioio.lib.api.exception.ConnectionLostException;
import ioio.lib.util.BaseIOIOLooper;
import ioio.lib.util.IOIOLooper;
import ioio.lib.util.android.IOIOActivity;
import android.os.Bundle;
import android.widget.SeekBar;
import android.widget.TextView;
import android.widget.ToggleButton;

public class IOIOSimpleApp extends IOIOActivity {
	private TextView textView_;
	private SeekBar seekBar_;
	private ToggleButton toggleButton_;

	@Override
	public void onCreate(Bundle savedInstanceState) {
		super.onCreate(savedInstanceState);
		setContentView(R.layout.main);

		textView_ = (TextView) findViewById(R.id.TextView);
		seekBar_ = (SeekBar) findViewById(R.id.SeekBar);
		toggleButton_ = (ToggleButton) findViewById(R.id.ToggleButton);

		enableUi(false);
	}

	class Looper extends BaseIOIOLooper {
		private AnalogInput input_;
		private PwmOutput pwmOutput_;
		private DigitalOutput led_;

		@Override
		public void setup() throws ConnectionLostException {
			led_ = ioio_.openDigitalOutput(IOIO.LED_PIN, true);
			input_ = ioio_.openAnalogInput(40);
			pwmOutput_ = ioio_.openPwmOutput(12, 100);
			enableUi(true);
```

```
		}

		@Override
		public void loop() throws ConnectionLostException, InterruptedException {
			setNumber(input_.getVoltage());
			pwmOutput_.setPulseWidth(500 + seekBar_.getProgress() * 2);
			led_.write(!toggleButton_.isChecked());
			Thread.sleep(10);
		}

		@Override
		public void disconnected() {
			enableUi(false);
		}
	}

	@Override
	protected IOIOLooper createIOIOLooper() {
		return new Looper();
	}

	private void enableUi(final boolean enable) {
		runOnUiThread(new Runnable() {
			@Override
			public void run() {
				seekBar_.setEnabled(enable);
				toggleButton_.setEnabled(enable);
			}
		});
	}

	private void setNumber(float f) {
		final String str = String.format("%.4f", f);
		runOnUiThread(new Runnable() {
			@Override
			public void run() {
				textView_.setText(str);
			}
		});
	}
}
```